

Epithelial-to-mesenchymal transition in clear cell renal cell cancer and renal fibrosis



Lea Zoe Landolt

Thesis for the Degree of Philosophiae Doctor (PhD)
University of Bergen, Norway
2019

UNIVERSITY OF BERGEN



Epithelial-to-mesenchymal transition in clear cell renal cell cancer and renal fibrosis

Lea Zoe Landolt



Thesis for the Degree of Philosophiae Doctor (PhD)
at the University of Bergen

2019

Date of defence: 16.01.2019

© Copyright Lea Zoe Landolt

The material in this publication is covered by the provisions of the Copyright Act.

Year: 2019

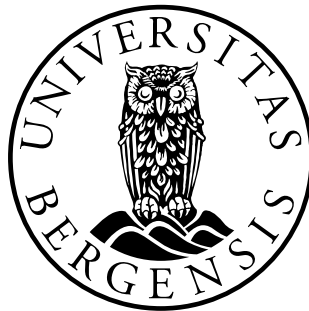
Title: Epithelial-to-mesenchymal transition in clear cell renal cell cancer and renal fibrosis

Name: Lea Zoe Landolt

Print: Skipnes Kommunikasjon / University of Bergen

Epithelial-to-mesenchymal transition in clear cell renal cell cancer and renal fibrosis

Lea Zoe Landolt



Thesis for the degree philosophiae doctor (PhD)
at the University of Bergen

2019

Date of defence:

© Copyright Lea Zoe Landolt

The material in this publication is covered by the provision of the Copyright Act.

Year: 2019

Title: Epithelial-to-mesenchymal transition in clear cell renal cell cancer and renal fibrosis

Name: Lea Zoe Landolt

Print: Skipnes Kommunikasjon / Univeristy of Bergen

Table of content

Abstract	8
List of publications	10
Abbreviations.....	11
1 Introduction	12
1.1 <u>Why study renal cell cancer and renal fibrosis?</u>	12
1.2 <u>The kidneys</u>	13
1.2.1 Structure and primary function of the kidney	14
1.2.2 Renal function	17
1.3 <u>Renal cell cancer</u>	17
1.3.1 Subtypes and histologic classification	17
1.3.2 Risk factors.....	18
1.3.3 Clinical features and diagnosis	19
1.3.4 Staging and prognostic tools.....	19
1.3.5 Tumor biology.....	21
1.3.6 Treatment	22
1.4 <u>Chronic kidney disease</u>	24
1.4.1 Definition and classification.....	24
1.4.2 Etiology	25
1.4.3 Clinical features and diagnosis	26
1.4.4 Progression of CKD	27
1.4.5 Treatment	27
1.4.6 Pathomechanisms of renal fibrosis.....	27
1.5 <u>Epithelial-to-mesenchymal transition</u>	32
1.5.1 Definition and occurrence in physiology and disease	32
1.5.2 Molecular pathways involved in EMT.....	34
1.5.3 TGF β signaling pathway	36
1.5.4 EMT in cancer	37
1.5.4.1 <i>EMT in renal cell cancer</i>	38
1.5.5 EMT in organ fibrosis.....	39
1.5.5.1 <i>EMT in renal fibrosis</i>	40
1.5.6 Targeting EMT.....	41
1.6 <u>AXL receptor tyrosine kinase</u>	42
1.6.1 Structure and signaling pathway	42
1.6.2 AXL in physiology	43
1.6.3 AXL and EMT	44
1.6.4 AXL in cancer	45
1.6.4.1 <i>AXL in renal cell cancer</i>	46
1.6.5 AXL in organ fibrosis.....	47
1.6.5.1 <i>AXL in renal fibrosis</i>	47
1.6.6 AXL inhibitors.....	49
1.7 <u>Renal registries and biopsy archives</u>	50
1.7.1 Storage methods of renal biopsy tissues	50
1.7.2 The Norwegian Renal Registry - patient and biopsy data.....	51
2 Aims of the thesis	52
3 Material and Methods	53

3.1	<u>Renal tissues, storage and handling</u>	53
3.1.1	Rat renal tissues (paper I).....	53
3.1.2	ccRCC and adjacent normal human renal tissues (paper I and II)	53
3.1.3	Murine renal tissues (paper III)	54
3.1.4	Human renal fibrosis tissues (paper III)	54
3.1.5	Laser-capture microdissection	55
3.2	<u>RNA extraction, sequencing and transcriptome analyses</u>	55
3.3	<u>Protein extraction and proteome analysis</u>	57
3.4	<u>Unilateral ureteral obstruction</u>	57
3.5	<u>BGB324 and vehicle treatment</u>	58
3.6	<u>Immunohistochemistry</u>	58
3.7	<u>Fibrosis quantification</u>	59
3.7.1	Sirius Red and semi quantitative computer-assisted analysis.....	59
3.7.2	Hydroxyproline content measurement.....	59
4	Summary of main results	60
4.1	Summary of results paper I.....	60
4.2	Summary of results paper II	61
4.3	Summary of results paper III.....	62
5	Discussion	64
5.1	<u>Methodological considerations</u>	64
5.1.1	How to obtain human renal tissues and what are the possible issues?	64
5.1.2	RNA extraction and assessment.....	66
5.1.3	From Sanger Sequencing to Next Generation Sequencing.....	67
5.1.4	RNA sequencing method in the context of FFPE.....	68
5.1.5	Implication of transcriptomic and proteomic data analyses	69
5.1.6	EMT gene signatures and EMT score	70
5.1.7	UUO as a renal fibrosis model	71
5.1.8	Experiment set up and choice of mice strain.....	73
5.1.9	How to quantify fibrosis in renal specimens?	73
5.2	<u>Discussion of the main results</u>	74
5.2.1	RNA extraction and sequencing of archival biopsies	74
5.2.2	EMT and fibrosis in ccRCC	77
5.2.3	EMT and AXL in renal fibrosis.....	80
6	Conclusions and further perspectives	85
6.1	Conclusions	85
6.2	Further perspectives.....	85
7	References	87

Scientific environment

This work was carried out within the Renal Research Group, Department of Clinical Medicine, Faculty of Medicine, at the University of Bergen, Norway, between 2015 and 2018 under the supervision of Professor Hans-Peter Marti, Professor Bjørn Egil Vikse and Professor James B. Lorens.

Collaborating partners were the Departments of Nephrology, Pathology and Urology of Haukeland University Hospital, Bergen; The Genomic Facility of the Department of Clinical Science, University of Bergen; The Department of Cancer Research and Molecular Medicine, Norwegian University of Science and Technology (NTNU), Trondheim, Norway; Spheromics, Kontiolathi, Finland and BerGenBio AS, Bergen.

Animal experiments were performed at the animal facilities of the Department of Clinical Medicine, University of Bergen.

This work was funded by a PhD grant from the University of Bergen. Financial support was also provided by BerGenBio AS (for the studies of paper III) and by a Helse Vest open project grant (#912167) to H.P. Marti.

Acknowledgments

First of all, I would like to thank my main supervisor Hans-Peter Marti for giving me the opportunity to work in the Renal Research Group, and for his guidance during my time as a PhD fellow. Hans-Peter has always been encouraging and I could not imagine a better supervisor than him.

Many thanks also to Bjørn Egil Vikse for his support and contribution during the writing phase, and also for giving me the possibility to work in Haugesund last winter - that helped me finish this thesis. Thank you also to Jim Lorens for his help and supervision despite busy time schedules.

I am very grateful to the whole Renal Research Group - particularly Jana, Jessica, Kenneth, Mohammad, Tarig, Trude, Øystein E., Dagny, Philipp and Even, to whom I owe this thesis. Thank you Trude and Øystein E. for introducing me to lab work and the "art" of RNA extraction. Also, I would like to thank Einar Svarstad, Camilla Tøndel, Thomas Knoop and Rannveig Skrunes for their support and for welcoming me in Bergen. Lots of thanks to Sabine Leh, for her patience, the good discussions and her enthusiasm!

The collaboration with BerGenBio, in particular with Gro Gausdal, Jim Lorens, Lavina Ahmed and Anthony Brown, was very fruitful and I am very happy to have been involved in it. I thank them for all their input into our projects and the many discussions. Thank you also to my co-authors Andreas Scherer and Christian Beisland for their help and contribution to the publications and the thesis.

A big thank to my colleagues and Ingegjerd Sekse from the Department of Nephrology for their help teaching the students and for the great "holiday from writing" during my time as a sommervikar this summer! Also, I would like to thank the administration of the Department of Clinical Medicine, especially Jorunn Skei, Ingvild Wallacher, Julie Hansen and Solveig Lund Witsø for their help - in the past years and during the submission process.

My deepest thanks go to my friends in Bergen and Switzerland for their company and distraction, and for cheering me on. Thank you also to the "Penthouse Crew" from the 9th floor for the great working atmosphere! Finally, I would like to thank my family, Hans, Claudine, Lunard, Malwina and Øystein for their loyalty and support.

Abstract

Background: Clear cell renal cell cancer (ccRCC) is a common cancer in humans and still has a high mortality. Chronic kidney disease (CKD) is a worldwide public health issue due to its increasing incidence and high morbidity and mortality related to accelerated cardiovascular diseases. Renal fibrosis is the histopathological correlate of CKD. Epithelial-to-mesenchymal transition (EMT) is a biological process where cells acquire mesenchymal characteristics such as loss of cell-cell adhesion, enhanced migratory capacity and production of extracellular matrix. In the case of cancer, EMT is involved in tumor progression, aggressiveness and therapy resistance. In the case of fibrosis, partial EMT drives the activation of myfibroblasts and the accumulation of extracellular matrix. AXL receptor tyrosine kinase is an EMT induced effector and is known to play a role in cancer aggressiveness, therapy resistance and fibrosis development. Renal biopsy archives such as the Kidney Biopsy Registry of the Norwegian Renal Registry are valuable sources for renal tissue analyses. Modern molecular analysis of archival renal biopsies could help to investigate pathomechanisms, and define potential biomarkers and new drug targets of renal diseases. The aims of this work were to: 1) evaluate the best method to extract RNA from archival formalin-fixed paraffin-embedded (FFPE) renal biopsies to enable RNA sequencing; 2) to study EMT markers in ccRCC tissues of our patient cohort; and 3) to detect AXL in unilateral ureteral obstruction (UUO), a murine renal fibrosis model, and to quantify fibrosis after inhibition of AXL by the selective small molecule BGB324 in UUO.

Methods: In [paper I](#), we tested seven commercially available RNA extraction kits on rat and human FFPE renal biopsy sections and on laser-capture microdissected (LCM) glomerular cross-sections to enable RNA sequencing from archival FFPE renal tissues. In [paper II](#), FFPE sample pairs of ccRCC and adjacent normal tissues from our ccRCC cohort were used to characterize EMT markers by immunohistochemistry (IHC) and to analyze RNA, miRNA sequencing and proteomic data with respect to EMT and fibrosis. In [paper III](#), we analyzed AXL in kidneys subjected to UUO in C57Bl/6 mice and assessed fibrosis extent by Sirius Red (SR) staining and hydroxyproline content after treatment with BGB324 or its vehicle. These analyses were supplemented by RNA sequencing including

pathway analyses and by ELISA. We later analyzed the presence of AXL in diabetic and nephrosclerotic FFPE human biopsy tissues by IHC and RNA sequencing.

Results: In paper I, four commercially available RNA extraction kits were suitable to isolate sufficient RNA from one human FFPE renal biopsy section and from around 100 LCM glomerular cross-sections with the Illumina TruSeq RNA Access Library Preparation kit. In paper II we demonstrated that EMT and fibrosis are prominent features in ccRCC samples of our cohort, that EMT related genes such as AXL, vimentin and matrix metalloproteinase 14 (MMP14) are associated to tumor stage in our cohort, and that expression levels of AXL, MMP14 and Klotho correlate with survival in publicly available datasets of ccRCC patient cohorts. In paper III, we found that AXL was distinctly more expressed in ligated compared to non-ligated kidneys in UUO. BGB324 treatment attenuated fibrosis development in ligated kidneys compared to ligated vehicle treated kidneys 15 days after obstruction. Tissue analyses and RNA sequencing data were compatible with reduced (partial) EMT and reduced inflammation in ligated BGB324 treated compared to the vehicle treated control.

Conclusion: Paper I: RNA sequencing from human FFPE renal biopsies is feasible from one single biopsy section and from around 100 LCM glomerular cross-sections using the Illumina TruSeq RNA Access Library Preparation kit. Archival renal biopsy tissues are thus suitable for transcriptome sequencing.

Paper II: EMT and fibrosis are substantial characteristics of ccRCC in our patient cohort and are associated with prognosis based on publicly available ccRCC datasets. Genes related to EMT including AXL may therefore be further evaluated as potential treatment targets.

Paper III: AXL is involved in fibrosis development in UUO and inhibition of AXL by BGB324 reduces fibrosis development of UUO. AXL is present also in fibrotic human renal biopsy tissues and AXL therefore represents a potential therapeutic target for renal fibrosis.

List of publications

Paper I

Landolt L, Marti HP, Beisland C, Flatberg A, Eikrem Ø

RNA extraction for RNA sequencing of archival renal tissues, *Scandinavian Journal of Clinical and Laboratory Investigations*, 2016; 13:1-9

Paper II

Landolt L, Eikrem Ø, Strauss P, Scherer A, Lovett DH, Beisland C, Finne K, Osman T, Ibrahim MM, Gausdal G, Ahmed L, Lorens JB, Thiery JP, Tan TZ, Sekulovic M, Marti HP

Clear cell renal cell carcinoma is linked to epithelial-to-mesenchymal transition and to fibrosis, *Physiological reports*, 2017, 5 (11): e13305

Corrigendum: Physiological reports, 2018, 6 (8): e13671.

Paper III

Landolt L, Jessica Furiol, Babickova J, Ahmed L, Eikrem Ø, Skogstrand T, Scherer A, Leh S, Lorens JB, Gausdal G, Suliman S, Marti HP, Osman T

Inhibition of AXL receptor tyrosine kinase reduces fibrosis development in experimental unilateral ureteral obstruction (*Manuscript*)

Abbreviations

ACEI	Angiotensin-converting enzyme inhibitor	MET	Mesenchymal-to-epithelial transition
αSMA	Alpha smooth muscle actin	miRNA	MicroRNA
AML	Acute myeloid leukemia	MMP	Matrix metalloproteinase
APC	Antigen presenting cell	mRNA	Messenger ribonucleic acid
bHLH	Basic helix-loop-helix	NaCl	Sodium chloride
BMP7	Bone morphogenetic protein 7	NGS	Next generation sequencing
CAV1	Caveolin1	NKBR	Norwegian Kidney Biopsy Registry
CDH1	E-cadherin	NRR	Norwegian Renal Registry
CKD	Chronic kidney disease	OS	Overall survival
CCL	C-C motif chemokine ligand	PAI1	Plasminogen activator inhibitor
ccRCC	Clear cell renal cell carcinoma	PAS	Periodic acid-Schiff
CTC	Circulating tumor cells	PCA	Principle component analysis
CTGF	Connective tissue growth factor	PD1	Programmed death 1
CTLA4	Cytotoxic T-lymphocyte antigen 4	PDGF	Platelet derived growth factor
DFS	Disease-free survival	PI3K	Phosphatidylinositol 3-kinase
ECM	Extracellular matrix	PLAU	Plasminogen activator urokinase
EGF	Epidermal growth factor	PtdSer	Phosphatidylserin
EMT	Epithelial-to-mesenchymal transition	RAAS	Renin-angiotensin-aldosterone system
EndMT	Endothelial-to-mesenchymal transition	rRNA	Ribosomal RNA
EPO	Erythropoietin	RTK	Receptor tyrosine kinase
ESRD	End-stage renal disease	SOCS	Suppressor of cytokine signaling
FC	Fold change	SR	Sirius Red
FFPE	Formalin-fixed paraffin-embedded	TCGA	The cancer genome database
GAS6	Growth arrest-specific protein 6	TEC	Tubular epithelial cell
GFR	Glomerular filtration rate	TGFα	Transforming growth factor alpha
HE	Hematoxylin (and) eosin	TGFβ	Transforming growth factor beta
HIF	Hypoxia inducible factor	TβRII	TGFβ type II receptor
HGF	Hepatocyte growth factor	TLR	Toll like receptor
IHC	Immunohistochemistry	TNFα	Tumor necrosis factor alpha
KL	Klotho	UUO	Unilateral ureteral obstruction
LCM	Laser-capture microdissected	VEGF	Vascular endothelial growth factor
LC-	Liquid chromatography-tandem mass	VHL	Von Hippel-Lindau
MS/MS	spectrometry	VIM	Vimentin
cpm	Counts per million	ZEB	Zinc-finger E-box binding protein
MARGS	Metzincins and related genes		

1 Introduction

1.1 Why study renal cell cancer and renal fibrosis?

Renal cancer is the sixth most common cancer in men and the tenth most common cancer in women (Siegel et al., 2018). In Norway, 876 patients were diagnosed with renal cell cancer (RCC) in 2016 and 222 have died from it. In the past years, incidence and survival of RCC has increased, but overall mortality remains high (Figure 1.1) (Larsen et al., 2017, Perazella et al., 2018). Clear cell RCC (ccRCC) is the most common RCC and often displays an aggressive disease course: Around 20% of cases are already advanced at time of diagnosis (Pichler et al., 2012, Dabestani et al., 2016, Siegel et al., 2018). Despite surgery, more than 20% of patients with initially localized cancer develop metastases after 5 years (Dabestani et al., 2016, Dabestani et al., 2018). Locally advanced ccRCC (Stage III) has a 5-year survival rate of around 50%. Patients with metastatic ccRCC, have a 5-year survival rate of 0-32% with established chemotherapy (Escudier et al., 2016, Choueiri et al., 2017b). There is therefore a need for more efficient and more targeted treatment strategies in both localized and advanced cancer cases.

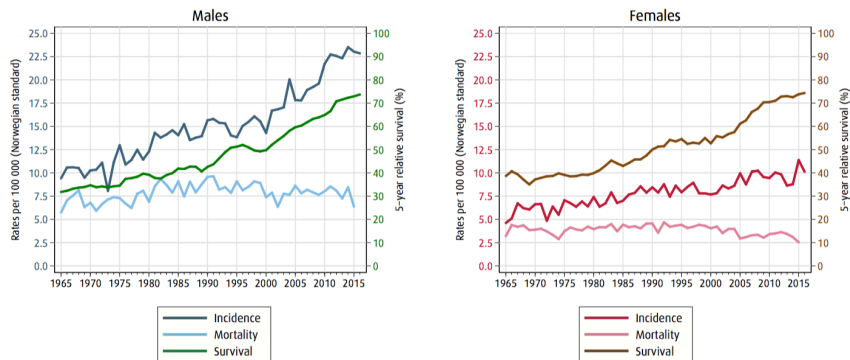


Figure 1.1: Trends in incidence, mortality rate and 5-year relative survival of renal cell cancer between 1965 and 2016 in Norway for males and females. From *Cancer in Norway 2016*, the Cancer Registry in Norway (Larsen et al., 2017) with permission.

Renal fibrosis is a common histological feature of moderate to advanced chronic kidney disease (CKD) irrespective of its cause. CKD - mainly caused by diabetes, hypertension and also glomerulonephritis - has a global prevalence of 11 to 13% and is a worldwide public health concern (Figure 1.2) (Eckardt et al., 2013, Hill et al., 2016, Levin et al., 2017). The high burden of CKD is due to increased

mortality, mainly caused by cardiovascular diseases, bone and infectious disease related morbidity, impaired quality of life and high economic costs (Levin et al., 2017). Between 1990 and 2013, there was a global increase of years of life lost due to CKD of more than 50%. The prevalence of CKD is expected to increase in the future, especially due to the rising prevalence of obesity and diabetes. In 2015, more than 400 million people were diabetic and it is expected that this number will rise to more than 640 million in 2050 (GBD, 2015, Kainz et al., 2015, Hsu et al., 2017, Ogurtsova et al., 2017).

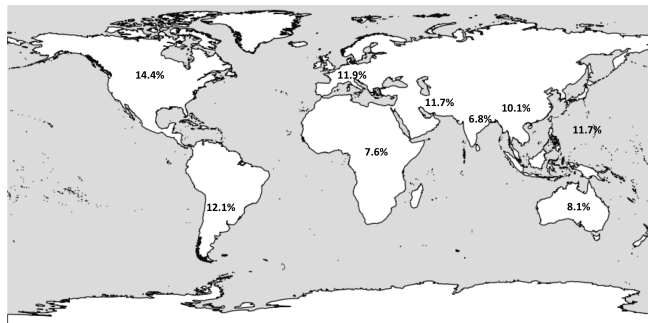


Figure 1.2: Global prevalence of CKD stage 3-5. Map generated using the public domain online tool SimpleMappr, <http://simplemappr.net>. Prevalence data from (Hill et al., 2016).

Renal fibrosis is progressive and, past a certain stage, becomes irreversible. There is no established and targeted therapy to slow the progression of renal fibrosis, besides attempts mostly with Angiotensin-converting enzyme inhibitors (ACEI) and the treatment of the underlying renal disease. In addition to the need for systematic action plans to prevent and monitor CKD at the global public health level, there is also a substantial need for increased biomedical research, which could lead to an improved understanding of the disease's pathomechanisms and potential treatment targets.

1.2 The kidneys

RCC and renal fibrosis are significant diseases arising in the renal tissues. To understand these entities, one needs to have a profound knowledge on the functioning of the kidneys. Thus, we must ask: How are the kidneys structured and why do we actually have kidneys? What are the risk factors and pathomechanisms leading to ccRCC and renal fibrosis and what role does epithelial-to-mesenchymal transition (EMT) play?

1.2.1 Structure and primary function of the kidney

Each human kidney consists of about 1.4 million nephrons - the functional unit of the kidney (Keller et al., 2003). One nephron comprises the renal corpuscle with glomerulus and Bowman's capsule, and the tubular system where the proximal tubule, loop of Henle, distal convoluted tubule and conducting tubule align (Figure 1.3) (Pollak et al., 2014). The primary functions of the kidney are summarized in table 1.

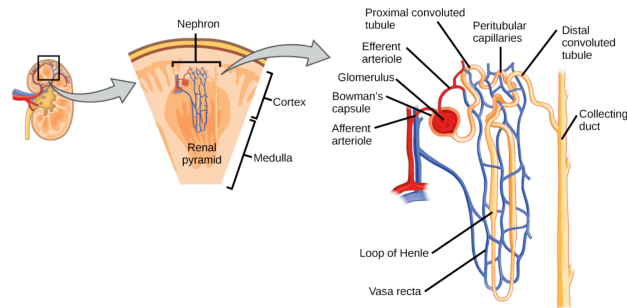


Figure 1.3: The nephron with glomeruli, proximal tubules and distal convoluted tubules in the cortex and loop of Henle and collecting ducts in the medulla. Illustration from OpenStax College, licensed under the Creative Commons Attribution-Share Alike 4.0.

Glomeruli are capillary networks and represent the filtering unit of the kidneys. Around 20% of the cardiac output passes through the capillary tuft of the glomeruli and around 160 liters of ultrafiltrate are filtered into the Bowman's capsule and the tubular system per day. The glomerular filtration barrier is made out of fenestrated endothelial cells of the glomerular capillaries, the glomerular basement membrane (GBM) and podocytes - uniquely specialized epithelial cells creating the slit diaphragms (Figure 1.4) (Pollak et al., 2014). The mesangium, consisting of mesangial cells and extracellular matrix (ECM), lies around the capillary tuft. Mesangial cells provide support to the capillaries and interact with the GBM where they influence the filtration pressure by contractility of their processes (Ghayur et al., 2008).

In the proximal tubule, around two thirds of the sodium present is resorbed from the ultrafiltrate. The acid-base balance is controlled by the secretion of acid, resorption of bicarbonate and production of the buffers ammonium and hydrogen phosphate (Curthoys et al., 2014, Hamm et al., 2015). The proximal tubule is also a locus for metabolism and elimination of drugs and toxins.

Nutrients such as glucose and amino acids but also anions are reabsorbed there and the proximal tubule epithelial cells (TEC) contribute to gluconeogenesis and convert 25-hydroxy-vitamin D to the active form 1.25-hydroxy-vitamin D (Curthoys et al., 2014). In the case of drugs and toxins, molecules or metabolites are secreted into the lumen and are thus eliminated by organic anion or cation transporters of the proximal tubule (Figure 1.4) (Nigam et al., 2015).

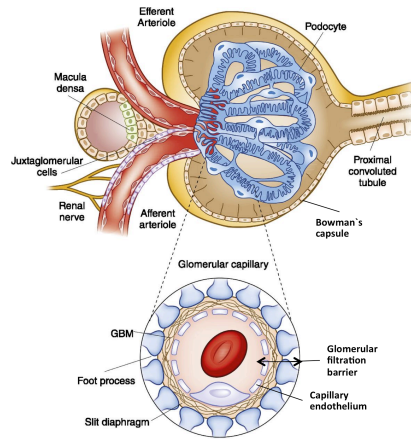


Figure 1.4: The renal corpuscle with glomerulus and Bowman's capsule leading into the proximal tubule. The glomerular filtration barrier comprises the capillary endothelium, the glomerular basement membrane (GBM) and the foot processes of the podocytes creating the slit diaphragm. The macula densa, the distal part of the thick ascending limb of Henle, joins the vascular pole of its corresponding glomerulus and takes part in the tubuloglomerular feedback. Modified from (Pollak et al., 2014) with permission.

The Henle loops function is to enable production of urine that is more concentrated than blood plasma (Figure 1.3) (Dantzler et al., 2014). Selective permeability and countercurrent of the descending and ascending limbs contribute to building the necessary osmolality gradient in the medulla (Mount, 2014, Palmer et al., 2015). The thick ascending limb of the Henle loop returns to its corresponding glomerulus and is involved in the tubuloglomerular feedback: A cluster of around 20 cells at the end of this segment form the macula densa. These cells are provided with particular sodium, potassium and chloride co-transporters. Uptake of sodium chloride in these cells leads to the secretion of adenosine by the juxtaglomerular cells of the extraglomerular mesangium and induction of vasoconstriction of the afferent arteriole of the glomerulus. This is

an important mechanism in the autoregulation of the glomerular perfusion (Mount, 2014, Palmer et al., 2015).

The short distal convoluted tubule, beginning directly distal of the macula densa, is involved in the resorption of 5-10% of filtered sodium and in the homeostasis of potassium, magnesium and calcium. Secretion of potassium in the distal convoluted tubule is voltage dependent and influenced by aldosterone release: The more sodium is resorbed, the more the following electric negativity in the tubular lumen attracts potassium, which is then increasingly secreted. Aldosterone leads to the expression of potassium channels, facilitating its secretion. Around 10% of filtered calcium and magnesium is actively reabsorbed in the distal convoluted tubule (Figure 1.3) (Reilly et al., 2000, Subramanya et al., 2014).

The collecting duct consists of cells with sodium, potassium and water channels. Resorption of sodium is controlled by aldosterone, whereas the expression of the water channel aquaporin depends on vasopressin. However, these processes are influenced by complex interactions of other autocrine and paracrine hormones such as prostaglandin E₂, endothelin, bradykinin, ATP, insulin and angiotensin II (Figure 1.3) (Pearce et al., 2015).

The renal interstitium constitutes 7-9% of the cortex and 30-40% of the medulla and is comprised of cells and ECM. Cortical interstitium consists of the peritubular, periarterial and the special interstitium. The latter forms the intra- and extraglomerular mesangium. The function of the interstitium is in providing scaffolding for the nephrons but also in the production of erythropoietin (EPO) and renin. The main cells are fibroblasts, a heterogeneous group of mesenchymal cells and the main source of ECM (Lemley et al., 1991, Zeisberg et al., 2015). Intertubular fibroblasts produce EPO, whereas it is the juxtaglomerular cells that produce renin (Castrop et al., 2010, Zeisberg et al., 2015, Souma et al., 2015). Renin is the enzyme that converts angiotensinogen to angiotensin I and is therefore a key protein of the renin-angiotensin-aldosterone system (RAAS) involved in blood pressure control (Zeisberg et al., 2015).

Compartment	Physiology	Systemic function
Glomerulus	Ultrafiltration of the blood	Acid-base balance
Proximal tubule	<ul style="list-style-type: none"> • Reabsorption of Na and H₂O • Secretion of H⁺, resorption of HCO₃⁻ and production of the buffers NH₃ and HPO₄⁻ • Conversion from 25-OH D3 to 1.25-OH D3 • Gluconeogenesis • Secretion of metabolites by OAT and OCT 	
Henle loop	<ul style="list-style-type: none"> • Reabsorption of Na • Creating osmotic gradient to produce hyperosmotic urine • Macula densa: Part of autoregulation 	Secretion of drugs and toxins
Distal convoluted tubule	<ul style="list-style-type: none"> • Reabsorption of Na, Ca and Mg • Secretion of K 	Glucose metabolism
Collecting duct	Reabsorption of H ₂ O, Na and K	Blood pressure control
Interstitial	<ul style="list-style-type: none"> • Production of erythropoietin • Production of renin involved in RAAS 	Electrolyte homeostasis
		Regulation of extracellular volume
		Erythropoiesis

Table 1: Primary functions of the renal structures. RAAS = Renin-angiotensin-aldosterone system.

1.2.2 Renal function

The most commonly used measure for renal function is the glomerular filtration rate (GFR), which is the amount of fluid or "ultrafiltrate" filtered out of the blood in the capillary tuft of the glomerulus into the Bowman's capsule (Pollak et al., 2014). As a surrogate marker, GFR is estimated (eGFR) by calculating the clearance of creatinine using gender, age and serum creatinine levels in the case of the CKD-EPI (chronic kidney disease epidemiology collaboration) equation (Levey et al., 2009, KDIGO, 2013).

1.3 Renal cell cancer

1.3.1 Subtypes and histologic classification

Around 80% of renal tumors are RCC, which are tumors arising from the cells of the nephron. More than 85% of RCC are ccRCC, followed by papillary RCC (around 10%), chromophobe RCC (around 2-3%) and other renal neoplasias such as collecting duct cancers or oncocytoma - the most common benign tumor of the kidney (Figure 1.5) (Patard et al., 2005, Moch et al., 2016, Shuch et al., 2015). Both ccRCC and papillary RCC likely arise from the cells of the proximal tubules, whereas chromophobe RCC and oncocytoma arise from the cells of the distal tubules (Gerharz et al., 1993, Shen et al., 2005, Shuch et al., 2015).

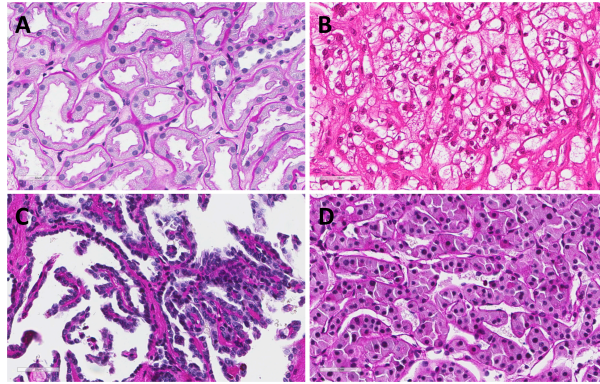


Figure 1.5: Renal cell cancer (RCC) histological subtypes. A) Normal renal tissue. Periodic acid-Schiff (PAS) staining. B) Clear cell RCC with typical clear cytoplasm due to accumulation of glycogen and lipids. Hematoxylin and eosin (HE) staining. C) Papillary RCC with papillary architecture with fibrovascular shaft. PAS. D) Oncocytoma, PAS. Author's own pictures. Magnification 40x.

1.3.2 Risk factors

The incidence of RCC is around two times higher in men than women and increases with age - peak incidence is at about 60-70 years (Levi et al., 2008, Larsen et al., 2017). The presence of RCC in first-degree family relatives is associated with a two-fold increased risk (Clague et al., 2009, Chow et al., 2010). Other main risk factors for RCC are smoking, obesity, hypertension, end-stage renal disease (ESRD) and renal transplantation (Chow et al., 2010).

The duration of smoking is strongly associated with ccRCC, with up to a 35% increase in risk compared to those who have never smoked. Smoking cessation led to a 60% decrease in risk for RCC after 10 years (Theis et al., 2008). Obesity is known to be a risk factor, in particular for ccRCC in both men and women, and the risk is linear to the body mass index (Wolk et al., 1996, Bergstrom et al., 2001, Lowrance et al., 2010, Wang et al., 2014). Hypertension was associated with an increased risk of 2.5 times in both women and men and was also independent of obesity. Antihypertensive medication only partly decreased the risk (Vatten et al., 2007, Weikert et al., 2008). ESRD is associated with increased risk for RCC and the risk depends on underlying renal diseases such as polycystic diseases but also on the duration of dialysis (Maisonneuve et al., 1999). The development of RCC after renal transplantation can arise from transmitted cancer from the graft or in the native kidney. Such transmission is rare and

estimated to be less than 0.03%. In the native kidney, the risk for RCC has been associated with immunosuppressive treatment, with a two to three fold increase in risk (Sprangers et al., 2017). Studies on the influence of dietary factors on RCC are inconsistent: Case-control studies but not cohort studies have shown a risk reduction with the consumption of three servings of fruits or vegetables per day (Weikert et al., 2006, Zhang et al., 2017). The consumption of red meat has been associated with an increased risk for RCC especially in premenopausal women (Rohrmann et al., 2015). Moderate alcohol consumption has been associated with lower risk for RCC in some studies (Lee et al., 2007, Wozniak et al., 2015). Other factors such as physical exercise and parity might influence the incidence of RCC (Chow et al., 2010). An increased risk was found in multiparous compared to nulliparous women (Lee et al., 2009). Physical activity was associated with a 22% risk reduction for RCC in a meta-analysis. The risk reduction was independent of other factors such as smoking or obesity (Behrens et al., 2013).

1.3.3 Clinical features and diagnosis

Typical local symptoms of RCC include flank pain, macrohematuria and a palpable abdominal mass, but only 10% of patients are diagnosed on the basis of such symptoms. Due to the increased use of abdominal imaging, around half of all RCCs are detected incidentally. Paraneoplastic syndromes may also occur, such as hypertension but also anemia, weight loss, fever, hypercalcemia and less frequent signs such as the new appearance of a varicocele, erythrocytosis and amyloidosis (Ljungberg et al., 2015, Capitanio et al., 2016, Perazella et al., 2018). Around 20% of RCCs are already advanced at the time of diagnosis (Kane et al., 2008, Pichler et al., 2012, Dabestani et al., 2016). The most common distant metastases are in the lung, bone and liver but less frequently in the adrenal gland and brain (Bianchi et al., 2012). Imaging, particularly computer tomography and magnetic resonance imaging, can help to identify RCC and to detect metastases (Capitanio et al., 2016, Perazella et al., 2018).

1.3.4 Staging and prognostic tools

The staging for ccRCC is by the standard Tumor - Node - Metastasis (TNM) system for renal cancer (Ljungberg et al., 2015, Escudier et al., 2016) (Table 2).

T1	Tumor \leq 7cm in greatest dimension	Stage I
T2	Tumor > 7cm in greatest dimension	Stage II
T3	Tumor extends into major veins or perinephric tissue but not into adrenal gland or beyond Gerota's fascia	Stage III
T3a	Tumor extends into renal vein, into its segmental branches, into perirenal fat or pelvicaliceal system	
T3b	Tumor extends into vena cava below the diaphragm	
T3c	Tumor extends into vena cava above the diaphragm or into wall of vena cava	
T4	Tumor invades beyond Gerota's fascia including into adrenal gland	Stage IV
N0	No regional lymph node metastasis	Stage I-II
N1	Metastasis in regional lymph node	T1-2: Stage III
cM0	Clinically no distant metastases	
cM1	Clinically distant metastases	Stage IV

Table 2: Standard Tumor - Node - Metastasis (TNM) classification and prognostic stages for renal cancer according to the Classification of malignant tumors, 8th edition (AJCC/UICC) (UICC, 2017).

In localized cancers, prognostic scores such as the Leibovich, SSIGN (stage, size, grade, necrosis) or UISS (UCLA integrated staging system) scores are often applied (Parker et al., 2017, Zisman et al., 2001, Leibovich et al., 2003, Escudier et al., 2016). These scores include histological parameters such as nuclear grading or the presence of necrosis, but also clinical parameters such as tumor size, TNM stage or clinical performance status. Traditionally, nuclear grade has been assessed using the Fuhrman grading score, which describes nuclear size, irregularity and nucleolar prominence (Fuhrman et al., 1982). In 2013, a new grading system (WHO/ISUP) was introduced and later validated. The WHO/ISUP system assesses nuclear polymorphism and nucleolar prominence and color (basophilic in grade I, eosinophilic in grade II and III) (Delahunt et al., 2013, Dagher et al., 2017).

In metastatic cancer, prognostic scores such as the International Metastatic RCC Database Consortium (IMDC) score are used, based on clinical performance status, time from diagnosis to treatment and biochemical parameters (calcium, hemoglobin, neutrophils, platelet count) are used (Heng et al., 2013, Escudier et al., 2016, Powles et al., 2017). Up to now, no molecular marker is routinely used. Since the 90s, more ccRCC have been incidentally detected at early stage. This is due to the increased use of imaging technologies. Incidental ccRCC are smaller

and have a lower TNM stage. This tendency and shift of stage (also called "stage migration"), did not have an influence on mortality but has led to increased survival, even after correction for lead-time bias (Figure 1.1). Early diagnosis is therefore favorable (Palsdottir et al., 2012, Capitanio et al., 2016).

1.3.5 Tumor biology

Generally, around 2-3% of RCC are assumed to be hereditary: The most common familial syndromes are mutations of the von Hippel-Lindau (VHL) tumor suppressor gene, which predisposes for ccRCC but also for hemangioblastoma and pheochromocytoma. There are different types of hereditary VHL mutations, each associated with an increased risk for particular cancers. Type 1 and 2b mutations of the VHL allele are especially associated with ccRCC (Kaelin, 2008, Kaelin, 2018). Birt-Hogg-Dubé syndrome is another hereditary RCC syndrome where the folliculin gene is mutated. Around one third of the affected patients develop RCC, mostly with chromophobe and oncocytoma components. ccRCC only account for 10% of the renal tumors in this syndrome (Schmidt et al., 2015). Around 80% of sporadic ccRCC cases are associated with alteration of the VHL alleles on chromosome 3 (Brugarolas, 2014). In physiological states, VHL is involved in degradation of the hypoxia inducible factors (HIF) by forming an ubiquitin ligase complex together with elongin B, C, cullin2 and RBX1. HIF is a transcription factor that activates genes responsible for adaptation under hypoxic conditions and has around 100-200 target genes. HIF has to be hydroxylated by proteins of the EGLN family to be recognized and degraded by VHL and the ubiquitin ligase complex. EGLN proteins are induced by hypoxia and EGLN2 is the main protein involved in hydroxylation of HIF (Kaelin, 2008, Kaelin, 2018). ccRCC due to VHL mutations occurs usually in two "hits": An inherited mutated VHL allele is followed by alteration of the remaining VHL allele. In cells with defective VHL, HIF2 α in particular accumulates. Target genes of HIF include EPO, vascular endothelial growth factor (VEGF), platelet derived growth factor B (PDGF), connective tissue growth factor (CTGF), matrix metalloproteinase 1 (MMP1), epidermal growth factor (EGFR) and transforming growth factor alpha (TGF β), among others (Figure 1.6). MET is also induced by HIF and leads to an

increased sensitization of cells to hepatocyte growth factor (HGF) and to invasive growth (Kaelin, 2008, Kaelin, 2018, Pennacchietti et al., 2003).

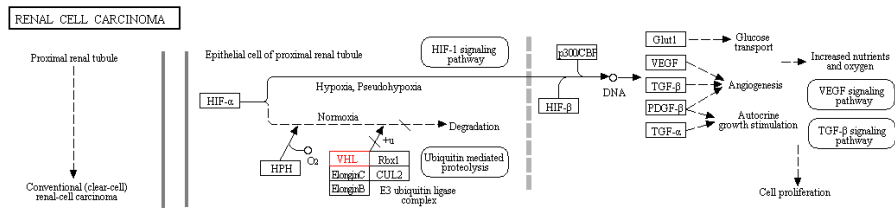


Figure 1.6: Principal pathway involved in ccRCC: The ubiquitin ligase complex including VHL, elongin B, C, cullin2 and RBX1 normally degrades HIF α in normoxia but not in hypoxic conditions. HIF accumulates in ccRCC due to VHL mutation and induces the expression of VEGF, TGF β , TGF α and PDGF. Pathway map 05211 from Kyoto Encyclopedia of Genes and Genomes (KEGG), with permission.

Altered VHL also induces non-HIF dependent pathways such as WNT/ β -catenin pathway, NF κ B, the AKT pathway and MET/HGF pathway. AKT is hydroxylated by EGLN1 and also targeted by the VHL ubiquitin-ligase complex under physiological conditions. When VHL is mutated, AKT has therefore increased activity (Kaelin, 2008, Kaelin, 2018).

Other gene alterations have been described and play a substantial role in the development of ccRCC. The most common involved genes involved (other than VHL) are PBRM (altered in 45% of ccRCC), SETD2 (10-15%) and BAP1 (10-15%), which are all located on chromosome 3. PBRM, SETD2 and BAP1 are also two-hit tumor suppressor genes. The region of chromosome 3 where these proteins are encoded is lost in around 90% of sporadic ccRCC. Different mutations of these involved proteins are associated with different biology and prognosis (Brugarolas, 2014, Frew et al., 2015). Intratumor molecular heterogeneity of ccRCC has also been demonstrated: More than 60% of all mutations cannot be found throughout the tumor (Gerlinger et al., 2012).

1.3.6 Treatment

In localized cancers, the treatment of choice is the removal of the tumor. In the case of small tumors (T1), a partial nephrectomy can be performed if feasible. In larger tumors, radical nephrectomy is the standard of care (Ljungberg et al., 2015, Escudier et al., 2016).

Study results on the effect of adjuvant therapy after tumor removal are conflicting: Three studies (S-TRAC, ASSURE and PROTECT) have compared receptor tyrosine kinase (RTK) inhibitors such as Sunitinib to placebo in an adjuvant setting in intermediate to high-risk patients as defined by UISS (S-TRAC), TNM alone (ASSURE) or TNM and Fuhrman grade (PROTECT). None of the studies showed increased overall survival in the intervention groups. Only the S-TRAC study showed prolonged disease-free survival (DFS) and thus led to the approval of Sunitinib (an RTK inhibitor that targets PDGFR and VEGFR in particular), as the only adjuvant treatment option in late 2017 (Ravaud et al., 2016, Motzer et al., 2018a, Salmasi et al., 2018). Both the ASSURE (Sunitinib or Sorafenib) and PROTECT (Pazopanib) studies revealed both dose dependent toxicity but also dose dependent clinical benefit (Haas et al., 2017, Motzer et al., 2017). However, adjuvant therapy with Sunitinib can be considered but is not a standard therapy in localized ccRCC (Bex et al., 2017).

In metastatic cancer, earlier recommendations included nephrectomy if possible, with the purpose of reducing tumor load (Ljungberg et al., 2015, Escudier et al., 2016). More recently, a study showed that in patients with metastatic ccRCC and intermediate to poor prognosis treatment with Sunitinib without nephrectomy did not worsen overall survival (OS) compared to nephrectomy combined with Sunitinib (Mejean et al., 2018). Thus, patients eligible for cytoreductive nephrectomy have to be selected carefully (Bex et al., 2018). Radiotherapy or resection of metastases might improve survival and local symptoms but is not routinely done. ccRCC is generally considered to be radioresistant (Dabestani et al., 2014, Ljungberg et al., 2015).

Systemic therapy is the standard in metastatic ccRCC and depends on the prognosis of the patient as graded by IMDC. However, this field of research is particularly dynamic and the subject of rapid development.

Up to now, the established first line treatment for patients with metastatic ccRCC with a good or intermediate prognosis has been Sunitinib, Pazopanib or Bevacizumab and interferon. Sunitinib and Pazopanib are multitarget RTK inhibitors, which inhibit VEGFR, PDGFR and other kinases. Bevacizumab, a monoclonal antibody, binds VEGFA and inhibits its binding and thus the activation of VEGFR. In patients with poor prognosis, Temsirolimus, an inhibitor

of the mammalian target of rapamycin (mTOR) has been recommended earlier (Ljungberg et al., 2015, Escudier et al., 2016, Choueiri et al., 2017b). Just recently, a study compared Nivolumab (an anti-programmed death 1 (PD1) antibody) together with Ipilimumab (an anti-cytotoxic T-lymphocyte antigen 4 (CTLA4) antibody) - both immune checkpoint inhibitors - to Sunitinib in metastatic ccRCC with intermediate or poor prognosis. Nivolumab plus Ipilimumab showed a benefit in OS: 15% more patients were alive after 18 months of follow up compared to patients treated with Sunitinib (Motzer et al., 2018b). This combination is currently advised as first line therapy in such patients, if available and safe in the context of toxicity. If these checkpoint inhibitors are not available or unfavorable, RTK inhibitors such as Sunitinib, Pazopanib or Cabozantinib are alternatives. In patients with good prognosis, Sunitinib or Pazopanib are currently still the first choices (Powles et al., 2017, Motzer et al., 2018b).

As second and third line treatments in patients with a favorable prognosis treated with RTK inhibitors, additional Nivolumab or Cabozantinib (a combined VEGFR, Met and AXL inhibitor) are options. Met and AXL are two proteins involved in alternative pathways responsible for resistance after VEGF targeted treatment (Rini et al., 2009, Choueiri et al., 2017a, Choueiri et al., 2017b, Powles et al., 2017). In patients with a poor prognosis already treated with checkpoint inhibitors, VEGF targeted RTK inhibitors are administered. Alternatives are Cabozantinib or Nivolumab alone in the case of the patient having already received RTK inhibitors (Ljungberg et al., 2015, Escudier et al., 2016, Powles et al., 2017, Escudier, 2017).

1.4 Chronic kidney disease

1.4.1 Definition and classification

CKD is defined as a reduced renal function with a GFR below 60ml/min/1.73m² for more than three months. Other conditions that define CKD regardless of the renal function are elevated markers of kidney damage such as albuminuria and structural abnormalities detected by renal biopsy or imaging (present for more than three months) and having undergone renal transplantation (KDIGO 2012). CKD is further classified by GFR and extent of albuminuria (Table 3). A GFR below 15ml/min is defined as ESRD (KDIGO, 2013).

			Albuminuria (mg/mmol creatinine)		
			A1	A2	A3
			<3mg/mmol	3-30mg/mmol	>30mg/mmol
GFR categories (ml/min/1.73m ²)	G1	>90			
	G2	60-89			
	G3a	45-59			
	G3b	30-44			
	G4	15-29			
	G5	<15			

Table 3: Prognosis of CKD based on GFR categories (G1-G5) and albuminuria (A1-A3). Green: Low risk, yellow: Moderate risk, orange: High risk, red: Very high risk for CKD progression. Modified from the KDIGO guidelines (KDIGO, 2013).

1.4.2 Etiology

The main causes for ESRD are diabetes, hypertension, glomerulonephritis (including vasculitis related glomerulopathies) and polycystic renal diseases (autosomal dominant polycystic kidney disease in particular). Other causes are chronic pyelonephritis, tubulointerstitial nephritis, systemic autoimmune diseases, amyloidosis, multiple myeloma and kidney tumors. There are geographical differences: In the US for example, the cause for ESRD is 46% diabetes and 28% hypertension whereas in Norway, the cause for ESRD is 34% hypertension and only 16% diabetes (Figure 1.7) (Webster et al., 2017, USRDS, 2017, Reisaeter, 2016).

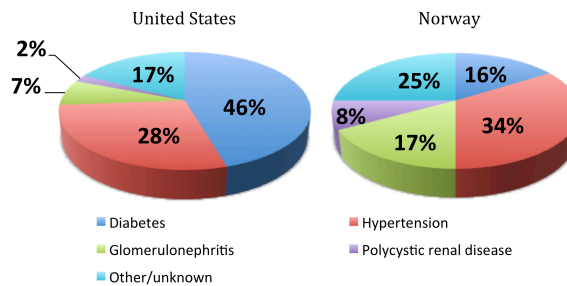


Figure 1.7: Causes of ESRD in the US and in Norway. Based on the annual report 2017 of the United States Renal Data System and the annual report 2016 of the Norwegian Renal Registry (USRDS, 2017, Reisaeter, 2016) with permission.

The burden of CKD is particularly high in low- and middle-income countries. This is due to rapid urbanization and the epidemiologic transition with increased prevalence of non-communicable diseases such as diabetes and hypertension. In addition, low access to health care and renal replacement therapy further increase the burden of CKD. In sub-Saharan Africa, the causes for CKD besides diabetes and hypertension also include communicable diseases such as HIV, hepatitis B and C, leishmaniasis, schistosomiasis and malaria. In addition, there is a known association between the widespread use of traditional and herbal medicine and acute kidney injury also leading to CKD (Stanifer et al., 2014, Stanifer et al., 2016, Silva et al., 2017). In past years, an emergence of CKD of unknown etiology but high mortality has been observed especially in Egypt, India and Sri Lanka in men from rural regions working in agriculture. The cause is still unknown but the combination of exposure to agents such as cadmium and arsenic, in addition to severe physical strain, heat and dehydration has been postulated as associated factors (Weaver et al., 2015, Stanifer et al., 2016).

1.4.3 Clinical features and diagnosis

CKD is often asymptomatic and only becomes overt in its advanced stages. Possible early symptoms are hypertension and peripheral edema. Symptoms in the advanced stages involve the failure of the primary functions of the kidneys (Table 1), which leads to metabolic acidosis, vitamin D deficiency and mineral bone disorder, retention of uremic toxins and decreased drug metabolism, hypertension, electrolyte abnormalities (such as high potassium or phosphate), malnutrition and extensive edema. Diagnosis of CKD and the underlying disease is performed by estimating the GFR with the means of serum creatinine measurements, quantification of albumin in the urine, imaging, and in particular, ultrasound and histological evaluation (Webster et al., 2017). Mortality is increased by up to six times in patients with CKD compared to patients with normal renal function and increases exponentially with progression of CKD. Mortality is driven by the higher risk for cardiovascular events and cardiovascular death even in the early stages (Go et al., 2004, Matsushita et al., 2010).

1.4.4 Progression of CKD

CKD is often a progressive disease. The rate of progression depends on multiple risk factors such as inadequately treated hypertension and diabetes but also sustained underlying renal diseases such as chronic glomerulonephritis. Other established risk factors are proteinuria, male gender as well as comorbidities and age (Tsai et al., 2016, Webster et al., 2017). Furthermore persistent hematuria has been linked to the progression of CKD (Moreno et al., 2016, Schulman et al., 2018). Higher level of serum uric acid and lower level of serum calcium have been associated with increased decline of renal function (Tsai et al., 2017, Janmaat et al., 2018). In clinical practice, the risk of progression is estimated through the classification of CKD by GFR and albuminuria (Table 3) (KDIGO, 2013).

1.4.5 Treatment

The management of CKD includes treatment of the underlying renal disease and its consequences, such as hypertension, edema, metabolic acidosis, hyperkalemia, hyperphosphatemia, vitamin D deficiency and anemia. The main medications to reduce proteinuria are ACEI or angiotensin II receptor inhibitors. Furthermore, cardiovascular risk factors have to be addressed to reduce cardiovascular morbidity and mortality - such as smoking cessation, lowering of lipids and regular physical activity (KDIGO, 2013). In ESRD, renal replacement therapy is either dialysis or transplantation (Webster et al., 2017).

1.4.6 Pathomechanisms of renal fibrosis

Renal fibrosis is the histopathological correlate of CKD and the common pathway for renal diseases regardless of the underlying disease and is a consequence of sustained injury and failed or maladaptive repair mechanisms. Morphologically, renal fibrosis is characterized by glomerulosclerosis, tubulointerstitial fibrosis and tubular atrophy (Figure 1.8) (Ferenbach et al., 2015, Lovisa et al., 2016). Histopathological features of renal fibrosis are the accumulation of extracellular matrix (ECM), fibroblast activation, inflammation, loss of tubular epithelial cells (TEC), and microvasculature rarefaction (Zeisberg et al., 2010, Ferenbach et al., 2015, Lovisa et al., 2016). The extent of tubulointerstitial fibrosis correlates with renal function and is therefore the crucial indicator of renal fibrosis and disease

progression (Kuncio et al., 1991). The cells involved in the development of renal fibrosis are fibroblasts, TEC, endothelial cells and immune cells (Lovisa et al., 2016).

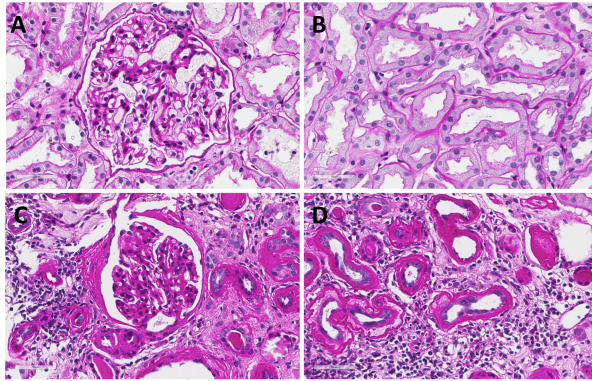


Figure 1.8: A) glomerulus and B) tubuli in normal human renal tissue. C) Glomerulosclerosis with mesangial expansion, thickening of the glomerular basement membrane and glomerular capillaries. D) Tubulointerstitial fibrosis with tubular atrophy, increased intertubular interstitium and infiltration with inflammatory cells. PAS staining. Author's own pictures. 40x magnification.

ECM is also present in normal renal tissue but undergoes qualitative and quantitative changes during renal fibrosis development. This includes increased production of collagen I and III. Fibroblasts are the main source of ECM. Fibroblasts are prototypical mesenchymal cells and the most important effector cell in fibrosis development (Zeisberg et al., 2010, Rockey et al., 2015). It has been long debated where fibroblasts contributing to renal fibrosis originate from. Fibroblasts in renal fibrosis are a heterogeneous group and arise mainly from the proliferation of resident renal fibroblasts and the infiltration of bone marrow derived cells. To a lesser extent, fibroblasts also originate by transdifferentiation from vascular endothelial cells and from TEC. It is debated if renal pericytes also contribute to fibroblasts. Upon fibrosis development, fibroblasts are activated to myofibroblasts and express alpha smooth muscle actin (α SMA) (Figure 1.9) (LeBleu et al., 2013, Mack et al., 2015).

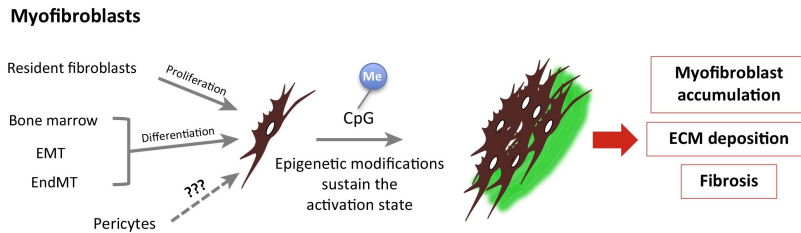



Figure 1.9: Different origins of myfibroblast and contribution to the development of renal fibrosis.  depicts myfibroblasts. Modified from (Lovisa et al., 2016) with permission.

Inflammation is already involved in the early phases of fibrosis development and comprises the infiltration of macrophages, lymphocytes, dendritic cells and mast cells. Macrophages seem to play a substantial role in renal fibrosis because of their ability to produce and secrete all possible proteins such as cytokines, matrix metalloproteinases (MMP) and growth factors. Macrophages are a heterogeneous group and display different phenotypes such as proinflammatory macrophages, which are recruited early after injury. Later in repair and eventually in the maladaptive phase and fibrosis progression, profibrotic macrophages are involved (Anders et al., 2011, Lovisa et al., 2016). Lymphocytes, especially CD4⁺ T-cells seem to be crucial players in the development of renal fibrosis: CD4⁺ T-cell depletion and mice without CD4⁺ T-cells had significantly less fibrosis development in murine renal fibrosis models than their wild type counterparts (Tapmeier et al., 2010). Dendritic cells are proinflammatory and act as antigen presenting cells (APC). Degranulation of mast cells is both proinflammatory and profibrotic (Lovisa et al., 2015).

In the context of renal fibrosis development, **TEC** display multiple responses to renal injury: This includes a shift of TEC towards a profibrotic phenotype, loss of function, tubular atrophy and inflammation. TEC are thus not only victims of injury but actively contribute to fibrosis development. The shift from normal TEC to a profibrotic phenotype is characterized, among other changes, by increased exhibition of mesenchymal features and is called **partial EMT** (described later in the text). TEC are then enabled to produce profibrotic cytokines such as TGF β , PDGF, CTGF, VEGF and WNT, but also chemokines such as the CC chemokine ligand (CCL) subfamily and proinflammatory cytokines, thus contributing to monocyte recruitment and inflammation (Liu et al., 2018).

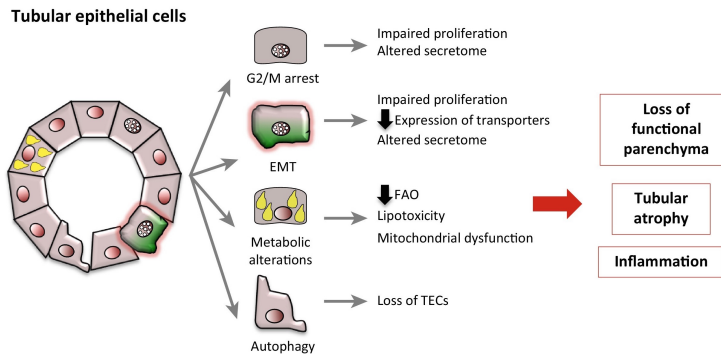


Figure 1.10: TEC and their modifications and contribution to the development of renal fibrosis. Modified from (Lovisa et al., 2016) with permission.

TEC also experience cell-cycle arrest, stop to proliferate and remain in the G2/M-phase (Lovisa et al., 2016, Liu et al., 2018). Furthermore, TEC undergo metabolic changes: In physiological states, the TEC metabolism consists of oxidation of fatty acids. In renal fibrosis tissues, a reduction in fatty acid oxidation but an increase in lipid deposition in TEC has been described. Lipid depositions and lipotoxicity lead to cell dysfunction and also contribute to a profibrotic phenotype of TEC (Kang et al., 2015, Lovisa et al., 2016). Autophagy is described as being both a response to injury potentially leading to recovery, but also a factor contributing to fibrosis development. Increased autophagy induces senescence in TEC, which predisposes them to maladaptive and profibrotic processes (Figure 1.10) (Baisantray et al., 2016, Lovisa et al., 2016, Liu et al., 2018).

Endothelial cells influence renal fibrosis development by increasing permeability, the rarefaction of capillaries and the generation of fibroblasts. Loss of cell-to-cell connections leads to increased permeability where macromolecules diffuse into the interstitium. This promotes inflammation and profibrotic changes. Loss of endothelial cells and endothelial cell integrity, as well as insufficient reparative mechanisms, contribute to the rarefaction of the microvasculature. This leads to an ischemic environment driving fibrosis development (Horbelt et al., 2007, Lovisa et al., 2016). Endothelial cells can also transdifferentiate into fibroblasts. This process is called endothelial-to-mesenchymal transition (EndMT) and it is thought that around 10% of the

fibroblasts in renal fibrosis derive from EndMT (LeBleu et al., 2013, Lovisa et al., 2016).

Tissue proteases, especially MMPs and the plasminogen-plasmin pathway, are other key players in renal fibrosis development. MMPs, especially MMP2 and MMP9, are produced by TEC and macrophages and are increasingly expressed upon TGF β activation. MMPs are able to degrade ECM, which seems paradox. However, they also release and activate profibrotic cytokines such as TGF β from the interstitium and thus the profibrotic effect outweighs in maladaptive repair conditions. MMP14, induced by SNAIL, activates MMP2 and MMP9 and is therefore also profibrotic. Plasminogen activator inhibitor 1 (PAI1) inhibits both tissue-type and urokinase-type plasminogen activators (tPA and uPA), which activate inactive plasminogen into plasmin and degrade ECM. PAI1 thus reduces ECM degradation, but is also involved in the activation of MMPs (Ma et al., 2009, Zeisberg et al., 2010, Ghosh et al., 2012, Zhao et al., 2013, Genovese et al., 2014).

Renal fibrosis is a dynamic disease and its development can be divided into 4 phases: 1) Injury phase and activation of TEC; 2) Recruitment and activation of fibroblasts with profibrotic cytokine release; 3) Fibrogenic phase with accumulation of ECM, and 4) progression of renal fibrosis and destruction of the renal architecture (Genovese et al., 2014, Rockey et al., 2015). The injury phase is characterized by the activation of repair mechanisms. But why do physiological repair mechanisms and regeneration after injury turn into maladaptive repair and fibrosis generation? One case may be when a persistent injury is sustained, such as hypertensive state, insufficiently treated diabetes or glomerulonephritis. Relapsing tubular injury such as ischemia can also promote fibrosis development. Ageing and previous injury leads to senescence of TEC and increased susceptibility to injury. Furthermore, epigenetic changes such as methylation or histone modifications of genes have been identified as possible reasons for the sustained activation of myofibroblasts and the progression of renal fibrosis (Figure 1.9). Kidney injury molecule 1 (KIM1) is increasingly expressed after injury and a chronically increased expression is associated with fibrosis progression. Finally, recruitment of myofibroblasts, inflammatory cells and, as described previously, the shift of tubular cells towards a profibrotic

phenotype, atrophy and microvascular rarefaction, drive further maladaptive repair and renal fibrosis development (Ferenbach et al., 2015, Lovisa et al., 2016).

1.5 Epithelial-to-mesenchymal transition

1.5.1 Definition and occurrence in physiology and disease

Epithelial integrity and suppression of plasticity is crucial to preserving the architecture and homeostasis of healthy tissue (Grande et al., 2015, Nieto et al., 2016). For over a century, epithelia were considered to be stable. This was proven otherwise when it became apparent that epithelial cells changed polarity and their appearance and began to migrate under the influence of growth factors in an in vitro experiment (Greenburg et al., 1982). This phenomenon was then called epithelial-mesenchymal transformation and later EMT. EMT is a cell plasticity mechanism involved in physiological processes such as embryogenesis and tissue regeneration. However EMT is also involved in the development of organ fibrosis and cancer progression (Carew et al., 2012). The classical definition of EMT is that epithelial cells lose their epithelial properties and convert into mesenchymal cells. This includes the disaggregation of epithelial units, which, in physiological states, rely on cell-cell adhesion, cell polarity and the close contact to the basement membrane. During EMT, epithelial cells acquire a mesenchymal phenotype. This includes the ability to migrate, invade tissue and produce ECM (Kalluri et al., 2009, Carew et al., 2012). In 2008, three types of EMT were described, depending on their functional result. These are summarized below (Figure 1.11).

Type I EMT happens during embryogenesis. Here EMT is a crucial process involved in implantation, where cells acquire invasive properties; during gastrulation, where the epithelial epiblast layer forms the mesoderm; and in the development of migrating neural crest cells from the neuroectoderm (Kalluri et al., 2009, Carew et al., 2012, Nieto et al., 2016).

Type II EMT occurs in the context of injury and inflammation and includes beneficial repair mechanism, in the case of wound healing, but also maladaptive and excessive repair mechanisms, in the case of the organ fibrosis development. After damage of e.g. the skin, inflammatory infiltrates with neutrophils and

macrophages trigger epithelial cells from the border of the wound to initiate re-epithelialization. Epithelial cells thus undergo EMT, detach from the basement membrane, migrate into the injured area and rebuild the epithelium, with the help of recruited myofibroblasts replacing the missing extracellular substance (Shaw et al., 2016, Nieto et al., 2016). In the case of organ fibrosis, persistent injury and inflammation induces a shift of epithelial cells to a mesenchymal phenotype or even to fibroblasts, which produce ECM and promote scarring of the tissue. This eventually destroys the organ architecture (Kalluri et al., 2009, Carew et al., 2012).

Type III EMT occurs in the development of cancers when cancerous epithelial cells transition to metastatic cells. This also includes the detachment from the cancerous epithelium and new functions gained, such as a migratory and invasive capacity. Tumors originating from epithelial tissues account for nearly 90% of all cancer types (Figure 1.11) (Carew et al., 2012, Nieto et al., 2016).

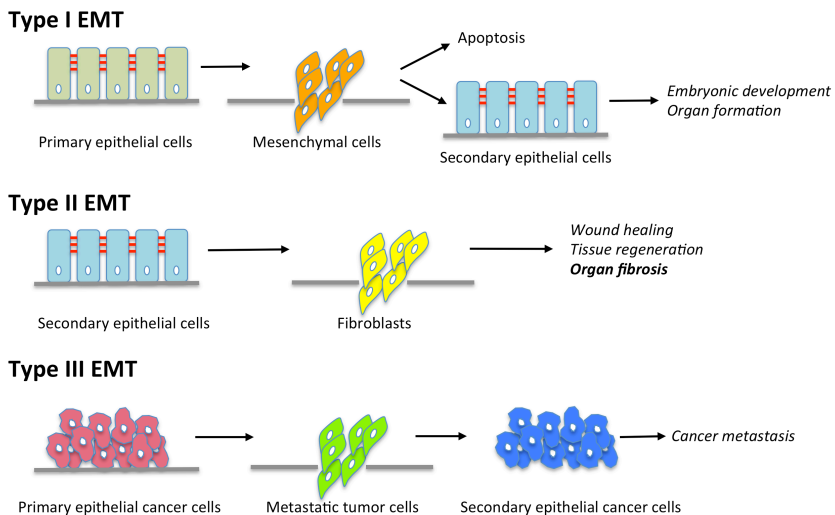


Figure 1.11: Different types of EMT according to its consequences in physiological states and diseases. Adapted from (Carew et al., 2012) with permission.

The reverse mechanism, named mesenchymal-to-epithelial transition (MET) occurs in the early development of the renal structures: Both glomeruli and TEC arise from the mesoderm via MET. The renal epithelium thus originates from mesenchymal tissue. It is postulated that this might render renal epithelial cells more prone to EMT at a later stage (Kalluri et al., 2009). In the case of wound

repair, the cells from the border of the wound undergo EMT but revert to epithelial cells to assure the epithelial integrity of the re-epithelialized tissue. MET is also thought to be involved in metastasis formation, as discussed later (Yao et al., 2011, Nieto et al., 2016).

It is suggested that EMT is not only a bidirectional dynamic process but that intermediate states also exist in EMT mechanisms supporting both organ fibrosis and cancer progression. Tissues or cells in these transitional states are thought to exhibit both epithelial and mesenchymal markers and might consequently transform back towards an epithelial phenotype or to an even more mesenchymal phenotype. The intermediate states are also described as partial EMT. This highlights the plasticity of cells undergoing EMT (Nieto et al., 2016).

Chronic inflammation and hypoxia are described as two common triggers of EMT in both fibrosis development and cancer progression (Lopez-Novoa et al., 2009). Inflammation as a consequence of injury, infection or autoimmunity, leads to the release of proinflammatory cytokines and also TGF β , which induces EMT. Hypoxia and HIF have also been described as profibrotic factors in renal fibrosis. Hypoxia through microvascular rarefaction in renal fibrosis and VHL alteration lead to increased expression and activation of HIF. HIF can act synergistically with TGF β and promote collagen production, EMT and inflammation (Haase, 2006, Lopez-Novoa et al., 2009).

1.5.2 Molecular pathways involved in EMT

The most important transcription factors involved in EMT are SNAIL, TWIST, basic helix-loop-helix (bHLH), and zinc-finger E-box binding protein (ZEB) (Figure 1.12). All these transcription factors suppress the expression of epithelial proteins, especially E-cadherin (CDH1), and induce expression of proteins associated with mesenchymal phenotypes such as vimentin (VIM), fibronectin, N-cadherin (CDH2), MMP2 and MMP9, by binding the E-box DNA through their zinc-finger domains. SNAIL (also known as SNAI1) and SNAI2 (also known as SLUG) are central in the activation of EMT in embryogenesis and disease. TGF β triggers the expression of SNAIL, the WNT family, NOTCH1, nuclear factor κ B (NF κ B) and other proteins. Posttranslational phosphorylation by different kinases (e.g. or PKD1) can either enhance or trigger its degradation. WNT and

AKT inhibit phosphorylation of SNAIL by GSK3 β , which increases SNAIL stability. SNAIL also induces the expression of TWIST and ZEB. **bHLH** proteins are transcription factors that function as regulators for different proteins including **TWIST**. **MAPK** phosphorylates TWIST and stabilizes and protects it from degradation. The expression of TWIST is induced by SNAIL, but also through hypoxia and HIF1 α , among other factors. In the case of cancer, TWIST can increase the expression of mesenchymal proteins and repress epithelial proteins independently of SNAIL. SNAIL directly activates the expression of **ZEB**. TGF β and the WNT protein family induce ZEB1 and ZEB2 expression. After translation, ZEB is regulated by sumoylation: The polycomb repressive complex (PRC2) adds small ubiquitin-like modifiers (sumo), which leads to ZEB2 being transported out of the nucleus and reduces its activity (Kalluri et al., 2009, Lamouille et al., 2014, Nieto et al., 2016).

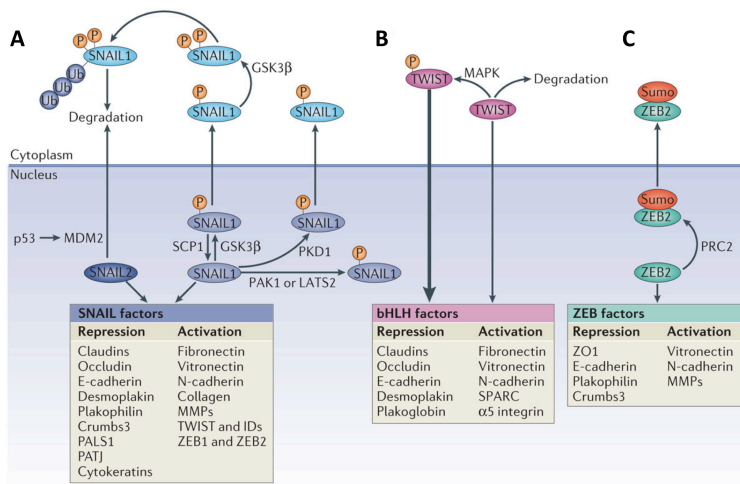


Figure 1.12: Major EMT transcription factors SNAIL (A), TWIST with bHLH (B) and ZEB (C), their signaling pathway and roles on repression of epithelial proteins and activation of mesenchymal proteins. Adapted from (Lamouille et al., 2014) with permission.

All these main transcription factors are regulated by various microRNA (miRNA). MiR200, for example, represses ZEB whereas miR34 represses SNAIL (Lamouille et al., 2014, Nieto et al., 2016). Markers of epithelial tissues are typically CDH1, cytokeratin, ZO-1, laminin-1 and collagen IV. Typical mesenchymal markers are VIM, CDH2 and α SMA (Kalluri et al., 2009, Nieto et al., 2016). Triggers of EMT are

TGF β in particular, but also fibroblast growth factor (FGF), epidermal growth factor (EGF) and platelet derived growth factor (PDGF) (Kalluri et al., 2009).

1.5.3 TGF β signaling pathway

The TGF β signaling pathway is substantially involved in both fibrosis and cancer development and TGF β is a strong inducer of EMT. In normal tissue, TGF β is crucial for tissue homeostasis and even has a tumor suppressive effect by e.g. inducing apoptosis, promoting differentiation or suppressing inflammation. The complex interaction of proteins involved in the TGF β pathways and the pleiotropic effects of TGF β enable tissues in dysregulated states to use TGF β to drive profibrotic states and to favor cancerogenesis. The effects of TGF β are thus dependent on the context of the tissues and cells involved (Massague, 2008, Meng et al., 2016). TGF β drives fibrosis development by activating fibroblasts to produce ECM, by reducing degradation of ECM, by inducing cell apoptosis and by promoting EMT. After translation, TGF β is kept latent in the interstitium. MMP2 and MMP9 activate TGF β by cleavage and release TGF β from the complex of binding proteins. The canonical pathway of TGF β includes the activation of SMAD2/3 via the TGF β receptor 1. SMAD4 then binds to SMAD2/3 and together they act as transcription factors - for example by inducing the expression of SNAIL. SMAD7, induced by SMAD3, is an inhibitor of the canonical pathway of TGF β and therefore anti-fibrotic. SMAD1 and 5 also are negative regulators by inhibiting SMAD3 induced transcription. In physiological states, SMAD2/3 and SMAD7 are in equilibrium but in the context of fibrosis and cancer development, SMAD7 is increasingly degraded by SMAD3 ubiquitin regulatory factor 2 (SMURF2). Bone morphogenic protein 7 (BMP7) is another anti-fibrotic factor, which activates SMAD1/5 and therefore reduces SMAD3 driven transcription and fibrosis development (Lamouille et al., 2014, Meng et al., 2016).

Non-canonical pathways of TGF β act via phosphatidylinositol 3-kinase (PI3K) and AKT and also via rho-like GTPase signaling pathways. Activation of AKT leads to a reduced degradation and activation of SNAIL and thus triggers EMT (Lovisa et al., 2016, Meng et al., 2016).

1.5.4 EMT in cancer

EMT is suggested to be involved in cancer progression, namely in invasion, metastasis formation, cancer stem cell development and therapy resistance.

EMT in cancer has been shown to occur particularly at the "invasive" front of the primary tumor. This might be triggered through the interaction of tumor cells with the surrounding microenvironment, consisting of inflammatory cells, cancer associated myofibroblasts and tumor associated macrophages. It is therefore thought that cancer cells at the invasive front of the tumor undergo EMT, which enables them to invade into the blood vessels and circulate (Nieto et al., 2016, Brabletz et al., 2017). Circulating tumor cells (CTC) are thought to be in an intermediate state between the epithelium and mesenchyme and express both epithelial and mesenchymal markers. CTC in clusters have been seen to metastasize more often than single cancer cells. In fact, CTC clusters express plakoglobin, a protein promoting desmosome and cell-to-cell connection. This further reflects the intermediate state of CTC displaying both epithelial and mesenchymal characteristics (Aceto et al., 2014). In contrast to the CTC, metastatic colonies have epithelial configurations, even though their origin can be traced back to the primary tumor. It is therefore suggested that circulating cells in intermediate EMT states undergo MET to enable metastatic colony formation (Yao et al., 2011, Nieto et al., 2016).

Cancer stem cells (CSC) are small subpopulations of tumor cells and contribute to cancer initiation, recurrence, metastasis and therapy resistance. Therapy resistance is thought to be due to the relatively low proliferation activity of CSC and also antiapoptotic and efficient mechanisms for DNA repair. EMT has been described as one mechanism leading to "stemness" of cancers and to CSC during tumor development. "Stemness" describes cell characteristics similar to stem cells, such as the ability of self-reproduction ("renewal") and differentiation. In particular SNAIL and ZEB have been seen to induce stemness in cancer cells (Nieto et al., 2016, Lathia et al., 2017).

Besides CSC as a reason for cancer therapy resistance, cells with a mesenchymal phenotype are generally less chemosensitive than cells with an epithelial phenotype. CTC with a more mesenchymal phenotype were less depleted by chemotherapeutics in pancreatic and breast cancer, compared to CTC with a

more epithelial phenotype. In the case of pancreatic cancer, EMT with an increased expression of SNAIL and ZEB did augment the expression of drug transporter and concentrating proteins and therefore contributed to resistance to gemcitabine (Zheng et al., 2015).

An EMT score quantifying EMT genes by their gene expression profile, can rank the EMT states of tissue samples but is not able to diagnose cancer. This is substantially due to tumor heterogeneity, as each cancer type can display a vast range of EMT "grades" on the spectrum of this EMT score. In the case of ovarian and colorectal cancer, a high "mesenchymal" EMT score correlates to lower DFS. However the EMT score cannot reliably predict the cancer's response to therapy (Tan et al., 2014).

1.5.4.1 EMT in renal cell cancer

In the context of ccRCC, EMT is, as described earlier, involved in invasion, metastasis formation, CSC development and therapy resistance. VHL mutations and accumulation of HIF in RCC have been shown to induce EMT with down-regulation of CDH1 and accumulation of ECM (Pantuck et al., 2010, Kaelin, 2018). MiR21, which is up-regulated in ccRCC, has an oncogenic effect on ccRCC development by promoting EMT, and thus also CSC (Cao et al., 2016). Increased cytoplasmic expression of TWIST and ZEB have been associated with more aggressive ccRCC and reduced survival rates compared to ccRCC with less TWIST or ZEB expression (Fang et al., 2013, Rasti et al., 2017). The expression of EMT markers in ccRCC is very heterogeneous. In high stage ccRCC, heterogeneity is even more pronounced than in lower stage ccRCC (Guarch et al., 2018).

VEGF targeted therapies have been the cornerstone of ccRCC therapy, but resistance is acquired in most of the patients. This is due to changes in the tumor and the tumor environment that leads to cancer progression that is less dependent on VEGF. A possible reason is the compensatory up-regulation of alternative pathways such as PI3K/AKT, and the increased production of other proangiogenic factors (Rini et al., 2009, Zhou et al., 2016). The role of AXL in resistance and EMT in renal cell cancer is discussed later in the text.

1.5.5 EMT in organ fibrosis

Organ fibrosis occurs as a consequence of disease and sustained injury in many tissues such as the heart, lungs, liver, skin, intestines and kidneys. All types of solid organ fibrosis have an analogue common pathway and course which involves the injury phase, the recruitment and activation of inflammatory cells and myofibroblasts, the production of ECM, and finally fibrosis progression, damage of the organ architecture and reduction of organ function (Genovese et al., 2014, Rockey et al., 2015).

In the case of the heart, it has been shown, that, after myocardial infarction, epicardial epithelial cells undergo EMT and promote tissue repair through the recruitment of fibroblasts and stem cells, an increase in cardiomyocyte proliferation and neovascularisation. This repair mechanism is initially necessary to protect the myocardial wall from rupture, but leads over time to the excessive production of ECM and fibrosis. This remodeling is due to the continuous strain, proinflammatory and profibrotic cytokines and also insufficient blood supply due to inadequate neovascularization. Remodeling leads over time to ventricular dysfunction. There are experimental attempts to enhance EMT in the post-myocardial infarction phase to increase the initially favorable tissue repair mechanisms (Blom et al., 2018).

EMT has been investigated and suggested to play a role also in pulmonary fibrosis development: Alveolar epithelial cells that are observed to express both epithelial and mesenchymal markers and up-regulated SNAIL and TWIST genes. Alveolar epithelial cells in the context of pulmonary fibrosis secrete profibrotic cytokines such as TGF β , and trigger the development, proliferation and activation of myofibroblasts from different sources (King et al., 2011, Richeldi et al., 2017).

In the liver, EMT also contributes to fibrosis development and is triggered through inflammation due to chronic hepatitis. TGF β and the EMT program give rise to hepatic myofibroblasts from different sources, such as hepatic stellate cells and bone marrow cells. Similar to pulmonary fibrosis, hepatic cells tend to display an intermediate EMT state and express both epithelial and mesenchymal markers (Zhao et al., 2016).

1.5.5.1 EMT in renal fibrosis

Originally, it was thought that injury activated EMT, which led TEC to disaggregate from the basement membrane and leave the tubular structure to fully become myofibroblasts, thereby contributing to fibrosis by the production of ECM. But when tracing the origin of myofibroblasts, only around 5% of myofibroblasts were found to develop directly from TEC through "complete" EMT (Figure 1.9). Recently, the notion of "partial EMT" has been suggested: In this case, also as a response to injury, TEC undergo changes, which lead to a shift in their proliferative activity, altered function and a modified expression profile. TEC undergo a G2 cell-cycle arrest, which reduces the repair and proliferation capacity of the cells. TEC also have a reduced function whereby less protein involved in secretion and absorption is expressed. The expression of profibrotic and proinflammatory cytokines is increased, which leads to recruitment and activation of fibroblasts and immune cells (Figure 1.10). Partial EMT was observed in 2015 in two studies, where both SNAIL and TWIST, thus crucial transcription factors involved in EMT, were silenced in TEC. This substantially reduced fibrosis development in murine fibrosis models. However TEC did not detach from the basement membrane or migrate, but remained within the epithelium and expressed both epithelial and mesenchymal markers (Figure 1.13) (Lovisa et al., 2015, Grande et al., 2015, Lovisa et al., 2016).

EMT markers such as α SMA, MMP9 and fibronectin, measured both in the kidney tissues and in the urine, have been associated with kidney diseases such as diabetic nephropathy (Rastaldi et al., 2002, Zheng et al., 2012). EMT is also described in renal transplant nephropathy, in both acute rejection and also in chronic allograft nephropathy (Wang et al., 2018). EMT markers in renal transplants have been associated with renal graft survival prognosis, and measurements of urinary VIM correlate with histological fibrosis extent in renal allografts (Hertig et al., 2006, Xu-Dubois et al., 2014, Mezni et al., 2018).

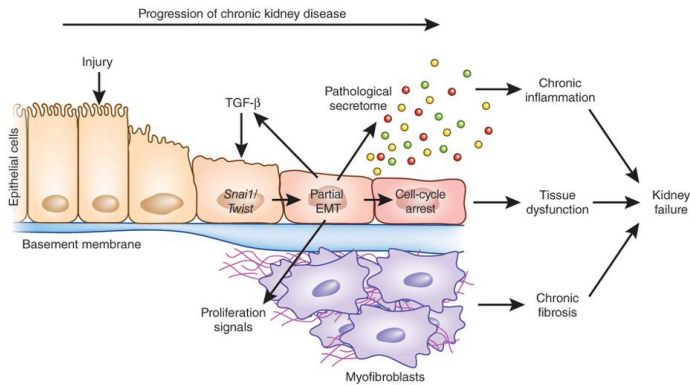


Figure 1.13: Progression of CKD with induction of SNAIL and TWIST expression in TEC as a response to injury and TGF β . TEC undergo cell cycle arrest and have increased expression of profibrotic and proinflammatory cytokines, which leads to tissue dysfunction, fibrosis development, inflammation and finally kidney failure. From (Ovadya et al., 2015) with permission.

1.5.6 Targeting EMT

The signaling pathways of TGF β and their interaction with other pathways are complex and the functions of TGF β are diverse, as previously discussed. TGF β can promote both anti-inflammatory states, which can be favorable in the case of injury, but acts also in a profibrotic manner and favors cancerogenesis. Blocking of the TGF β type II receptor (T β RII) - the receptor responsible for the profibrotic function of TGF β - did not show reduced fibrosis development in murine renal fibrosis models. TGF β inhibition is thus not enough to stop fibrosis development (Neelisetty et al., 2015). Deletion of T β RII during the development of mice even led to an increased fibrosis development after the induction of fibrosis by ureteral obstruction. It is thought that this was a consequence of compensatory increased TGF β expression and activation of the alternate TGF β pathways, for example of Rho (Gewin et al., 2010, Kopp, 2010). In 2014, a phase I clinical study was stopped after failing to show any effect of a TGF β blocker in reducing the progression of diabetic nephropathy (ClinicalTrials.gov, 2014).

Another approach has been to increase SMAD7 expression but decrease SMAD3, and thus decrease the activity of the canonical TGF β pathway. This was seen to be promising and reduced fibrosis development in a murine renal fibrosis model (Meng et al., 2015). BMP7, which reduces SMAD3 driven transcription by activation of SMAD1/5, has also been investigated as a component to inhibit

EMT. BMP7 counteracts EMT and reduces fibrosis development in different murine renal fibrosis models, such as ureteral obstruction and nephrotoxic serum nephritis (Hruska et al., 2000, Zeisberg et al., 2003, Meng et al., 2013, Boor et al., 2015). However, in an in vitro model, where TEC lines were exposed to TGF β and BMP7, BMP7 failed to reduce expression of EMT markers compared to exposure of cells to TGF β alone (Dudas et al., 2009).

1.6 AXL receptor tyrosine kinase

1.6.1 Structure and signaling pathway

AXL (from ancient Greek "ἄκλιτος", meaning uncontrolled) was first isolated in 1988 and first described in 1991 in patients with chronic myeloid leukemia (Liu et al., 1988, O'Bryan et al., 1991, Janssen et al., 1991). AXL, also known as ark, UFO, tyro7 and JTK11, is a transmembrane RTK and belongs to the TAM RTK family together with TYRO3 and MER (also called MERTK) (Korshunov, 2012). In 1995, growth arrest-specific protein 6 (GAS6) was detected to be the sole ligand to AXL, whereas protein S also binds to TYRO3 and MER (Stitt et al., 1995, Korshunov, 2012). Both GAS6 and protein S have vitamin K dependent gamma-carboxylated glutamic acid residues in the N-terminal GLA domain. GAS6 binding to AXL leads to receptor dimerization that requires GLA domain interaction with phosphatidylserine (PtdSer). AXL may also be activated independently of GAS6, for example by the dimerization of AXL receptors in the context of high AXL expression or heterodimerization with other RTK. GAS6 independent receptor activation may be more common in the context of disease (Korshunov, 2012, Meyer et al., 2015, Gay et al., 2017).

Upon receptor activation, tyrosine residues on the cytoplasmic domain of the receptor are phosphorylated and activate several signaling pathways such as PI3K/AKT and GRB2/MAPK/ERK. PI3/AKT promotes cell survival and the MAPK/ERK pathway increases cell proliferation. AXL signaling is associated with EMT through TWIST and SNAIL, cell migration via p38, and MMP9 invasion through the degradation of ECM, such as basement membranes. AXL also activates the suppressor of cytokine signaling 1 and 3 (SOCS1/3) in myeloid cells, which reduces the immune reaction through different mechanisms, as discussed later (Figure 1.14) (Korshunov, 2012, Gay et al., 2017).

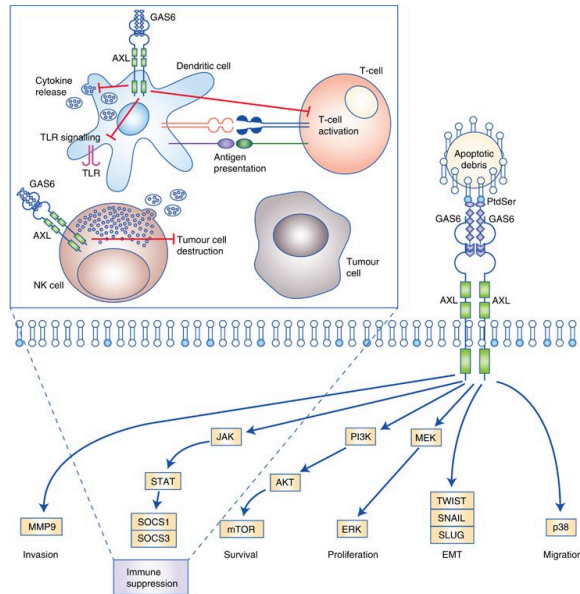


Figure 1.14: Molecular signaling pathway of the AXL receptor and resulting processes. The pathway via STAT and SOCS1/3 expression leads to immunosuppression through different mechanisms such as the increased clearance of apoptotic material (efferocytosis), tissue repair, the reduction of Toll-like receptor (TLR) signaling and cytokine production in dendritic cells and reduced activation of T-cells and natural killer cells. From (Gay et al., 2017) with permission.

1.6.2 AXL in physiology

Under physiological conditions, the TAM family is involved in tissue repair and regulates innate immunity through different mechanisms:

A) After apoptosis, cells externalize PtdSer that activate AXL/MER receptors on macrophages. This leads to efferocytosis that clears apoptotic material and promotes tissue repair (Graham et al., 2014, Gay et al., 2017). B) AXL also reduces Toll-like receptor (TLR) dependent inflammatory signaling: Activation of TLR on APC, such as dendritic cells, induces STAT1 up-regulation, which increases AXL expression and SOCS1/3 signaling and thus decreases inflammatory response and cytokine production mediated by TLR. C) Further, activated T-cells switch PtdSer to the extracellular portion of the cells, leading to the activation of AXL/MER on APC and the reduction of T-cell activation and expression of proinflammatory cytokines. D) AXL/MER also decrease the activity of natural killer cells. E) Finally, particularly MER inhibits proinflammatory macrophages but triggers profibrotic macrophages to produce profibrotic

cytokines such as TGF β , which promotes tissue repair. In physiology, AXL and MER thus reduce the immune response and promote repair (Figure 1.14) (Graham et al., 2014, Gay et al., 2017).

Under normal physiological conditions, AXL is expressed in myeloid cells, such as dendritic cells, in various tissues and in microglia and astrocytes in the brain. In normal renal tissues, AXL is not or very low expressed (Fiebeler et al., 2004, Meertens et al., 2017, Gay et al., 2017).

Viral diseases exploit the immunosuppressive capacity of TAM RTK, especially AXL. It is suggested that AXL is involved in the entry of the Zika virus in glia cells and promoting Zika-associated encephalitis and also microcephaly. Zika is shown to specifically activate AXL on dendritic cells to antagonize the anti-viral interferon response (Meertens et al., 2017, Chen et al., 2018). Further, AXL has been associated with the Dengue, West Nile and Ebola viruses, working as an entry-receptor. In chronic hepatitis C, increased expression of AXL is also associated with the reduced antiviral response of hepatocytes to interferon alpha signaling (Read et al., 2015, Gay et al., 2017).

The abrogation of the TAM family of kinases, especially AXL, leads to increased inflammation and autoimmunity (Korshunov, 2012, Graham et al., 2014, Gay et al., 2017). Depletion of AXL/MER led to increased expression of proinflammatory cytokines and also to increased risk for inflammation-associated colon cancer in an experimental colitis model in mice (Bosurgi et al., 2013, Akalu et al., 2017).

1.6.3 AXL and EMT

AXL is closely associated with EMT mechanisms: The EMT program induces the expression of AXL, in particular by the up-regulation of SNAIL, TWIST and ZEB (Gjerdrum et al., 2010, Schoumacher et al., 2017). In addition, AXL leads to the increased expression of EMT-associated transcription factors SNAIL and TWIST, which produces a positive feedback loop. AXL is thus both a downstream effector of EMT but also promotes EMT. In the case of EMT related therapy resistant cancer, AXL targeting reverses drug resistance, pointing towards the up-regulation of AXL and related pathways as a crucial mechanism in EMT related resistance to therapy (Schoumacher et al., 2017). On the expression level, high

scores of EMT markers have consistently been associated with increased AXL expression across a variety of cancers (Mak et al., 2016).

1.6.4 AXL in cancer

The up-regulation of AXL is associated with cancer aggressiveness and resistance. AXL promotes cancer aggressiveness by driving tumor growth, migration and metastasis, and by dampening the anti-tumor immune reaction. Tumor growth is nurtured by increased cell survival signaling, through the suppression of anti-apoptotic factors, and also angiogenesis. AXL facilitates invasion, migration and potential metastasis of tumor cells through the enhancement of EMT signaling, but also through the direct activation of e.g. MMP9, and the regulation of adhesion proteins. The suppression of the innate immune system by AXL promotes the immune evasion of cancer cells (Graham et al., 2014, Gay et al., 2017, Akalu et al., 2017, Davidsen et al., 2017).

Increased expression of AXL has been observed in a wide variety of solid cancers in association with EMT gene expression patterns - and correlating with poor prognosis (Gjerdrum et al., 2010, Mak et al., 2016, Schoumacher et al., 2017). AXL has also been seen to be involved in hematologic malignancies, such as acute myeloid leukemia (AML). More than 50% of AML patients show up-regulation of AXL, which is associated with an increased proliferation and survival of cancer cells and greater resistance to treatment by e.g. doxorubicin and cytarabine. Additionally, AML cells trigger stromal cells of the bone marrow to produce GAS6, which activates the up-regulated AXL on the AML cells. Small molecule inhibition of AXL kinase activity leads to reduced proliferation and increased apoptosis of AML cells (Ben-Batalla et al., 2013, Janning et al., 2015).

AXL is involved in cancer chemotherapeutic resistance through both intrinsic and acquired mechanisms. Together with MER, AXL promotes survival and has been shown to therefore enhance the resistance of tumor cells to chemotherapeutics upon increased expressions. This is also due to further activation of EMT, the development of CSC, the maintenance of a mesenchymal phenotype of tumor cells (making tumor cells less chemosensitive) and immune evasion mechanisms. AXL has also been seen to be up-regulated in cancers resistant to RTK inhibitors - such as Imatinib in chronic myeloid leukemia, EGFR

inhibitors (e.g. Lapatinib, Erlotinib) in breast cancer and non-small cell lung cancer, and VEGF targeted therapies in cancers such as RCC (discussed later) (Graham et al., 2014). The blocking of AXL leads to a reduced resistance and improves the effect of standard chemotherapy in different experimental cancer studies such as pancreatic cancer, ovarian, breast cancer, and non-small cell lung cancers (Kariolis et al., 2017, Zhang et al., 2018, Yule et al., 2018). Also in the context of resistance to immunotherapy agents, such as checkpoint inhibitors, AXL is thought to play a role: AXL, and other EMT related genes, were more up-regulated in melanoma samples of patients resistant to PD1 inhibitor compared to patients responding to immunotherapy. Further, inhibition of AXL combined with immune checkpoint inhibitors has shown to increase inflammation with cytotoxic T-cells in experimental lung and breast cancer models, thus enforcing the anti-tumor response by checkpoint inhibitors (Wnuk-Lipinska et al., 2017). It is thus suggested, that blocking of AXL may increase the efficacy of the treatment with checkpoint inhibitors (Hugo et al., 2016, Gay et al., 2017, Akalu et al., 2017).

1.6.4.1 AXL in renal cell cancer

AXL is known to be up-regulated in ccRCC, especially in those cells lacking VHL and to have oncogenic properties (Gustafsson et al., 2009a). Levels of AXL up-regulation are associated with clinical conditions such as advanced tumor stage, invasion of the capsule, but also with paraneoplastic signs such as low hemoglobin, albumin, increased erythrocyte sedimentation rate or C-reactive protein. In addition, the expression of AXL in ccRCC tissue has been seen to independently predict survival of patients. Interestingly, increased expression of GAS6 but low AXL was associated with the best survival. This implies that the GAS6/AXL interaction is complex and might differ between different cancer types (Gustafsson et al., 2009b). In 2015, it was seen that inhibition of AXL leads to the reduced activation of the AKT/PI3 pathway, increased apoptosis and reduced tumor growth in a murine xenograft model. AXL was then postulated to be a potential target in ccRCC treatment (Yu et al., 2015).

Therapy with the VEGFR inhibitor Sunitinib increases the expression of AXL and MET and leads to Sunitinib resistance. Accordingly, treatment of ccRCC with Cabozantinib (a VEGFR, AXL and MET inhibitor) reduces Sunitinib resistance.

Treatment with Cabozantinib has been seen to reverse the desensitization of ccRCC cells to Sunitinib (Zhou et al., 2016, Gay et al., 2017).

1.6.5 AXL in organ fibrosis

AXL in the context of solid organ fibrosis has been investigated in particular in liver, lung and renal fibrosis. In a mouse liver fibrosis model, it was seen that GAS6 was expressed especially in Kupffer cells (specialized hepatic macrophages) but AXL more in immigrated monocytes/macrophages and hepatic stellate cells. AXL knockout mice had reduced liver fibrosis development, and the blocking of AXL through BGB324 in wild type mice led to a reduced activation of hepatic stellate cells and decreased liver fibrosis development (Barcena et al., 2015). AXL also seems to be a valuable biomarker in liver diseases: AXL in the serum was significantly higher in patients with liver fibrosis and cirrhosis and correlated with the stage of liver fibrosis (Stauffer et al., 2017). In lung fibrosis, AXL has been seen to be up-regulated in biopsy tissues of patients with idiopathic lung fibrosis. The inhibition of AXL by BGB324 was shown to lead to significantly less fibrosis development in two different mouse lung fibrosis models as measured by hydroxyproline quantification (Espindola et al., 2018). These findings imply a role of AXL targeting in the clinical setting of both liver and lung fibrosis.

1.6.5.1 AXL in renal fibrosis

AXL or GAS6 are not or very low expressed in normal renal tissue, but up-regulated in various murine renal disease models, such as a rat immunogenic mesangio-proliferative glomerulonephritis model (Yanagita et al., 2001, Fiebeler et al., 2004). Upon induction of diabetes in a rat type 1 diabetes model, expression of both AXL and GAS6 increased in renal mesangial cells and endothelial cells in particular, along with glomerular hypertrophy. Depletion of GAS6 reduced glomerular hypertrophy development, which is an early sign of diabetic nephropathy (Nagai et al., 2003). Both studies showed a reduced mesangial cell proliferation upon low-dose treatment with warfarin. This may result from inhibition of gamma-carboxylation of GAS6 and protein S (Yanagita et al., 2001, Nagai et al., 2003). In a mouse model where podocytes were depleted by targeting with diphtheria toxin, the depletion of around 20% of

podocytes led to proteinuria and to successful repair mechanisms. This was accompanied by increased levels of urinary GAS6 and increased AXL expression in TEC. AXL may thus play a role in supporting TEC proliferation (Guo et al., 2012). In a murine hypertension model, depletion of AXL in immune cells of the bone marrow led to less increase in blood pressure upon treatment with cortisone. This was accompanied by less expression of proinflammatory cytokines. In the advanced phase of cortisone-induced hypertension, AXL knockout mice had reduced vascular remodeling but increased occurrence of apoptosis. This suggested that AXL plays a role in both the initial propagation of hypertension related to inflammation and also in later stages through the remodeling of vascular cell (Batchu et al., 2013).

In a murine glomerulonephritis model using nephrotoxic serum, AXL knockout mice had reduced AKT activation, and increased survival and renal function compared to wild type mice (Zhen et al., 2016). The same author recently published a study showing that treatment with the selective small molecule AXL RTK inhibitor BGB324 also led to significantly reduced AKT activation, renal inflammation and improved renal function in an murine anti-GBM antibody induced nephritis model (Zhen et al., 2018).

In contrast, another study showed an increased development of tubulointerstitial fibrosis in AXL knockout mice compared to wild type mice in a murine renal fibrosis model that included a subtotal nephrectomy and high phosphate diet. In this study, AXL was therefore described as a protective factor in the context of fibrosis development (Hyde et al., 2014).

In human studies, AXL/GAS6 expression was demonstrated in human renal tissue biopsies of patients with IgA-nephropathy, immune-complex glomerulonephritis, lupus-nephritis, ANCA-associated glomerulonephritis and acute graft rejection (Fiebeler et al., 2004, Zhen et al., 2018). AXL/GAS6 was expressed in vessels and glomeruli but also diffusely in the renal tubules of fibrotic renal tissues. Stimulation of renal tissue with angiotensin II led to increased expression of AXL and GAS6 as well (Fiebeler et al., 2004).

All soluble TAM RTK, including AXL, can be detected in serum and urine and were significantly higher in the serum of diabetic patients with or without

proteinuria compared to healthy controls. Soluble AXL is shed into the urine, probably from TEC, in healthy and diabetic patients (Ochodnický et al., 2017).

1.6.6 AXL inhibitors

Several AXL inhibitors are being tested on the market. Most inhibit several RTK, such as Cabozantinib, which inhibits VEGFR, MET and AXL. Cabozantinib is the only AXL RTK inhibitor approved at the moment and is used for medullary thyroid cancer and metastatic ccRCC (Myers et al., 2016).

BGB324 (also known as R428 or Bemcentinib) is the first-in-class selective inhibitor of AXL RTK (Holland et al., 2010, Myers et al., 2016). BGB324 is a small molecule with a molecular weight of 506.6g/mol and is administered perorally. BGB324 is not a cytochrome P450 substrate but inhibits cytochrome P450 isoenzymes 3A4 and 2D6. BGB324 is a RTK inhibitor highly selective for AXL and is 50-100 fold more selective for AXL than TYRO3 or MER and more than 100 fold more selective for AXL than for other RTK such as EGFR and HER2. The concentration of BGB324 at which 50% of AXL RTK activity is inhibited (IC₅₀, half maximal inhibitory concentration) is 14nM (Holland et al., 2010, Graham et al., 2014). Other pharmacokinetic data (e.g. half life, bioavailability and volume distribution) are not available from publications. In comparison, Cabozantinib is around 40 fold more selective for VEGFR2 than Met and more than 200 fold more selective for VEGFR2 than for AXL RTK (Yakes et al., 2011).

BGB324 has been tested in different experimental cancer models, and has lately been shown to increase chemosensitivity to gemcitabine in a pancreatic cancer model (Ludwig et al., 2018). Another study showed that ccRCC cells exposed to Sunitinib lead to an increased expression of AXL, and that subsequent exposure of the cells to BGB324 increases susceptibility to Sunitinib (van der Mijn et al., 2016).

In the context of fibrosis, BGB324 has been seen to reduce fibrosis in a murine hepatic liver fibrosis model, ameliorate fibrotic mechanisms in idiopathic pulmonary fibrosis and improve the renal function in a murine anti-GBM antibody induced nephritis mouse model (Barcena et al., 2015, Espindola et al., 2018, Zhen et al., 2018).

BGB324 is the first selective AXL inhibitor to enter clinical trials (Sheridan, 2013). BGB324 is currently being tested in different phase 2 studies against melanoma (NCT02872259), non-small cell lung cancer (NCT02424617, NCT02922777), acute myeloid leukemia or myelodysplastic syndrome (NCT02488408), triple negative or inflammatory breast cancer (NCT03184558), pancreatic cancer (NCT03649321) and malign mesothelioma (NCT03654833) (ClinicalTrials.gov, 2018). Positive results have been reported from phase II studies of BGB324 in non-small cell lung cancer in combination with targeted and immune checkpoint inhibitors (Yule et al., 2018).

Other selective AXL inhibitors have recently entered clinical trials, e.g. DS-1205 (Jimbo et al., 2017).

1.7 Renal registries and biopsy archives

The systematic collection of data on patients with renal diseases is a valuable resource for research into epidemiology, treatment courses and outcomes of CKD and helps to evaluate patient care. In 2015, there were around 50 renal registries worldwide, comprising each more than 300 patients with ESRD and including data on renal replacement therapy and other patient characteristics, such as treatment outcomes. Most registries are in Europe. There is a lack of adequate renal registries in the most populated countries such as China, India and Russia and, to our current knowledge, no existing renal registries in Africa (Liu et al., 2015).

1.7.1 Storage methods of renal biopsy tissues

The gold standard to conserve tissue specimens for molecular research, is freezing of fresh tissues ("fresh frozen tissues") to temperatures below -80°C. However, freezing of tissues requires extensive and expensive infrastructure, which is not available everywhere. Historically and also nowadays, most tissue specimens, thus also renal biopsy tissues, are formalin-fixed and paraffin-embedded (FFPE), although formalin fixation leads to a certain degree of degradation of proteins, DNA and also RNA. FFPE is the storage method of choice because FFPE biopsy tissues can be stored at room temperature for many decades and because of good conservation of tissue morphology (von Ahlfen et al., 2007, Arreaza et al., 2016).

1.7.2 The Norwegian Renal Registry - patient and biopsy data

The Norwegian Renal Registry (NRR), previously "the Norwegian Nephrology Registry", was established in 1980. Patients with ESRD, and since 2016 also patients with CKD stage 5, are registered here based on informed consent. Upon reaching CKD stage 5 or initiation of chronic renal replacement therapy (kidney transplantation or chronic dialysis treatment), patient data, are reported annually until treatment cessation or death. By the end of 2016, data from more than 10'000 patients receiving renal replacement therapy have been collected and around 500 new patients are registered every year (Reisaeter, 2016).

The Norwegian Kidney Biopsy Registry (NKBR) was established in 1988, and registers clinical and pathological data from kidney biopsies (including biopsy scans) from native kidneys. In 2016, the NKBR was integrated into the NRR as an own section. Up to now, data from around 13'000 biopsies have been collected. Patients registered in the NRR (and thus their clinical and biopsy data) can be identified by a unique personal identification number and linked to other national registries such as the Norwegian National Cause of Death Registry or to the Norwegian Population Registry.

In comparison to Norway, Switzerland has since 2008 had the Swiss Transplant Cohort Study (STCS), where patient and biopsy data are collected systematically after transplantation. Since 2013, there is also a national renal registry for patients with ESRD - the Swiss Renal Registry and Quality Assessment Program, SRRQAP (Lu et al., 2017). Biopsies or its data are however not systematically collected. In addition, Swiss social security numbers are not directly linked to hospital admission or to the use of health care services.

The NRR has, for example, been used to study the association between preeclampsia or low birth weight and the risk of ESRD, and to estimate the risk of death in first grade relatives of ESRD patients (Vikse et al., 2008b, Vikse et al., 2008a, Skrunes et al., 2016). Renal tissues from the NKBR have for example been analyzed in the case of IgA nephropathy, where histological scores were correlated to clinical outcome (Knoop et al., 2017). Proteomic analysis has been performed on microdissected glomeruli in IgA nephropathy to study complement proteins (Paunas et al., 2017). However, RNA extraction or sequencing has not been performed on these archival biopsies before.

2 Aims of the thesis

Rationale

The rationale for this thesis was that the NRR includes more than 13'000 archival renal biopsies, which are an underused source for modern molecular analysis techniques, such as RNA sequencing, to be used for research and ultimately routine analyses.

The rationale for investigating EMT in ccRCC and renal fibrosis was that (partial) EMT plays a role in ccRCC and CKD development, and that AXL RTK may represent a target for potential new treatment strategies.

Hypotheses

Hypotheses of the studies were: 1) RNA sequencing can be performed from human FFPE renal biopsy sections and from laser-capture microdissected (LCM) glomerular cross-sections (Paper I); 2) ccRCC tissues are characterized by EMT markers and EMT related genes represent potential treatment targets (Paper II); and 3) AXL is involved in fibrosis development in murine unilateral ureteral obstruction (UUO) and inhibition of AXL by BGB324 reduces fibrosis development in UUO (Paper III).

Aims

The aims of this thesis were 1) to evaluate the best method to extract RNA from FFPE renal biopsy sections and from LCM glomerular cross-sections to enable RNA sequencing (Paper I); 2) to analyze EMT markers in FFPE ccRCC tissues and to assess their association to prognosis (Paper II); and 3) to detect AXL in murine UUO and to quantify fibrosis after inhibition of AXL by BGB324 treatment in UUO (Paper III).

3 Material and Methods

3.1 Renal tissues, storage and handling

The renal tissues used in this work were obtained from different sources summarized below (Table 4).

Paper	Renal tissue used	Origin and mode of sampling
I	Normal rat renal tissue	- Own previous animal experiment (whole kidneys)
	Normal human renal tissue	- Prospective collection of renal tissue samples adjacent to ccRCC after nephrectomy (core biopsies)
II	Normal human renal tissue	- Prospective collection of renal tissue samples adjacent to ccRCC after nephrectomy (core biopsies)
	Human ccRCC tissue	- Prospective collection of ccRCC tissues after nephrectomy (core biopsies)
III	Normal and fibrotic mouse renal tissue	- Own animal experiments (whole kidneys)
	Normal and fibrotic human renal tissue	- Norwegian Kidney Biopsy Registry of the Norwegian Renal Registry (core biopsies)

Table 4: Summary of origin and mode of sampling of renal tissues used in the articles presented in this work.

3.1.1 Rat renal tissues (paper I)

In paper I, we first tested RNA extraction methods on rat renal tissue. Tissues corresponded to normal renal tissues from male Wistar rats from an experiment previously performed by our research group (Skogstrand et al., 2013).

3.1.2 ccRCC and adjacent normal human renal tissues (paper I and II)

In paper I and II, both normal human renal and ccRCC tissues originated from patients referred to Haukeland University Hospital, either for partial or full nephrectomy due to ccRCC. From each patient, core biopsies were taken with a 16 gauge needle from both ccRCC tissue and from adjacent normal renal tissue immediately after the removal of the tumor or kidney. Renal tissue biopsies were then stored as FFPE blocks and later used for RNA and protein extraction and analysis, and for immunohistochemistry (IHC). The ethics committee of Western Norway has approved this study (REK Vest, 78/05). In paper I, only normal renal tissues from two patients who were operated in June 2015 were used. In the case

of paper II, normal renal and ccRCC tissues from 26 patients, which underwent surgery for RCC between November 2013 and September 2015 were used.

3.1.3 Murine renal tissues (paper III)

Renal tissues from mice used in paper III were from our own animal experiment, which has been approved by the Norwegian Food Safety Authority (Case number 16/116548, FOTS ID 8675 and case number 17/129461, FOTS ID 8675). The intervention (UUO) is discussed below. Upon sacrifice of the mice, renal tissues were partly stored in RNA later and frozen to -80°C and partly FFPE. RNA later stored tissues were used for RNA extraction, RNA sequencing and for the measurement of hydroxyproline content. FFPE tissues were used for IHC and fibrosis quantification using Sirius Red (SR) (see below). Male C57Bl/6J OlaHsd mice were used.

3.1.4 Human renal fibrosis tissues (paper III)

In paper III, human FFPE renal biopsy tissues with either benign nephrosclerosis or diabetic nephropathy and normal renal tissues were obtained from the Renal Biopsy Registry of the NRR. The ethics committee of Western Norway has given consent to this study (REK Vest, 2013/553). Benign nephrosclerosis corresponds to the histopathological term for "hypertensive nephropathy", which is the term typically used in the context of the clinic. Clinical information such as serum creatinine, eGFR and comorbidities were extracted from the relevant hospital charts. The inclusion criteria consisted of patients from Haukeland University Hospital with benign nephrosclerosis, type 2 diabetic patients exhibiting diabetic nephropathy, and $\text{eGFR} \geq 35 \text{ml/min/1.73m}^2$. Patients with primary renal diseases such as glomerulonephritis or systemic diseases such as Lupus erythematosus were excluded, as well as patients testing positive for ANCA antibodies. In the case of normal renal tissues, patients with hypertension or diabetes mellitus were excluded. The histopathological diagnosis of normal renal tissues corresponded to "normal tissue or slight unspecific changes" and all patients included had normal eGFR of over 60ml/min/1.73m^2 . Slides were reviewed with the renal pathologist at the pathology institute of Haukeland University Hospital.

3.1.5 Laser-capture microdissection

LCM is a method, which uses laser beams to extract specific tissue regions. In the context of paper I, we dissected glomerular cross-sections from both whole rat renal tissues sections and human renal biopsy sections. In practice, FFPE sections were deparaffinized, stained with Hematoxylin Eosin (HE) and then mounted on nuclease free membrane slides, in order to reduce RNA degradation. Glomeruli were then visualized and selected and then a guiding line was manually drawn around them. The laser then cuts the selected tissue and both membrane and glomeruli are catapulted up into an Eppendorf tube lid containing lysis buffer for the first step of RNA extraction (Figure 3.1).

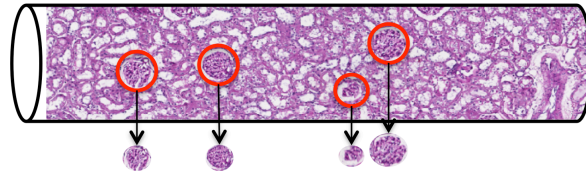


Figure 3.1: Schematic illustration of a human renal core biopsy and how the glomeruli cross-sections are identified, marked and cut out of the HE stained tissue by LCM. Author's own pictures.

3.2 RNA extraction, sequencing and transcriptome analyses

Paper I

Here, seven commercial RNA extraction kits using filter-based methods were used to extract RNA from FFPE rat whole renal sections and from LCM glomerular cross-sections. Of these seven kits, the four performing best in the context of RNA quantity were then chosen for use in extracting RNA from normal human FFPE renal biopsy sections and LCM glomerular cross-sections. RNA quantity was assessed using Nanodrop, a spectrophotometric method, and Qubit, a procedure, which uses fluorescence staining and measurement. RNA quality was assessed by calculating the percentage of RNA fragments longer than 200 base pairs (The DV200 metric), performed using a BioAnalyzer from Agilent. The RNA library from human FFPE LCM glomerular cross-sections was generated by using the TruSeq RNA Access Library Preparation kit (Illumina), and then sequencing was performed with an Illumina NS500 instrument. The RNA was not analyzed further, and only the numbers of reads per samples were used as a read-out.

Paper II

In paper II, the miRNeasy FFPE RNA extraction kit from Qiagen was used to extract RNA and miRNA from human FFPE renal biopsy sections. RNA and miRNA libraries were generated using the TruSeq RNA Access Library Preparation kit for mRNA and the TruSeq Small RNA Library Preparation kit for miRNA sequencing (both from Illumina). Sequencing was performed with an Illumina HiSeq2500 instrument. Reads were then aligned to the GRCh38 human reference genome. Sequencing data were published on Gene Expression Omnibus as GSE76207 and GSE82122. To analyze our transcriptomic data, a set of EMT genes from two different studies and one gene database were merged. The studies included 43 (Chen et al., 2014) and 131 (Groger et al., 2012) EMT genes. The EMT gene database contained 377 genes (Zhao et al., 2015), however we removed 20 included EMT related miRNA from this list. Merging the lists and adding the genes GAS6 and ZEB1, resulted in 483 EMT genes of interest. The 137 genes found to be differentially regulated genes underwent unsupervised hierarchical cluster analysis, principal component analyses (PCA) and regression analysis of both mRNA expression levels and tumor stages. 468 ccRCC samples with mRNA sequencing and 217 ccRCC samples with miRNA sequencing from a patient cohort of the Cancer Genome Atlas (TCGA) were used to perform survival analyses using the selected genes of interest. Later, a linear discriminant analysis based on a previously published metzincins and related genes (MARGS) panel was applied to study the association of our samples with known fibrosis classifier genes (Rodder et al., 2009, Rodder et al., 2011). In addition, an EMT score was applied to the RNA sequencing data. The EMT score uses a particular common EMT gene expression signature and grades EMT states in a continuous spectrum between mesenchymal (+1) and epithelial (-1) (Tan et al., 2014).

Paper III

Mouse renal tissues: In paper III, the RNeasy mini kit from Qiagen was used to extract RNA from RNAlater stored whole mice renal sections. The RNA library was generated using the TruSeq stranded mRNA library preparation kit (Illumina) and RNA was then sequenced with an Illumina HiSeq4000 instrument. Reads were aligned to the GRCm38.p7 mouse reference genome. Sequencing

data was analyzed using PCA on all genes identified as being differentially expressed, as well as those genes found on a public gene list of fibrosis related genes from www.SABioscience.com. To demonstrate any changes or differences in the molecular processes of ligated BGB324 treated versus ligated vehicle treated kidneys, a perturbation score was generated. Here, the log₂ counts per million (log₂cpm) reads of each ligated sample was divided by the average log₂cpm reads of the matched contralateral non-ligated tissue. Ratios below 1 were converted to the inverse. For all genes contained in the different gene lists, the average ratio was determined for each sample, which concluded in the "perturbation score" per sample group, in our case this was BGB324 treated versus vehicle treated mice. Gene lists were taken from www.SABioscience.com and also from previous publications (Mosser et al., 2008, Rodder et al., 2009, Rodder et al., 2011). As a control, the perturbation score was also generated from a list of 100 random genes, which did not show significant perturbation.

Human renal tissues: For RNA extraction of archival human FFPE renal tissues, we used the High Pure FFPE tissue RNA isolation kit (Roche). RNA sequencing libraries for each sample (n=6 for each nephrosclerotic, diabetic and normal renal tissue samples) were prepared using the TruSeq stranded mRNA library preparation kit (Illumina), according to the manufacturers protocol. Paired end sequencing with 75bp reads was performed on an Illumina HiSeq2500 platform. Reads were then aligned to the GRCh38 human reference genome.

3.3 Protein extraction and proteome analysis

In paper II, proteins from human FFPE normal renal and ccRCC biopsy tissues were extracted using a filter aided sample preparation method (Wisniewski, 2013). Proteins were quantified and identified in a label-free manner by a Q-Exactive HF Orbitrap liquid chromatography-tandem mass spectrometry (LC-MS/MS) and identified by alignment to the UniprotKB/SwissProt database for human proteins.

3.4 Unilateral ureteral obstruction

UUO is an established murine renal fibrosis model that was used in paper III. During surgery under gas anesthesia, the left ureter is ligated with a silk suture below the lower renal pole. Ligated kidneys subsequently undergo

hydronephrosis and fibrosis development is observed typically after only three days. Mice were then sacrificed at 7 or 15 days (Figure 3.2). Upon sacrifice, kidneys were harvested and parts of each kidney were stored in both RNAlater and FFPE. Blood and serum respectively were taken by heart puncture upon sacrifice.

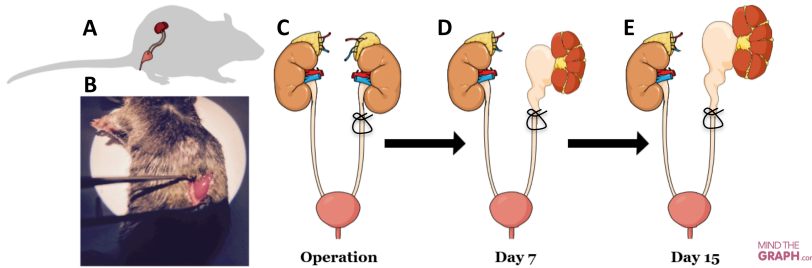


Figure 3.2: Schematic illustration of the kidney in mice (A) and of the operation where the kidney is located through a subcostal incision (B). The left ureter is then ligated (C). Hydronephrosis develops and mice are sacrificed on day 7 (D) or 15 (E). This figure was made with Mind The Graph.com (www.mindthegraph.com), licensed under the Creative Common Attribution-Share Alike 4.0. The picture in B) was taken by us for this study.

3.5 BGB324 and vehicle treatment

For the experiments in paper III, BGB324 was dissolved in its vehicle consisting of hydroxypropylmethylcellulose (HPMC) and Tween 80, and applied in a dosage of 50mg per kilogram weight twice a day via oral gavage, as recommended by the manufacturer based on their own previous studies (BerGenBio). The control group was treated only with the vehicle.

3.6 Immunohistochemistry

IHC was performed with sections from both human and murine FFPE renal tissues using standard methods. In paper II, both normal renal and ccRCC tissues were stained with AXL, VIM, CDH1 and MMP14. Staining results were then assessed visually. In paper III, staining with AXL, VIM, CDH1, α SMA and F4/80 was performed in ligated and non-ligated murine renal tissues. AXL was also stained in normal and diseased human renal biopsy tissues. IHC staining in murine tissues was quantified using Aperio, an image analysis system, as described below.

3.7 Fibrosis quantification

3.7.1 Sirius Red and semi quantitative computer-assisted analysis

For quantification of fibrosis in paper III, murine FFPE renal tissues were stained with SR (Figure 3.3, B), scanned and analyzed with the color deconvolution algorithm (Version 9) of the Aperio image analysis system, a computer-assisted semi-automated quantitative image analysis method. In short, areas of interest are marked, the algorithm is tuned by adapting its input parameters to the detection threshold, and the area is then analyzed. The output consists of a markup image (Figure 3.3, C) with color-coded weak (yellow), medium (orange) and strong (red) positive intensity of SR or IHC staining and therefore of fibrosis or IHC positivity. Total positive pixel percentage of each sample was used to compare between ligated and non-ligated mice renal tissues.

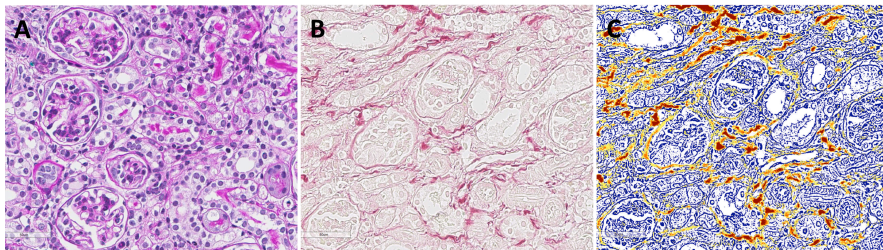


Figure 3.3: Mice renal fibrosis tissue analysis with color deconvolution algorithm of Aperio. A) PAS staining, B) Sirius Red (SR) staining, C) Markup image of applied color deconvolution algorithm from Aperio image analysis systems with intensity ranges of SR stained collagen.

3.7.2 Hydroxyproline content measurement

In addition to SR staining and computer-assisted analysis, we measured hydroxyproline content from mice renal tissues stored in RNAlater to quantify fibrosis in paper III. Hydroxyproline quantification was performed with a commercially available kit based on a colorimetric assay. Tissues were hydrolyzed in HCl 6M and hydroxyproline content was measured at 570nm after addition of the kit specific reagents. Results of hydroxyproline quantities of each sample were normalized to the total protein content of the same sample.

4 Summary of main results

4.1 Summary of results paper I

RNA extraction for RNA sequencing of archival renal tissues

Background: The analysis of RNA sequencing data can give insight into the underlying mechanisms of disease. Archival FFPE renal biopsy tissues are an underused source of material for modern molecular techniques such as RNA sequencing. The aim of this paper was to evaluate the most best method to extract RNA from FFPE renal biopsy sections and LCM glomerular cross-sections to enable RNA sequencing.

Methods: Seven different commercially available RNA extraction kits were tested on rat and normal human FFPE renal tissues. RNA was first extracted from both rat FFPE whole kidney sections (n=8, each with one or two 5 μ m sections used in each kit) and other samples composed of 80-101 rat LCM glomerular cross-sections (n=4 for each kit) using all seven RNA extraction kits. Later, the four RNA extraction kits, which yielded the highest quantity of extracted RNA, were tested on human FFPE renal biopsy sections (n=4, each with two 10 μ m sections used in each kit) and other samples composed of 80-160 human LCM glomerular cross-sections (n=2 for each kit). RNA from human LCM glomerular cross-sections was sequenced using the TruSeq RNA Access Library Preparation kit (Illumina).

Results: Four of the RNA extraction kits used yielded a sufficient quantity and quality of RNA from a single 10 μ m human renal biopsy section to enable sequencing (137ng RNA \pm 31ng at DV200 76% \pm 8% for the High Pure FFPE kit; 84ng RNA \pm 19ng at DV200 72% \pm 7% for the ExpressArt kit; 64ng RNA \pm 22ng at DV200 62% \pm 5% for the RNeasy FFPE kit and 53ng RNA \pm 18ng at DV200 51% \pm 13% for the miRNeasy FFPE kit). Two RNA extraction kits were found to be particularly suitable, allowing extraction of sufficient high quality RNA from around 100 LCM glomerular cross-sections (54ng RNA \pm 16ng at DV200 89% for the High Pure FFPE kit and 138ng RNA \pm 43ng at DV200 82% \pm 6% for the ExpressArt kit). RNA sequencing of RNA extracted from the human LCM samples with three of the kits was successful: RNA extracted with the High Pure FFPE kit yielded 24.1 million reads, the miRNeasy kit yielded 12.3 million reads and the

ExpressArt kit yielded 10.1 million reads per sample successfully mapped to the genome. Conclusion: RNA can be extracted from one human FFPE renal biopsy section or from around 100 LCM glomerular cross-sections from human FFPE renal biopsies to enable successful RNA sequencing using the Illumina TruSeq RNA Access Library Preparation kit. Archival renal biopsy tissues are thus suitable for transcriptome sequencing.

4.2 Summary of results paper II

ccRCC is linked to EMT and to Fibrosis

Background: ccRCC has a high morbidity and mortality. EMT is known to play a role in ccRCC development and progression. The aim of this study was to analyze markers of EMT in FFPE ccRCC tissues and to assess their association to prognosis.

Methods: RNA was extracted from FFPE ccRCC and adjacent normal tissues of patients undergoing partial or full nephrectomy due to ccRCC (n=26) and sequenced using the TruSeq Access Library preparation kit. MiRNA of a subgroup of 12 patients was sequenced using the TruSeq small RNA library preparation kit (both Illumina). Proteins from a subgroup of 11 patients were isolated and analyzed using a LC-MS/MS in a label-free manner.

Results: A generic EMT score with 315 EMT related genes showed significantly higher ("mesenchymal") values for tumor samples compared to its corresponding normal renal tissue sample in 25 out of 26 samples. 399 genes out of 483 EMT related genes compiled from public sources were detected and 137 of these genes were differentially expressed in our dataset. VIM, AXL and MMP14 were among the genes with the highest contribution towards the explanation of the variance in a PCA using the 137 differentially expressed genes. IHC showed more staining of VIM, AXL, and MMP14 but reduced CDH1 staining in ccRCC tissues compared to normal renal tissues. VIM, CDH1 and MMP14 were also detected in the proteomic dataset. Caveolin1 (CAV1), VIM, IGFBP3, ITGA5, MMP14 and AXL were found to be associated with cancer stage in our cohort. High expression of AXL and MMP14 was associated with worse survival, while Klotho (KL) was associated with improved survival in a publicly available TCGA dataset. MiR34 was distinctly up-regulated in our dataset but did not correlate

with survival in a TCGA cohort. A set of differentially expressed collagen genes (COL1A1, 1A2, 3A1 and 5A1) and a set of 11 genes out of the 20 most regulated genes outperformed MMP14 and AXL in a survival analysis with the TCGA cohort. Finally, a fibrosis classifier gene set with 10 or 19 metzincins and related genes (MARGS) was able to classify all samples correctly into ccRCC and normal renal tissues and also correlated with survival in the TCGA cohort.

Conclusion: EMT and fibrosis are substantial characteristics of ccRCC in our patient cohort and are associated with prognosis based on TCGA cohorts. EMT related genes including AXL may therefore be further evaluated as potential treatment targets.

4.3 Summary of results paper III

Inhibition of AXL RTK prevents fibrosis development in experimental UUO

Background: Renal fibrosis represents the histological evidence of CKD. EMT is known to be involved in fibrosis development. AXL is a known effector of EMT. The aim of the study was to detect AXL in murine UUO and to quantify fibrosis after AXL inhibition with BGB324 treatment in UUO.

Methods: C57Bl/6 mice were treated with BGB324 (n=6 for 7 days and n=16 for 15 days), ACEI (n=10 for 15 days), ACEI + BGB324 (n=10 for 15 days) or only vehicle (n=6 for 7 days and n=16 for 15 days) by oral gavage. Treatment was initiated one day before ureteral ligation and mice were sacrificed on day 7 or on day 15 after UUO. Ligated and non-ligated renal tissues were stored in RNAlater or FFPE and analyzed by fibrosis quantification (SR and Aperio image analysis, hydroxyproline content), IHC, western blot, ELISA and RNA sequencing.

Results: After 7 days of ligation, there were no differences in fibrosis development between BGB324 treated and vehicle treated ligated kidneys. After 15 days, the amount of fibrosis had not increased in the BGB324 treated ligated kidneys, but was significantly higher in the vehicle treated ligated kidneys (6.3% positive pixels \pm 3.3% in BGB324 treated versus 14.7% \pm 6.1% in vehicle treated ligated kidneys, $p < 0.0001$, one-way ANOVA with Bonferroni correction). BGB324 treated ligated kidneys also displayed significantly less fibrosis compared to ACEI treated ligated kidneys (11.9% \pm 4.4% positive pixels in the ligated ACEI treated kidneys, $p = 0.026$). BGB324 + ACEI did not have an additive effect

compared to BGB324 treatment alone. Hydroxyproline contents were in accordance to SR staining quantification when comparing BGB324 or BGB324 + ACEI to vehicle treated ligated kidneys. IHC staining showed significantly less VIM staining and less α SMA positive activated myofibroblasts in the ligated BGB324 treated compared to the ligated vehicle treated control after 15 days, which was compatible with less induction of (partial) EMT. This was also reflected on RNA sequencing level: EMT related genes such as AXL, SNAIL1, 2, TWIST, STAT1, TGF β 1, AKT3, MMP2, elastin and SMAD2/4 were less expressed in ligated BGB324 treated compared to ligated vehicle treated kidneys. IHC of F4/80, mainly staining macrophages, showed distinctly less F4/80 positive cells in ligated BGB324 treated compared to ligated vehicle treated kidneys, which was compatible with reduced inflammation related to macrophages. This was supported by less alteration of genes in a macrophage marker gene set as measured by a perturbation score in BGB324 treated kidneys, and less expression of the chemokines CCL2, CCL7, CCL12 and CCL17 by BGB324 treatment. Pathway analysis also revealed a down-regulation of pathways related to the immune system and cytokine secretion in ligated BGB324 treated kidneys, further documenting the reduction of inflammation by BGB324. Hypothetically, BGB324 thus reduces fibrosis development in UUO by attenuation of (partial) EMT and by reduction of the inflammatory response. In diabetic and nephrosclerotic human FFPE renal biopsy tissues, AXL was identified both in IHC and on RNA sequencing level. AXL expression was found to be significantly up-regulated in diseased compared to normal human renal tissues.

Conclusion: AXL is involved in fibrosis development in UUO and inhibition of AXL by BGB324 reduces fibrosis development in UUO. AXL is present also in diabetic and nephrosclerotic human renal tissues and AXL therefore represents a potential therapeutic target for renal fibrosis.

5 Discussion

5.1 Methodological considerations

5.1.1 How to obtain human renal tissues and what are the possible issues?

Research on the tissue morphology and the molecular mechanisms of diseases is dependent on the comparison between pathologic and physiological tissue. In general, human tissues can be obtained from archives, biobanks or from prospective collections of samples of a particular cohort (Bell et al., 2009). In our studies renal tissues were obtained from our own animal experiments, from prospective sample collection and from the Renal Biopsy Registry of the Norwegian Renal Registry (Table 4).

It is especially challenging to obtain healthy, normal human tissues. Reasons are that organ biopsies or surgical resections are only performed in the case of a relevant indication and suspected disease. Historically, normal tissues have been harvested from autopsies, however the rate of autopsies is decreasing (Chesters et al., 1983, WHO, 2018). In the context of cancer research, surgical resection can unveil normal tissue of the resected organ, which is adjacent to the tumor. This is typically the case in renal, breast, lung, prostate and thyroid cancers (Zeng et al., 2018). Other possible sources of normal tissues arise from cancer screening programs, for example normal gastric tissue sourced from national screening programs with gastroscopy to detect gastric cancer, such as in Korea and Japan (Zhao et al., 2018).

In paper I, we only used normal tissues taken from a previous rat experiment and from our ccRCC cohort to evaluate RNA extraction for RNA sequencing. The motivation for this choice was primarily that a large amount of tissues was required to test all seven kits and we assumed that normal tissue would yield the best reproducibility between the samples and also because of the high availability of normal rat tissues and such "non-cancer" normal samples.

In paper II, mRNA and miRNA sequencing, proteome analysis and IHC were performed on ccRCC tissues and the matched adjacent normal tissue from the same patient. Patients with eGFR <60ml/min/1.73m², with known diabetes, hypertension or other renal diseases were excluded to assure the normal tissue

collected was as "healthy" as possible. However, during surgery, blood supply is typically stopped before nephrectomy. In the case of partial nephrectomy, the resected tissues, including both the tumor and scarce amount of normal tissues, are also exposed to ischemia. Ischemia is known to very quickly induce changes on the level of gene expression also in the adjacent normal tissues (Spruessel et al., 2004). Further, tumor heterogeneity is known to be a prominent feature in ccRCC (Gerlinger et al., 2012). In this paper, we did not take this into consideration and only sampled tissues from one location per sample. We did however avoid bleeding or visibly cystic or necrotic areas. The role of these factors (ischemia, possible paracrine secretion and tumor heterogeneity) on the results of our study in paper II is discussed in 5.2.2.

In paper III, we also used normal human FFPE renal tissue, but this time from the Renal Biopsy Registry of the NRR. Here, the term "normal biopsy tissues" corresponds to the diagnosis "normal tissue or slight unspecific changes" (also coded "diagnosis 29" in the archive). However, even these "healthy" renal tissues may be problematic to use when it comes to their molecular analysis and any comparisons to diseased renal tissues: For example, these biopsies have been taken due to a particular indication, often due to proteinuria of unknown cause or (functional or transient) renal failure. The diagnosis "normal tissue or slight unspecific changes" might still be true and the proteinuria caused through interfering systemic inflammation, postural or transient proteinuria. However, renal tissues may also suffer sampling issues in the case of heterogeneous disease, or when early renal changes occur that were not visible by the eye or through electron microscopy. Whether or not, in the case of this archival "normal renal tissues", changes or alterations have already occurred on the gene expression level, is unclear. The fibrotic human renal tissue used in paper III originated from patients with hypertensive nephrosclerosis or diabetic nephropathy. We excluded patients with an eGFR $<30\text{ml}/\text{min}/1.73\text{m}^2$, because we wanted to study changes in tissue morphology and gene expression in the context of EMT and AXL in moderate stage CKD. Our prospect was then to initiate an experiment involving the inhibition of the AXL in mice to reduce the development of fibrosis. We assumed that ESRD and thus extensive fibrosis would not be reversible and thus excluded these patients from this analysis.

5.1.2 RNA extraction and assessment

The performance of RNA sequencing methods depends on the degree of RNA degradation and thus on the quality of tissue storage and extraction methods as well as on the sequencing technique itself. Upon tissue harvesting, biopsies or tissue samples can be FFPE or stored in RNA stabilizing solutions such as RNAlater and frozen at -80°C to prevent degradation. FFPE samples are kept at room temperature and can be stored for decades. Tissue archives usually use FFPE as a storage method.

Seven RNA extraction kits were used in paper I. These were chosen based on commercial availability and their specificity for RNA extraction from FFPE tissues. In addition, the kits were all filter based, which was the most convenient methods available to us at the time of the study. Other RNA extraction methods, such as RNA separation through organic extraction or via magnetic particle processing, were not considered. Automated RNA extraction methods have been shown to be effective and practical in different studies, however, we did not have such equipment available and therefore did not take semi-automated or automated techniques into account (Bohmann et al., 2009, Kocjan et al., 2015).

In paper II and III, we used the RNA extraction kits found to perform best according to our earlier studies. To assess RNA quantity, we used Nanodrop spectrophotometry, as the guidelines of Illumina recommended this method (Illumina, 2014a). In addition, in paper I, we measured quantities using Qubit, as this method is considered to have more specificity for RNA measurement and is therefore more precise. However, the minimal concentration measurable with Qubit is $2\text{ng}/\mu\text{l}$, which was higher than the concentration of some of the RNA samples extracted from LCM glomerular cross-sections. To assess RNA quality, we used DV200 values instead of the conventional RNA Integrity Number (RIN). Our reasons for this were that the RIN has been shown to correlate poorly with library preparation yield and sequencing success, and also because DV200 is considered more reliable in predicting the sequencing success of RNA from FFPE tissues. In addition, the Illumina guidelines for RNA quantity and quality for sequencing are based on the DV200 metric (Illumina, 2014a). An exception to this is that samples with low DV200 values may still result in successful sequencing when utilizing RNA extracted with the miRNeasy FFPE kit from

Qiagen. We assume, that small RNA fragments such as miRNA lead to a left-shift in the BioAnalyzer analysis and thus result in false low DV200 values. DV200 percentages must therefore be assessed with caution (Paper I, figure 6).

5.1.3 From Sanger Sequencing to Next Generation Sequencing

The human genome project, which aimed to sequence the entire human genome using Sanger sequencing, took approximately 14 years and was published in 2004 (International Human Genome Sequencing, 2004). Sanger sequencing is based on polymerase chain reaction to replicate DNA fragments, while incorporating chain-terminating nucleotides result in many fragments of differing sizes, which are then sorted and the terminal nucleotide of each fragment is read through gel electrophoresis, revealing the overall order of nucleotides. Following the completion of the human genome project, the development of new sequencing technologies was highly funded with the aim of reducing the duration and the costs of genome sequencing. In 2005, the first sequencing platforms were released by various companies using different techniques, but all of these platforms were described as next generation sequencing (NGS), massive parallel sequencing or high-throughput sequencing systems. In contrast to Sanger sequencing, NGS applies a cell-free system for library preparation, is independent of electrophoreses and finally, allows the simultaneous sequencing of millions of reactions in parallel (Buermans et al., 2014, van Dijk et al., 2014).

Transcriptome sequencing using NGS includes four steps: Library preparation, cluster generation, sequencing and analysis of the raw data. Library preparation in the case of RNA consists of fragmentation and the production of cDNA from the fragmented RNA. Around 95% of the total extracted RNA will consist of ribosomal RNA (rRNA), which must be removed before sequencing. This is performed by several different methods, such as the capturing of any coding RNA fragments or the selective removal of rRNA. The cDNA is then loaded on to a flow cell, which is characteristic for each of the platforms. The cDNA fragments are then amplified by PCR to generate clusters. The sequencing method the Illumina platforms use corresponds to a "sequencing by synthesis" method, which consists of the successive addition and integration of fluorescent

deoxyribonucleotide triphosphate and subsequent reading of the nucleotides by light excitation. After quality control, the reads are then assembled to join the overlapping sequences into contigs. Contigs are then identified through comparison to a reference genome, a process also called alignment (Figure 5.1) (Griffith et al., 2015, Illumina, 2017). In the case of the human genome, the Genome Reference Consortium Human Genome build 38 (GRCh38), released in December 2013, is currently used. It consists of a combination of the genomes of many volunteers (Schneider et al., 2017).

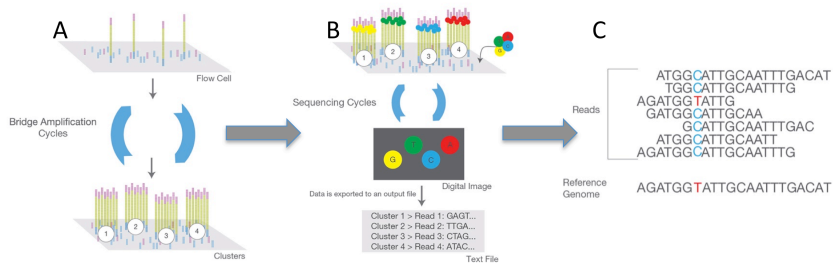


Figure 5.1: After fragmentation and cDNA generation, the library is loaded on to a flow cell by hybridization with the flow cell surface. Each fragment is then amplified into a clonal cluster (Cluster amplification, A). For the sequencing, fluorescence labeled nucleotides are added to the flow cell. Each round, any attached nucleotides are imaged and nucleotide identity is registered using the wavelength and intensity of the emission (Sequencing, B). The reads are then aligned and compared to a reference genome (Alignment, C). Figure from Illumina Inc., publicly available at <https://emea.illumina.com/company/news-center/multimedia-images.html>.

5.1.4 RNA sequencing method in the context of FFPE

RNA from FFPE tissues is known to be of inferior quality and lower quantity than other sources due to the cross-linkage of RNA and other molecules with formalin, but also due to degradation during fixation, embedding and storage. This is why, until recently, RNA from FFPE tissues was not considered to be suitable for RNA sequencing. However, in April 2014, Illumina, one of the main sequencing platform providers, released the TruSeq Access library preparation protocol (now called TruSeq Exome). This library preparation kit was specifically developed for transcriptome sequencing of degraded RNA such as RNA from FFPE tissues. It includes a particular protocol, where "capture probes" specifically select coding RNA and therefore enriches mRNA for the library. This results in reduced contamination from rRNA and increased detection and

identification of coding RNA fragments (Illumina, 2014b). Different Illumina platforms were used to sequence RNA in all articles presented in this study. This was due to resources and different availability of sequencing platforms in the collaborating genomic facilities at the time of study.

5.1.5 Implication of transcriptomic and proteomic data analyses

Transcriptome and proteome analyses reveal changes in gene expression on the mRNA and protein level. One protein-coding gene does not translate into one protein, but instead can give rise to up to many different proteins. This is possible due to processes such as alternative splicing and posttranslational modifications (Ponomarenko et al., 2016). However, mRNA levels tend to correlate with protein abundances most of the time: The ratio between mRNA and protein abundance remains relatively constant in all human tissues (Lundberg et al., 2010, Wilhelm et al., 2014). In addition, around 45% of all 20'000 protein-coding genes are expressed in all tissues and are therefore considered to be essential in structure and homeostasis of all cells (Uhlen et al., 2015). The detection of amino acid sequences with current technologies is limited and resolution is not as precise as in sequencing methods, which provides a resolution of a single nucleotide. Contrary to modern sequencing methods, protein detection by spectrometry does not rely on PCR based amplification. This is why, in contrast to RNA in sequencing methods, low abundance proteins are still challenging to detect with current technology (Ponomarenko et al., 2016).

In the proteome analysis of paper II, a total of 3613 proteins were identified with at least two unique peptides in normal and ccRCC FFPE tissue samples from our cohort. This is less than 20% of the approximately 20'000 protein-coding genes present in the human genome, thus only the most abundant proteins are represented in the proteomic dataset. This is likely the reason why AXL was not detected on the proteome level, although being clearly up-regulated in ccRCC tissue in the corresponding transcriptomic data.

Limitations of both transcriptomic and proteomic data include many technical issues, such as the viability of RNA and protein extraction procedures and the frequent problem of rRNA contamination in the case of transcriptome

sequencing. Further, transcriptomic and proteomic data represent only a "snap shot" in time of the gene expression profile of a particular tissue or cell types and does not include the whole picture of disease development or expression dynamics (Griffith et al., 2015).

5.1.6 EMT gene signatures and EMT score

In this work, we used three different EMT gene signatures to analyze our RNA sequencing data in the context of EMT (Figure 5.2).

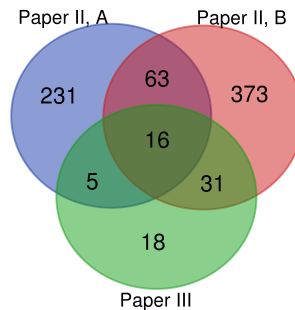


Figure 5.2: Venn diagram of three EMT gene signatures used in paper II and III: Overlap of gene signatures of the EMT score by (Tan et al., 2014) (Paper II, A, 315 genes), our own customized EMT gene list (Paper II, B, 483 genes) and the commercial available EMT gene set from SABiosciences.com (Paper III, 70 genes). Venn diagram was drawn with the public online tool available on <http://bioinformatics.psb.ugent.be>.

In paper II, we applied an EMT score, which comprises a particular common EMT gene expression signature based on 315 genes (145 epithelial, 170 mesenchymal genes) derived from multiple cancer tissues such as breast, lung and colorectal cancer. This EMT score ranks tissues on a spectrum between "epithelial" (-1) and "mesenchymal" (+1). The EMT score reflects the dynamics of EMT and considers intermediate states (Figure 5.2, A) (Tan et al., 2014). In the same paper II, we customized an own list with 483 genes by compiling gene sets from an online EMT gene database (dbEMT) (Zhao et al., 2015), two publications (Groger et al., 2012, Chen et al., 2014) and adding various genes of interest such as GAS6 and AKT3. AXL had already been included through the dbEMT database (Figure 5.2, B). Zhao et al., have collected 357 EMT associated genes and 20 EMT associated miRNA out of an extensive literature search on sequencing and microarray experiments in different diseases and cancers. The gene signature of Groger et al., consisted of genes found to be associated with EMT and cancer progression.

The gene signature of Chen et al., included genes associated with EMT in ccRCC. In paper III, a compact 70 genes long EMT gene signature was used from a commercially available microarray chip from SABiosciences.com.

There is not a great overlap between these gene lists used in these studies. Overlapping genes included CDH1, CDH2, TWIST, VIM, ZEB1 and ZEB2. In a recent metaanalysis, 24 human and 17 mouse EMT gene sets were analyzed, and a low correspondence between these lists was found. The authors even hypothesized that different EMT types may be a reason for this disparity and identified five clusters of EMT gene expression. Partly, these clusters reflected different cell types, which would imply the existence of different EMT pathways specificities in different cells (Liang et al., 2016). These findings emphasize the incompleteness of our current techniques and both the complexities and difficulties associated with assessing the EMT with generic gene signatures.

5.1.7 UUO as a renal fibrosis model

Animal models are necessary to study the mechanisms of disease development and to evaluate novel therapies in pre-clinical settings. In the case of renal fibrosis, there are many different murine models in which genetic changes, surgical or pharmacological interventions can lead to renal injury and fibrosis development. More specifically, models exist which are established to recapitulate particular disease pathogenesis, such as anti-GBM glomerulonephritis models, anti-Thy 1.1 nephritis models used to study mesangioproliferative glomerulonephritis, a HIV associated nephropathy transgenic mice model, a folic acid induced nephropathy models and a hypertensive rat model, where hypertension occurs spontaneously in a particular strain (spontaneously hypertensive rats) or is induced by clipping of a renal artery (two kidney one clip model) (Yang et al., 2010, Eddy et al., 2012).

However, despite renal fibrosis development being a common final pathway of different pathomechanisms, none of the existing murine models can exactly reflect human conditions. There are murine renal fibrosis models, which more generally reflect renal fibrosis development mechanisms, such as the sub-total nephrectomy (also called 5/6 nephrectomy) and the UUO model, performed since the 1970s (Chevalier et al., 2009, Yang et al., 2010, Eddy et al., 2012).

Ureteral obstruction and consequently obstructive nephropathy is nowadays a rare cause for renal fibrosis and CKD in human. However, the UUO model recapitulates all main mechanisms of fibrosis development, including accumulation of ECM, especially in the interstitium, fibroblast activation, inflammation, loss of TEC and microvascular rarefaction, as described in 1.5.6. Compared to sub-total nephrectomy, in which glomerulosclerosis is particularly pronounced, it is interstitial fibrosis that develops in UUO. Interstitial fibrosis appears to correlate with renal fibrosis and CKD in humans. This is why UUO has been one of the most widely used models to study renal fibrosis (Chevalier et al., 2009, Eddy et al., 2012). EMT is a known feature of UUO and VIM has been shown to be essential for the development of fibrosis in this renal fibrosis model (Wang et al., 2018). Partial EMT has also been demonstrated in this model, which therefore was particularly suited for our study presented in paper III (Chevalier et al., 2009, Grande et al., 2015, Lovisa et al., 2015). In addition, UUO represents a reliable and reproducible renal fibrosis model that is easily setup in the lab. Another advantage of UUO as a renal fibrosis model is, that the unaffected right kidney can be used as a control. Our research group also already had experience with performing UUO from previous experiments (Tveitaras et al., 2015).

The main disadvantage of UUO as a model to study renal fibrosis development is the missing functional endpoint and read-out: GFR - at least as expressed by creatinine levels - remains normal in mice, because the contralateral non-ligated kidney compensates for the affected kidney in global renal function. The serum creatinine therefore remains normal. Also, due to complete ligation of the ureter, no proteinuria is measurable. Another limiting aspect is the aggressive nature of the model: The injury caused by complete ligation of the ureter is drastic, leading to diminished perfusion after only 24 hours, inflammation with a peak after 2-3 days, fibrosis development after only 1 week and end-stage renal fibrosis after only 2 weeks. This pace does obviously not reflect renal fibrosis development in humans. However, in the context of our experiment involving the inhibition of AXL and the proven effect on fibrosis development, despite the harsh fibrosis induction by UUO, this strengthens the relevance of our findings.

5.1.8 Experiment set up and choice of mice strain

The experiment set up presented in paper III involves the pre-treatment of mice with BGB324 one day before UUO operation, despite the fact that this concept cannot be translated into the clinical setting. However, in this case, the rationale for pre-treating animals was to evaluate, as a proof of concept, if inhibition of AXL does reduce fibrosis development. Taking into account that UUO has an aggressive pace of fibrosis development, we sought to preload mice with BGB324 and therefore make BGB324 in the tissues available already at the time of ligation to assure an effect of BGB324 from the development of the very first changes on. We also considered that AXL and thus BGB324 has an effect on inflammation and that inflammation occurs already in the first three days after UUO (Chevalier et al., 2009). C57Bl/6 mice were used because they are the most known and characterized mouse strain and because their genome corresponds to the reference mouse genome. In the context of UUO, C57Bl/6 mice are the most used mice as models and also have been shown to be relatively susceptible to the development of fibrosis, especially tubulointerstitial fibrosis, as compared to BALB/c mice (Chevalier et al., 2009, Puri et al., 2010). Interestingly, in subtotal nephrectomy models, C57Bl/6 mice are resistant to the development of glomerulosclerosis (Yang et al., 2010, Eddy et al., 2012).

5.1.9 How to quantify fibrosis in renal specimens?

Renal fibrosis is characterized by the accumulation of ECM, which consists mainly of collagen types I and III. Collagen type IV, however, is represented in all basement membranes, and therefore also in the renal tubules and GBM (Zeisberg et al., 2010). The extent of interstitial fibrosis is known to correlate well with renal function and is a validated marker (Farris et al., 2014). Standard stainings for fibrosis quantification are trichrome stainings such as Masson, SR and IHC staining with collagen III. In the case of paper III, we quantified fibrosis by computer-assisted analysis of SR staining of whole renal tissue sections and hydroxyproline measurement of renal tissue samples from mice. SR staining is specific for collagen I and III under polarized light. SR is especially convenient for fibrosis quantification by computer-assisted techniques, because of a high contrast between collagen staining (red) and the background (yellow) (Figure

3.3). In paper III we assessed SR stainings in un-polarized light, meaning that collagen type IV was also included and measured. Trichrome stainings are cheaper and can also be analyzed with computer-assisted methods. However, both SR and trichrome stainings do not perform well when it comes to reproducibility within and between pathologic laboratories (Farris et al., 2014). In our hands and experience, SR stainings were more reliable than trichrome stainings such as Masson. However, we did increase reproducibility and observer-independence by analysis of the sections with semi-automated computer-assisted methods like those described in 3.8.1.

Hydroxyproline is a major component of collagen and can also be used to quantify fibrosis as has been shown in different studies using the UUO model (Chevalier et al., 2009, Lovisa et al., 2015). The hydroxyproline content of a sample can be normalized to the sample weight or to the protein content. In our case, we considered the protein content to be more precise than the sample weight, which may easily change upon, e.g., evaporation of the storage media.

Other methods for fibrosis quantification are, for example, PCR of collagen genes, especially COL1A1, or the detection of collagen by second harmonic generation imaging. This method is performed on unstained tissues and is based on the analysis of the interaction of photons from a laser beam with nonlinear material, such as fibrillar collagen. This method is thus specific for collagen I (which is fibrillar) but collagen IV (which is not) does not yield a signal (Strupler et al., 2007). Combining second harmonic generation imaging with fluorescence labeling has been seen to be even more specific for quantifying fibrosis in renal tissues (Ranjit et al., 2016).

5.2 Discussion of the main results

5.2.1 RNA extraction and sequencing of archival biopsies

FFPE is the routine storage method for biopsies, autopsy tissues and therefore also for tissue archives. FFPE has been the storage method of choice mainly due to its high quality preservation of tissue morphology (von Ahlfen et al., 2007). In the case of the Kidney Biopsy Registry of the NRR, around 13'000 renal biopsies have been collected as FFPE blocks since 1988, making this a readily available, but underused source of renal tissue material.

Transcriptome sequencing can give insight into dysregulated genes and pathways and thus can help to elucidate the pathomechanisms of renal diseases. Transcriptome sequencing also allows for the identification of new disease biomarkers, to assess prognosis, prediction and effectiveness of treatment, and may provide new drug targets for novel treatment strategies for renal diseases.

In addition, the use of archival tissues allows us to perform transcriptome analysis without depending on fresh tissues derived from recent biopsies or operations. This can help to increase the sample size of studies, particularly in the case of rare or very rare diseases, such as Fabry disease or specific glomerulopathies. The overriding aim of this study was therefore to enable RNA sequencing in the context of archival FFPE renal biopsy tissues. The hypothesis was, that RNA sequencing can be performed from human FFPE renal biopsy sections and from LCM glomerular cross-sections.

After Illumina released the TruSeq Access library preparation kit (now called TruSeq Exome), it has become easier to sequence samples containing low quality RNA. In a first step, our research group investigated the suitability of RNA extracted from FFPE tissues for RNA sequencing and analysis. For this purpose, paired core biopsies from ccRCC and adjacent normal tissues were collected from patients undergoing partial or full nephrectomy and stored in RNAlater and FFPE. The comparison of RNA sequencing results from the RNA extracted from tissues from both storage methods revealed a high correlation coefficient and therefore comparable results (Eikrem et al., 2016b). These results, and derived set of tumor classifier markers, were validated in a second cohort of patients (Eikrem et al., 2016a). RNA sequencing from FFPE renal biopsies is thus feasible. However, whilst archival renal biopsies are readily available, tissue quantity is limited and tissues therefore very precious. This is why we wanted to evaluate the most efficient method to enable successful RNA sequencing from archival biopsies.

The primary functions of the kidney comprise the electrolyte exchange capabilities and the metabolic capacity of the renal compartments, glomerulus and tubular systems, in close interaction with the interstitium. Primary renal diseases such as glomerulopathies largely affect the glomeruli but also cause changes to the tubules and the interstitium upon progression. Common systemic

diseases such as diabetes and hypertension manifest themselves first in the glomeruli, and in the case of hypertension, in the vasculature and only later in the other compartments (Olson et al., 2015, Olson, 2015). Other systemic diseases such as Fabry disease, have been shown to affect glomerular cells, TEC and also endothelial cells (Eikrem et al., 2017). Selective RNA sequencing of renal compartments can therefore give rise to more specific information about disease mechanisms and any potential biomarkers than that revealed by other molecular analyses, such as RNA sequencing from whole tissue sections.

RNA extraction from FFPE LCM renal compartments is challenging. This is mainly due to the lower tissue quantity, caused by the selective microdissection of glomerular cross-sections. In addition, sections are stained with HE, and mounted on slides, during which RNA can further degrade. LCM glomerular cross-sections from rats had been already used for protein extraction and proteome analysis by members of our research group (Finne et al., 2014). We therefore evaluated if RNA sequencing was possible also from rat and from human LCM glomerular cross-sections.

Quantitative analyses with Nanodrop showed consistently lower amounts of RNA for samples from LCM glomerular cross-sections. Nevertheless, RNA sequencing from FFPE LCM glomerular cross-sections was shown to be feasible and reliable even though we selected only specific renal compartments and both the quantity and quality of RNA was undermined by the storage method and duration.

The principle limitations of this study include that only a few specific RNA extraction kits were available for our use (discussed in 5.1.2) and that these methods were tested on normal renal tissues, whereas within the archives, diseased renal tissues obviously prevail. As mentioned, diseased human tissue is only taken by indication and renal biopsy can lead to complications but this is rare (Tondel et al., 2012). Still, biopsies from the archives are precious tissues and so we did not have sufficient materials to use simply to test the method. Further, according to the genomic facilities, sequencing of our samples was unproblematic, implying that this method of sequencing is sufficiently sensitive and that even lower quantities of RNA may lead to successful sequencing results.

In our study we have shown that one single human FFPE renal biopsy section or around 100 LCM glomerular cross-sections were necessary to enable RNA sequencing using the Illumina TruSeq RNA Access Library Preparation kit. These findings support the use of renal biopsy archives for transcriptome analysis of both biopsy sections and LCM renal compartments.

5.2.2 EMT and fibrosis in ccRCC

ccRCC is a common cancer in both men and women and the most common RCC. Despite extensive research, ccRCC often recurs after operation and still has an unfavorable prognosis. During the past decades, mortality has remained high, but survival has increased. This is probably both due to improved therapies, but also to earlier, often incidental diagnosis through increases in the use of imaging technologies. EMT has been seen to be involved in overall cancer aggressiveness and influences tumor cell migration and invasiveness, metastasis formation but also development of CSC and resistance to chemotherapeutics. AXL, commonly overexpressed in cancers with adverse prognosis, contributes to cancer progression especially by enhancing EMT and driving cancer resistance through different mechanisms.

The hypothesis of this study was that ccRCC tissues are characterized by EMT markers and that EMT related genes represent potential treatment targets. We have therefore analyzed the grade of EMT, EMT markers and fibrosis in ccRCC tissues of patients from our cohort by RNA and miRNA sequencing, transcriptome analysis and proteome analysis. Survival analyses of EMT or fibrosis related genes of interest were performed on ccRCC RNA and miRNA data from TCGA cohorts.

A generic EMT cancer gene expression signature showed a significant increase of the EMT score within pairs of normal renal tissue and corresponding matched ccRCC tissue in our transcriptomic data. The spectrum of normal renal and ccRCC tissues on the EMT score axis was spread out and overlapping, which made the EMT score unsuitable for diagnostic purpose. The wide spectrum in ccRCC EMT score and the more "mesenchymal" phenotype has been demonstrated already in the original publication (Tan et al., 2014). This may reflect the development of renal structures such as TEC from the intermediate

mesoderm during embryogenesis (Kalluri et al., 2009, Tan et al., 2014). Interestingly, normal renal tissue, which is adjacent to ccRCC tissue, showed a relatively "mesenchymal" phenotype (Paper II, figure 1). Here, a combination of the paracrine secretion of cytokines and the local tumor microenvironment, as well as ischemia during surgical resection, may have influenced the normal renal tissue and rendered their expression profiles "mesenchymal". However, there was no difference of the EMT score between normal renal tissue samples taken from full nephrectomy compared to normal renal tissues taken from partial nephrectomy, where tumorous tissue is in close proximity (data not shown).

Only 71 genes included in the EMT score gene signature were included in our EMT gene list where 399 of a total of 483 genes were detected (EMT gene signatures in general are discussed in 5.1.6). With our customized EMT gene list, we found that VIM, MMP14 and AXL were among the critical genes, which explained the variance between ccRCC and normal tissue in a PCA (Paper II, figure 3). AXL was also up-regulated in ccRCC tissue compared to normal renal tissues on the RNA level, but was not detected in our proteomic dataset (discussed in 5.1.5). There was also a modest but relevant association of AXL expression with cancer stage in our patients (Paper II, figure 4). In the publicly available TCGA cohort, increased expression of AXL was associated with reduced survival as shown in the Kaplan-Meier analyses (Paper II, figure 8C). Interestingly, the degree of EMT as measured by the EMT score, has not been associated with cancer treatment resistance (Tan et al., 2014). AXL however, has been proven to directly be associated with acquired resistance in the context of RTK inhibitor resistance in ccRCC (Zhou et al., 2016). This has been proven to be relevant in the clinic, where treatment with Cabozantinib is an effective treatment option, particularly after the use of VEGF targeted therapy with, e.g., Sunitinib (Choueiri et al., 2017a, Choueiri et al., 2017b).

MMP14 is known to be involved in ccRCC development and has been associated with VHL mutations, EMT and nuclear grade alterations according to Fuhrman (Mahimkar et al., 2011). In our study, MMP14 was associated with AXL expression and was significantly more expressed in ccRCC compared to normal tissues. This was confirmed by our proteome analysis and IHC. In addition, MMP14 expression was also associated with tumor stage in our cohort and with

unfavorable prognosis in TCGA patients. On miRNA level, miR34a was one of the most significantly up-regulated miRNA in ccRCC compared to normal tissue and its expression correlated well with both AXL and MMP14. MiR34a is known to target both AXL and MMP14 (Jia et al., 2014, Cho et al., 2016). In the case of AXL, a complex feedback loop leads to AXL inducing the expression of miR34a, which, contrast, promotes AXL down-regulation (Cho et al., 2016). This could be the reason why we found an up-regulation of AXL alongside miR34a. In the case of MMP14, miR34a reduces the expression of MMP14, as seen in lung tumor cells (Jia et al., 2014). The reasons why both miR34a and MMP14 were up-regulated in our cancer cohort could possibly include tumor heterogeneity and network complexity with the influence of other regulators. These interlaced networks and functions of miRNA might also be the reason why, in contrary to AXL and MMP14, miR34a expression did not correlate with survival in the TCGA cohort.

ITGA5 and CAV1 were also among prominently differentially expressed genes between ccRCC and normal tissues. Both ITGA5 and CAV1 expression have recently been described as being associated with worse prognosis in ccRCC (Poplawski et al., 2017, Ruan et al., 2017). This is in accordance with our data, where ITGA5 and CAV1 had a strong association with tumor stage (Paper II, figure 4).

KL was also among the most down-regulated genes in ccRCC tissue compared to normal tissue. KL was included in our EMT gene list because it negatively regulates and inhibits EMT related genes such as AKT and SNAIL (Zhu et al., 2013). Accordingly, increased expression of KL was associated with improved survival in our analysis of the TCGA dataset (Paper II, figure 8).

In the context of our survival analysis, we found a set of four collagen genes and a set of 11 highly dysregulated genes, which did outperform AXL and MMP14 in predicting the survival of patients in the TCGA cohort. Three out of the four collagen genes were included within our EMT gene list. In accordance with these findings, the MARGS panel correctly assigned all samples to either ccRCC or normal tissue and was also found to be associated with patient survival. This reflects the close link between EMT and fibrosis development and provides a connection between the mechanisms of ccRCC development and those involved in renal fibrosis.

We therefore conclude that EMT and fibrosis are substantial characteristics of ccRCC in our patient cohort and are associated with prognosis based on TCGA cohorts.

There are several limitations of this study. Particularly, biopsies of ccRCC tissues have only been taken from one tumor site. This means that tumor heterogeneity is not taken into account, while it is known to be common in ccRCC and can lead to the misinterpretation of ccRCC genomic characteristics (Gerlinger et al., 2012). In addition, this study is merely descriptive. ccRCC cell studies or animal models treated with the inhibition of EMT genes or the depletion of genes of interest would provide further support for our findings.

However the results of our study support the relevance of EMT related genes including AXL in ccRCC and provide further rationale for studies on EMT targeted treatment strategies in ccRCC.

5.2.3 EMT and AXL in renal fibrosis

CKD is a global public health issue due to its high incidence and prevalence, high mortality, especially of cardiovascular nature, reduced quality of life and high costs of treatment and renal replacement therapy, if these are available at all. Prevalence of CKD is expected to rise particularly due to increases in the prevalence of obesity, diabetes and hypertension. These diseases, from a public health perspective, are ultimately driven by ageing and longevity of humans, the effects of urbanization and globalisation, increasing sedentarism and the nutritional transition leading to an increase in these metabolic disorders. Renal fibrosis is the histopathological correlate to CKD. Causal therapy, such as treatment of diabetes mellitus, hypertension or the underlying renal disease and alleviation of aggravating factors such as secondary hypertension and proteinuria can reduce, but not halt, progression of CKD.

Efforts to address and tackle renal fibrosis and thus CKD must be made on all levels: From primary prevention, where interventions prevent or address obesity, diabetes and hypertension before CKD develops, to secondary prevention, where CKD is detected early and (if available) specific treatments are initiated timely, but also to tertiary prevention in advanced stages of CKD, where CKD and fibrosis are established and progression can be reduced. Besides

symptomatic treatment and control of progression factors, there is an urgent need for targeted therapy to halt fibrosis development and progression.

EMT, first described in the 1980s, was understood as a process where epithelial cells undergo a complete shift towards mesenchymal cells. In the context of renal fibrosis, EMT was thought to lead to TEC detaching from the basement membrane and transforming into myofibroblasts directly contributing to fibrosis development. This notion of "complete EMT" became highly controversial, when modern lineage tracing was introduced: None, or only very few, myofibroblasts were shown to truly originate from TEC and not around one third, as described before (Iwano et al., 2002, LeBleu et al., 2013, Mack et al., 2015).

In 2015, the idea of a "partial EMT" was first described in two articles where TWIST and SNAIL were either deleted or up-regulated in TEC. An EMT gene expression profile was induced upon gene reactivation but TEC remained attached to the basement membrane. These findings demonstrated, that despite not complying with the original concept of "complete" EMT, EMT of TEC occurs "partially" and is a crucial mechanism in renal fibrosis development (Grande et al., 2015, Lovisa et al., 2015, Ovadya et al., 2015).

AXL is an EMT induced effector that drives EMT but also promotes cell survival, cell proliferation and dampens the immune response. AXL is known to be expressed in different murine renal disease models but also in human renal diseases (Yanagita et al., 2001, Nagai et al., 2003, Fiebeler et al., 2004).

The hypothesis of our study was that AXL is involved in fibrosis development in UUO and that inhibition of AXL by BGB324 reduces fibrosis development in UUO. We have therefore demonstrated the presence of AXL in ligated and non-ligated kidneys in UUO, quantified fibrosis and analyzed tissues of kidneys after treatment with BGB324 or its vehicle.

AXL was substantially more expressed in ligated compared to non-ligated kidney tissues after 15 days of UUO (Paper III, figure 2). This implicated that the UUO model is an appropriate model to study AXL inhibition with BGB324.

The effect of BGB324 on reducing fibrosis development in UUO was not detected after 7 days, but became apparent after 15 days of obstruction: Fibrosis quantity had increased in the vehicle treated ligated kidneys compared to 7 days of obstruction, but had not increased in the BGB324 treated ligated kidneys (Paper

III, figure 4). BGB324 treated ligated kidneys had more than 50% less fibrosis, as seen by SR staining, and around 30% less fibrosis as measured by hydroxyproline quantification after 15 days of obstruction. BGB324 treatment also led to significantly less fibrosis development, as measured with SR in ligated kidneys compared to mice treated with ACEI, the gold standard for CKD therapy. ACEI alone did not reduce fibrosis development in UUO as measured with SR and hydroxyproline and, accordingly, BGB324 + ACEI did not have an additive effect compared to BGB324 treatment alone (Paper III, figure 5).

We can only speculate why BGB324 treatment reduced fibrosis development in UUO. On one hand, we have observed the reduced activation of EMT gene expression in ligated BGB324 treated kidneys, as seen with less VIM and α SMA staining in IHC and, correspondingly, the down-regulation of EMT related genes, such as SNAIL, TWIST and ZEB, and less perturbation in an EMT gene score in ligated BGB324 treated compared to their vehicle treated control. This indicates an attenuated induction of (partial) EMT by BGB324 treatment.

On the other hand, we have observed less inflammation in ligated kidneys treated by BGB324: This was reflected by markedly less F4/80 positive inflammatory cells and less α SMA positive activated myofibroblasts in ligated BGB324 treated kidneys compared to the vehicle treated controls (Paper III, figure 8). F4/80 is mainly expressed by macrophages. Accordingly, on the transcriptome levels, ligated BGB324 treated kidneys showed less deviation of gene expression in a gene set related to macrophage markers. Furthermore, the expression of the chemokines CCL2, CCL7, CCL12 and CCL17 was reduced by BGB324 (Paper III, figure 9). CCL2, CCL7 and CCL 12 are known to play a role in fibrosis development, where they act both proinflammatory and also are chemoattractant to fibroblasts, and thus promote fibrosis development (Moore et al., 2006). CCL2, CCL7 and CCL 12 are known to bind to the chemokine receptor 2 (CCR2), which is expressed on monocytes upon activation and promotes their recruitment (Anders et al., 2011). Finally, in a pathway analysis, pathways related to the immune system and cytokine secretion were down-regulated (Paper III, figure 10). This further supports a reduction of inflammation in ligated kidney tissues by BGB324 treatment.

BGB324 has mostly been tested in cancer and lately has entered phase II in several cancer studies. BGB324 is orally administered and current data suggest no severe adverse side effects. BGB324 was seen to improve the effect of RTK (e.g. EGFR or VEGFR) targeted therapies in different cancers, and of immune checkpoint inhibitors (PD1 and CTLA4 inhibitors) in experimental cancer models by reducing immune evasion mechanisms and thus resistance to these treatment modalities (Gay et al., 2017, Wnuk-Lipinska et al., 2017, Akalu et al., 2017, Yule et al., 2018). BGB324 has also been proven to reduce fibrosis in an experimental liver fibrosis experiment. This was accompanied by less F4/80 positive cells and less expression of cytokines (Barcena et al., 2015). In idiopathic lung fibrosis, AXL was seen to be up-regulated as compared to normal human lung tissue, and BGB324 led also to reduction of fibrosis development in two mouse lung fibrosis models (Espindola et al., 2018). In a murine anti-GBM antibody induced nephritis model, mice treated with BGB324 showed improved renal function compared its control, and AXL knockout mice had improved survival, less inflammation and also increased GFR in a nephrotoxic serum nephritis model. The extent of fibrosis was not analyzed in these studies (Zhen et al., 2018, Zhen et al., 2016). However, the studies on liver fibrosis and in particular in renal fibrosis with improved renal function and reduced inflammation by AXL inhibition support our findings in UUO.

In archival fibrotic renal tissues from patients with diabetic nephropathy or hypertensive nephrosclerosis, AXL was present in IHC and more expressed in diseased renal tissues compared to normal renal tissues on RNA level (Paper III, figure 11). This implies a potential clinical relevance - as AXL also could be blocked in human renal diseases.

UUO can be described as a drastic but high throughput murine renal fibrosis model and has been proven to induce EMT. Limitations of our study are beside the missing functional endpoint and the time point of therapy induction before ligation of the ureter (discussed in 5.1.7 and 5.1.8 respectively) also the missing detailed characterization of inflammatory infiltrates. Inflammatory cells were only characterized by F4/80 staining, which mainly stain a macrophage subpopulation but also particular dendritic cells. However, F4/80 positive macrophages are known to be a prominent feature of inflammatory infiltrates

during renal fibrosis development in UUO (Chevalier et al., 2009, Lee et al., 2011, Grande et al., 2015, Lovisa et al., 2015). Still, further assessment of inflammatory cells such as additional IHC stainings or flow cytometry would give insight into how BGB324 treatment affects inflammation after ligation of the ureter. At last, to our knowledge, UUO has not yet been performed with appropriate AXL knockout mice. Such functional studies would further strengthen our results.

However, the reduction of fibrosis development through BGB324 treatment, as compared to vehicle treatment and also ACEI, the gold standard therapy of renal fibrosis, was substantial. Possibly, fibrosis development was reduced by BGB324 due to an attenuated induction of (partial) EMT and through the reduced inflammatory response. The effect of AXL inhibition in our UUO study is a proof of concept and supports the relevance of AXL in fibrosis development in UUO. In addition, the detection of AXL in diseased human renal biopsy tissues implicates a potential relevance of AXL also in human renal diseases and provides the rationale to study in detail the effect of AXL inhibition on renal fibrosis in other murine renal fibrosis models and ultimately in humans.

6 Conclusions and further perspectives

6.1 Conclusions

I RNA can be extracted from one human FFPE renal biopsy section or from around 100 LCM glomerular cross-sections from human FFPE renal biopsies to enable successful RNA sequencing using the Illumina TruSeq RNA Access Library Preparation kit. Archival renal biopsy tissues are thus suitable for transcriptome sequencing (Paper I).

II EMT and fibrosis are substantial characteristics of ccRCC in our patient cohort and are associated with prognosis based on publicly available datasets of ccRCC patient cohorts. Genes related to EMT including AXL may therefore be further evaluated as potential treatment targets (Paper II).

III AXL is involved in fibrosis development in UUO and inhibition of AXL by BGB324 reduces fibrosis development in UUO. AXL is present also in diabetic and nephrosclerotic human renal tissues and AXL therefore represents a potential therapeutic target for renal fibrosis (Paper III).

6.2 Further perspectives

Archival FFPE renal biopsy tissues such as those from the Renal Biopsy Registry of the NRR are now accessible for RNA sequencing and tissues can be exploited to study pathomechanisms, to define biomarkers and new drug targets. The transcriptome profiles of primary renal diseases, such as glomerulopathies, or rare storage diseases, such as Fabry disease, can be analyzed using archival biopsies - also in collaborations with other registries and thus allowing researchers to generate a larger sample size. Particularly, different compartments of the kidneys, such as glomeruli, proximal or distal tubules, interstitium or vasculature can be analyzed separately using LCM method to separately evaluate their role in the disease's development.

The issue of the lack of "ideal" normal renal tissues in Nephrology related research will remain for as long as tissue bioengineering does not provide an

alternate solution. The comparison of transcriptome sequencing data of different "normal" renal tissues, such as native kidney biopsies or preimplantation biopsies from renal allografts, could help to distinguish characteristics and differences of these specimens. This might also help us to identify possible systematical mistakes made previously by using "normal" tissues as controls, in particular in studies applying molecular analyses such as RNA sequencing.

Efforts to evaluate the effect of AXL inhibition on chemotherapy resistance are ongoing. Cabozantinib, a drug, which also blocks AXL, is an established treatment option in advanced ccRCC. However, the relevance of selective AXL inhibitors such as BGB324 on the resistance to VEGF targeted therapies and immune checkpoint inhibitors is promising, but has not yet been assessed. Further studies, for example, on the effect of BGB324 on growth and metastasis of ccRCC in a xenograft model, could yield answers. In addition, the issue of tumor heterogeneity could potentially be addressed in our ccRCC cohort and this may help to further improve the evaluation of EMT in ccRCC. Measurement of soluble AXL in serum or urine by ELISA is validated and commercially available. Studies on the correlation of soluble AXL levels to tumor stage, prognosis or treatment response - also in the context of therapy resistance - could lead to the use of soluble AXL as a prognostic or predictive tool.

EMT related genes including AXL are possible targets for new treatment strategies in fibrotic diseases. Efforts should be made to further characterize EMT and AXL in different renal fibrosis models, e.g. by complementing transcriptomic data with proteome analyses. Also, the study of the effect of inhibition of EMT and AXL on renal fibrosis - in the context of EMT but also inflammation - should be pursued. Targeting EMT and AXL is promising and could, in the future, potentially assist existing treatments in reducing fibrosis development and CKD progression in highly prevalent renal diseases, such as hypertensive or diabetic nephropathies, but also in allograft nephropathy and in rare progressive renal diseases. Also we postulate that the association between soluble AXL in serum or urine with renal function, fibrosis grade or outcome may allow us to assess the role of soluble AXL as a diagnostic or prognostic tool.

7 References

- Aceto, N., Bardia, A., Miyamoto, D. T., Donaldson, M. C., et al. Circulating tumor cell clusters are oligoclonal precursors of breast cancer metastasis. *Cell*, 2014, 158(5):1110-1122
- Akalu, Y. T., Rothlin, C. V. & Ghosh, S. TAM receptor tyrosine kinases as emerging targets of innate immune checkpoint blockade for cancer therapy. *Immunol Rev*, 2017, 276(1):165-177
- Anders, H. J. & Ryu, M. Renal microenvironments and macrophage phenotypes determine progression or resolution of renal inflammation and fibrosis. *Kidney Int*, 2011, 80(9):915-25
- Arreaza, G., Qiu, P., Pang, L., Albright, A., et al. Pre-Analytical Considerations for Successful Next-Generation Sequencing (NGS): Challenges and Opportunities for Formalin-Fixed and Paraffin-Embedded Tumor Tissue (FFPE) Samples. *Int J Mol Sci*, 2016, 17(9):
- Baisantry, A., Bhayana, S., Rong, S., Ermeling, E., et al. Autophagy Induces Prosenescent Changes in Proximal Tubular S3 Segments. *J Am Soc Nephrol*, 2016, 27(6):1609-16
- Barcena, C., Stefanovic, M., Tutusaus, A., Joannas, L., et al. Gas6/Axl pathway is activated in chronic liver disease and its targeting reduces fibrosis via hepatic stellate cell inactivation. *J Hepatol*, 2015, 63(3):670-8
- Batchu, S. N., Hughson, A., Gerloff, J., Fowell, D. J., et al. Role of Axl in early kidney inflammation and progression of salt-dependent hypertension. *Hypertension*, 2013, 62(2):302-9
- Behrens, G. & Leitzmann, M. F. The association between physical activity and renal cancer: systematic review and meta-analysis. *British Journal of Cancer*, 2013, 108789-811
- Bell, W. C., Sexton, K. C. & Grizzle, W. E. How to efficiently obtain human tissues to support specific biomedical research projects. *Cancer Epidemiol Biomarkers Prev*, 2009, 18(6):1676-9
- Ben-Batalla, I., Schultze, A., Wroblewski, M., Erdmann, R., et al. Axl, a prognostic and therapeutic target in acute myeloid leukemia mediates paracrine crosstalk of leukemia cells with bone marrow stroma. *Blood*, 2013, 122(14):2443-52
- Bergstrom, A., Hsieh, C. C., Lindblad, P., Lu, C. M., et al. Obesity and renal cell cancer--a quantitative review. *Br J Cancer*, 2001, 85(7):984-90
- Bex, A., Albiges, L., Ljungberg, B., Bensalah, K., et al. Updated European Association of Urology Guidelines for Cytoreductive Nephrectomy in Patients with Synchronous Metastatic Clear-cell Renal Cell Carcinoma. *Eur Urol*, 2018, 10.1016/j.eururo.2018.08.008
- Bex, A., Albiges, L., Ljungberg, B., Bensalah, K., et al. Updated European Association of Urology Guidelines Regarding Adjuvant Therapy for Renal Cell Carcinoma. *Eur Urol*, 2017, 71(5):719-722
- Bianchi, M., Sun, M., Jeldres, C., Shariat, S. F., et al. Distribution of metastatic sites in renal cell carcinoma: a population-based analysis. *Ann Oncol*, 2012, 23(4):973-80
- Blom, J. N. & Feng, Q. Cardiac repair by epicardial EMT: Current targets and a potential role for the primary cilium. *Pharmacol Ther*, 2018, 186114-129
- Bohmann, K., Hennig, G., Rogel, U., Poremba, C., et al. RNA extraction from archival formalin-fixed paraffin-embedded tissue: a comparison of manual, semiautomated, and fully automated purification methods. *Clin Chem*, 2009, 55(9):1719-27
- Boor, P. & Floege, J. Renal allograft fibrosis: biology and therapeutic targets. *Am J Transplant*, 2015, 15(4):863-86
- Bosurgi, L., Bernink, J. H., Delgado Cuevas, V., Gagliani, N., et al. Paradoxical role of the proto-oncogene Axl and Mer receptor tyrosine kinases in colon cancer. *Proc Natl Acad Sci U S A*, 2013, 110(32):13091-6
- Brabletz, S., Brabletz, T. & Stemmler, M. P. Road to perdition: Zeb1-dependent and -independent ways to metastasis. *Cell Cycle*, 2017, 16(19):1729-1730
- Brugarolas, J. Molecular genetics of clear-cell renal cell carcinoma. *J Clin Oncol*, 2014, 32(18):1968-76
- Buermans, H. P. & den Dunnen, J. T. Next generation sequencing technology: Advances and applications. *Biochim Biophys Acta*, 2014, 1842(10):1932-1941
- Cao, J., Liu, J., Xu, R., Zhu, X., et al. MicroRNA-21 stimulates epithelial-to-mesenchymal transition and tumorigenesis in clear cell renal cells. *Mol Med Rep*, 2016, 13(1):75-82
- Capitanio, U. & Montorsi, F. Renal cancer. *Lancet*, 2016, 387(10021):894-906

- Carew, R. M., Wang, B. & Kantharidis, P. The role of EMT in renal fibrosis. *Cell Tissue Res*, 2012, 347(1):103-16
- Castrop, H., Hocherl, K., Kurtz, A., Schweda, F., et al. Physiology of kidney renin. *Physiol Rev*, 2010, 90(2):607-73
- Chen, D., Gassenmaier, M., Maruschke, M., Riesenberger, R., et al. Expression and prognostic significance of a comprehensive epithelial-mesenchymal transition gene set in renal cell carcinoma. *J Urol*, 2014, 191(2):479-86
- Chen, J., Yang, Y. F., Yang, Y., Zou, P., et al. AXL promotes Zika virus infection in astrocytes by antagonizing type I interferon signalling. *Nat Microbiol*, 2018, 3(3):302-309
- Chesters, P. M., Heritage, J. & McCance, D. J. Persistence of DNA sequences of BK virus and JC virus in normal human tissues and in diseased tissues. *J Infect Dis*, 1983, 147(4):676-84
- Chevalier, R. L., Forbes, M. S. & Thornhill, B. A. Ureteral obstruction as a model of renal interstitial fibrosis and obstructive nephropathy. *Kidney Int*, 2009, 75(11):1145-52
- Cho, C. Y., Huang, J. S., Shiah, S. G., Chung, S. Y., et al. Negative feedback regulation of AXL by miR-34a modulates apoptosis in lung cancer cells. *RNA*, 2016, 22(2):303-15
- Choueiri, T. K., Halabi, S., Sanford, B. L., Hahn, O., et al. Cabozantinib Versus Sunitinib As Initial Targeted Therapy for Patients With Metastatic Renal Cell Carcinoma of Poor or Intermediate Risk: The Alliance A031203 CABOSUN Trial. *J Clin Oncol*, 2017a, 35(6):591-597
- Choueiri, T. K. & Motzer, R. J. Systemic Therapy for Metastatic Renal-Cell Carcinoma. *N Engl J Med*, 2017b, 376(4):354-366
- Chow, W. H., Dong, L. M. & Devesa, S. S. Epidemiology and risk factors for kidney cancer. *Nat Rev Urol*, 2010, 7(5):245-57
- Clague, J., Lin, J., Cassidy, A., Matin, S., et al. Family history and risk of renal cell carcinoma: results from a case-control study and systematic meta-analysis. *Cancer Epidemiol Biomarkers Prev*, 2009, 18(3):801-7
- ClinicalTrials.gov. U.S. National Library of Medicine. 2014.
<https://clinicaltrials.gov/ct2/show/NCT01113801>
- ClinicalTrials.gov. U.S. National Library of Medicine. 2018.
<https://clinicaltrials.gov/ct2/results?cond=&term=BGB324&cntry=&state=&city=&dist=>
- Curthoys, N. P. & Moe, O. W. Proximal tubule function and response to acidosis. *Clin J Am Soc Nephrol*, 2014, 9(9):1627-38
- Dabestani, S., Beisland, C., Stewart, G. D., Bensalah, K., et al. Long-term Outcomes of Follow-up for Initially Localised Clear Cell Renal Cell Carcinoma: RECUR Database Analysis. *Eur Urol Focus*, 2018, 10.1016/j.euf.2018.02.010
- Dabestani, S., Marconi, L., Hofmann, F., Stewart, F., et al. Local treatments for metastases of renal cell carcinoma: a systematic review. *Lancet Oncol*, 2014, 15(12):e549-61
- Dabestani, S., Thorstenson, A., Lindblad, P., Harmenberg, U., et al. Renal cell carcinoma recurrences and metastases in primary non-metastatic patients: a population-based study. *World J Urol*, 2016, 34(8):1081-6
- Dagher, J., Delahunt, B., Rioux-Leclercq, N., Egevad, L., et al. Clear cell renal cell carcinoma: validation of World Health Organization/International Society of Urological Pathology grading. *Histopathology*, 2017, 71(6):918-925
- Dantzler, W. H., Layton, A. T., Layton, H. E. & Pannabecker, T. L. Urine-concentrating mechanism in the inner medulla: function of the thin limbs of the loops of Henle. *Clin J Am Soc Nephrol*, 2014, 9(10):1781-9
- Davidson, K.T., Haaland, G.S., Lie, M.K., Lorens, J.B., et al. The Role of Axl Receptor Tyrosine Kinase in Tumor Cell Plasticity and Therapy Resistance. In: Akslen L, Watnick R. (eds) Biomarkers of the Tumor Microenvironment. Springer, Cham. 2017, Vol. 978-3-319-39145-8
- Delahunt, B., Chevillat, J. C., Martignoni, G., Humphrey, P. A., et al. The International Society of Urological Pathology (ISUP) grading system for renal cell carcinoma and other prognostic parameters. *Am J Surg Pathol*, 2013, 37(10):1490-504
- Dudas, P. L., Argentieri, R. L. & Farrell, F. X. BMP-7 fails to attenuate TGF-beta1-induced epithelial-to-mesenchymal transition in human proximal tubule epithelial cells. *Nephrol Dial Transplant*, 2009, 24(5):1406-16
- Eckardt, K. U., Coresh, J., Devuyst, O., Johnson, R. J., et al. Evolving importance of kidney disease: from subspecialty to global health burden. *Lancet*, 2013, 382(9887):158-69

- Eddy, A. A., Lopez-Guisa, J. M., Okamura, D. M. & Yamaguchi, I. Investigating mechanisms of chronic kidney disease in mouse models. *Pediatr Nephrol*, 2012, 27(8):1233-47
- Eikrem, O. S., Strauss, P., Beisland, C., Scherer, A., et al. Development and confirmation of potential gene classifiers of human clear cell renal cell carcinoma using next-generation RNA sequencing. *Scand J Urol*, 2016a, 50(6):452-462
- Eikrem, O., Skrunes, R., Tondel, C., Leh, S., et al. Pathomechanisms of renal Fabry disease. *Cell Tissue Res*, 2017, 369(1):53-62
- Eikrem, Oystein Solberg, Beisland, Christian, Hjelle, Karin, Flatberg, Arnar, et al. Transcriptome Sequencing (RNAseq) enables utilization of Formalin-Fixed, Paraffin-Embedded Biopsies with Clear Cell Renal Cell Cancer for Exploration of Disease Biology and Biomarker Development. *PLoS One*, 2016b, 11(2):e0149743
- Escudier, B. eUpdate: Renal Cell Carcinoma Treatment recommendations (published 10th April 2017) 2017, <http://www.esmo.org/Guidelines/Genitourinary-Cancers/Renal-Cell-Carcinoma/eUpdate-Renal-Cell-Carcinoma-Treatment-Recommendations>
- Escudier, B., Porta, C., Schmidinger, M., Rioux-Leclercq, N., et al. Renal cell carcinoma: ESMO Clinical Practice Guidelines for diagnosis, treatment and follow-up. *Ann Oncol*, 2016, 27(suppl 5):v58-v68
- Espindola, M. S., Habieli, D. M., Narayanan, R., Jones, I., et al. Targeting of TAM Receptors Ameliorates Fibrotic Mechanisms in Idiopathic Pulmonary Fibrosis. *Am J Respir Crit Care Med*, 2018, 197(11):1443-1456
- Fang, Y., Wei, J., Cao, J., Zhao, H., et al. Protein expression of ZEB2 in renal cell carcinoma and its prognostic significance in patient survival. *PLoS One*, 2013, 8(5):e62558
- Farris, A. B. & Alpers, C. E. What is the best way to measure renal fibrosis?: A pathologist's perspective. *Kidney Int Suppl*, 2014, 4(1):9-15
- Ferenbach, D. A. & Bonventre, J. V. Mechanisms of maladaptive repair after AKI leading to accelerated kidney ageing and CKD. *Nat Rev Nephrol*, 2015, 11(5):264-76
- Fiebeler, A., Park, J. K., Muller, D. N., Lindschau, C., et al. Growth arrest specific protein 6/Axl signaling in human inflammatory renal diseases. *Am J Kidney Dis*, 2004, 43(2):286-95
- Finne, K., Vethe, H., Skogstrand, T., Leh, S., et al. Proteomic analysis of formalin-fixed paraffin-embedded glomeruli suggests depletion of glomerular filtration barrier proteins in two-kidney, one-clip hypertensive rats. *Nephrol Dial Transplant*, 2014, 29(12):2217-27
- Frew, I. J. & Moch, H. A clearer view of the molecular complexity of clear cell renal cell carcinoma. *Annu Rev Pathol*, 2015, 10263-89
- Fuhrman, S. A., Lasky, L. C. & Limas, C. Prognostic significance of morphologic parameters in renal cell carcinoma. *Am J Surg Pathol*, 1982, 6(7):655-63
- Gay, C. M., Balaji, K. & Byers, L. A. Giving AXL the axe: targeting AXL in human malignancy. *Br J Cancer*, 2017, 116(4):415-423
- GBD. Global Burden of Disease 2013 Mortality and Causes of Death Collaborators: Global, regional, and national age-sex specific all-cause and cause-specific mortality for 240 causes of death, 1990-2013: a systematic analysis for the Global Burden of Disease Study 2013. *Lancet*, 2015, 385(9963):117-71
- Genovese, F., Manresa, A. A., Leeming, D. J., Karsdal, M. A., et al. The extracellular matrix in the kidney: a source of novel non-invasive biomarkers of kidney fibrosis? *Fibrogenesis Tissue Repair*, 2014, 7(1):4
- Gerharz, C. D., Moll, R., Storkel, S., Ramp, U., et al. Ultrastructural appearance and cytoskeletal architecture of the clear, chromophilic, and chromophobe types of human renal cell carcinoma in vitro. *Am J Pathol*, 1993, 142(3):851-9
- Gerlinger, M., Rowan, A. J., Horswell, S., Math, M., et al. Intratumor heterogeneity and branched evolution revealed by multiregion sequencing. *N Engl J Med*, 2012, 366(10):883-892
- Gewin, L., Bulus, N., Mermaugh, G., Moeckel, G., et al. TGF-beta receptor deletion in the renal collecting system exacerbates fibrosis. *J Am Soc Nephrol*, 2010, 21(8):1334-43
- Ghayur, M. N., Krepinsky, J. C. & Janssen, L. J. Contractility of the Renal Glomerulus and Mesangial Cells: Lingering Doubts and Strategies for the Future. *Med Hypotheses Res*, 2008, 4(1):1-9
- Ghosh, A. K. & Vaughan, D. E. PAI-1 in tissue fibrosis. *J Cell Physiol*, 2012, 227(2):493-507
- Gjerdrum, C., Tiron, C., Hoiby, T., Stefansson, I., et al. Axl is an essential epithelial-to-mesenchymal transition-induced regulator of breast cancer metastasis and patient survival. *Proc Natl Acad Sci U S A*, 2010, 107(3):1124-9
- Go, A. S., Chertow, G. M., Fan, D., McCulloch, C. E., et al. Chronic kidney disease and the risks of death, cardiovascular events, and hospitalization. *N Engl J Med*, 2004, 351(13):1296-305

- Graham, D. K., DeRyckere, D., Davies, K. D. & Earp, H. S. The TAM family: phosphatidylserine sensing receptor tyrosine kinases gone awry in cancer. *Nat Rev Cancer*, 2014, 14(12):769-85
- Grande, M. T., Sanchez-Laorden, B., Lopez-Blau, C., De Frutos, C. A., et al. Snail1-induced partial epithelial-to-mesenchymal transition drives renal fibrosis in mice and can be targeted to reverse established disease. *Nat Med*, 2015, 21(9):989-97
- Greenburg, G. & Hay, E. D. Epithelia suspended in collagen gels can lose polarity and express characteristics of migrating mesenchymal cells. *J Cell Biol*, 1982, 95(1):333-9
- Griffith, M., Walker, J. R., Spies, N. C., Ainscough, B. J., et al. Informatics for RNA Sequencing: A Web Resource for Analysis on the Cloud. *PLoS Comput Biol*, 2015, 11(8):e1004393
- Groger, C. J., Grubinger, M., Waldhor, T., Vierlinger, K., et al. Meta-analysis of gene expression signatures defining the epithelial to mesenchymal transition during cancer progression. *PLoS One*, 2012, 7(12):e51136
- Guarch, R., Lawrie, C. H., Larrinaga, G., Angulo, J. C., et al. High levels of intratumor heterogeneity characterize the expression of epithelial-mesenchymal transition markers in high-grade clear cell renal cell carcinoma. *Ann Diagn Pathol*, 2018, 3427-30
- Guo, J. K., Marlier, A., Shi, H., Shan, A., et al. Increased tubular proliferation as an adaptive response to glomerular albuminuria. *J Am Soc Nephrol*, 2012, 23(3):429-37
- Gustafsson, A., Bostrom, A. K., Ljungberg, B., Axelson, H., et al. Gas6 and the receptor tyrosine kinase Axl in clear cell renal cell carcinoma. *PLoS One*, 2009a, 4(10):e7575
- Gustafsson, A., Martuszewska, D., Johansson, M., Ekman, C., et al. Differential expression of Axl and Gas6 in renal cell carcinoma reflecting tumor advancement and survival. *Clin Cancer Res*, 2009b, 15(14):4742-9
- Haas, N. B., Manola, J., Dutcher, J. P., Flaherty, K. T., et al. Adjuvant Treatment for High-Risk Clear Cell Renal Cancer: Updated Results of a High-Risk Subset of the ASSURE Randomized Trial. *JAMA Oncol*, 2017, 3(9):1249-1252
- Haase, V. H. The VHL/HIF oxygen-sensing pathway and its relevance to kidney disease. *Kidney Int*, 2006, 69(8):1302-7
- Hamm, L. L., Nakhoul, N. & Hering-Smith, K. S. Acid-Base Homeostasis. *Clin J Am Soc Nephrol*, 2015, 10(12):2232-42
- Heng, D. Y., Xie, W., Regan, M. M., Harshman, L. C., et al. External validation and comparison with other models of the International Metastatic Renal-Cell Carcinoma Database Consortium prognostic model: a population-based study. *Lancet Oncol*, 2013, 14(2):141-8
- Hertig, A., Verine, J., Mougenot, B., Jouanneau, C., et al. Risk factors for early epithelial to mesenchymal transition in renal grafts. *Am J Transplant*, 2006, 6(12):2937-46
- Hill, N. R., Fatoba, S. T., Oke, J. L., Hirst, J. A., et al. Global Prevalence of Chronic Kidney Disease - A Systematic Review and Meta-Analysis. *PLoS One*, 2016, 11(7):e0158765
- Holland, S. J., Pan, A., Franci, C., Hu, Y., et al. R428, a selective small molecule inhibitor of Axl kinase, blocks tumor spread and prolongs survival in models of metastatic breast cancer. *Cancer Res*, 2010, 70(4):1544-54
- Horbelt, M., Lee, S. Y., Mang, H. E., Knipe, N. L., et al. Acute and chronic microvascular alterations in a mouse model of ischemic acute kidney injury. *Am J Physiol Renal Physiol*, 2007, 293(3):F688-95
- Hruska, K. A., Guo, G., Wozniak, M., Martin, D., et al. Osteogenic protein-1 prevents renal fibrogenesis associated with ureteral obstruction. *Am J Physiol Renal Physiol*, 2000, 279(1):F130-43
- Hsu, R. K. & Powe, N. R. Recent trends in the prevalence of chronic kidney disease: not the same old song. *Curr Opin Nephrol Hypertens*, 2017, 26(3):187-196
- Hugo, W., Zaretsky, J. M., Sun, L., Song, C., et al. Genomic and Transcriptomic Features of Response to Anti-PD-1 Therapy in Metastatic Melanoma. *Cell*, 2016, 165(1):35-44
- Hyde, G. D., Taylor, R. F., Ashton, N., Borland, S. J., et al. Axl tyrosine kinase protects against tubulo-interstitial apoptosis and progression of renal failure in a murine model of chronic kidney disease and hyperphosphataemia. *PLoS One*, 2014, 9(7):e102096
- Illumina. Evaluating RNA Quality from FFPE Samples. Guidelines for obtaining high-quality RNA sequencing results from degraded RNA with the TruSeq® RNA Access Library Preparation Kit (Technical Note: RNA Sequencing). Illumina, Inc, 2014a, 1-5. Pub. No. 470-2014-001, <http://www.illumina.com/documents/products/technotes/technote-truseq-rna-access.pdf>

- Illumina. TruSeq RNA Access Library Prep Guide. Illumina, Inc, 2014b, 1-96. Pub. No. RS-301-9001DOC, https://support.illumina.com/content/dam/illumina-support/documentation/chemistry_documentation/samplepreps_truseq/truseq_rnaaccess/truseq_rna-access-library-prep-guide-15049525-b.pdf
- Illumina. An introduction to Next-Generation Sequencing Technology. Illumina, Inc, 2017, 1-16. Pub. No. 770-2012-008-B, https://www.illumina.com/content/dam/illumina-marketing/documents/products/illumina_sequencing_introduction.pdf
- International Human Genome Sequencing, Consortium. Finishing the euchromatic sequence of the human genome. *Nature*, 2004, 431(7011):931-45
- Iwano, M., Plieth, D., Danoff, T. M., Xue, C., et al. Evidence that fibroblasts derive from epithelium during tissue fibrosis. *J Clin Invest*, 2002, 110(3):341-50
- Janmaat, C. J., van Diepen, M., Gasparini, A., Evans, M., et al. Lower serum calcium is independently associated with CKD progression. *Sci Rep*, 2018, 8(1):5148
- Janning, M., Ben-Batalla, I. & Loges, S. Axl inhibition: a potential road to a novel acute myeloid leukemia therapy? *Expert Rev Hematol*, 2015, 8(2):135-8
- Janssen, J. W., Schulz, A. S., Steenvoorden, A. C., Schmidberger, M., et al. A novel putative tyrosine kinase receptor with oncogenic potential. *Oncogene*, 1991, 6(11):2113-20
- Jia, L. F., Wei, S. B., Mitchelson, K., Gao, Y., et al. miR-34a inhibits migration and invasion of tongue squamous cell carcinoma via targeting MMP9 and MMP14. *PLoS One*, 2014, 9(9):e108435
- Jimbo, T., Taira, T., Komatsu, K., Kumazawa, K, et al. 395P-DS-1205b, a novel, selective, small-molecule inhibitor of AXL, delays the onset of resistance and overcomes acquired resistance to EGFR-TKIs in a human EGFR mutant NSCLC T790M negative xenograft model. *Annals of Oncology*, 2017, 28(suppl_5):v122-v141
- Kaelin, W. G., Jr. The von Hippel-Lindau tumour suppressor protein: O2 sensing and cancer. *Nat Rev Cancer*, 2008, 8(11):865-73
- Kaelin, W. G., Jr. The von Hippel-Lindau Tumor Suppressor Protein. *Annual Review of Cancer Biology*, 2018, 291-109
- Kainz, A., Hronsky, M., Stel, V. S., Jager, K. J., et al. Prediction of prevalence of chronic kidney disease in diabetic patients in countries of the European Union up to 2025. *Nephrol Dial Transplant*, 2015, 30 Suppl 4iv113-8
- Kalluri, R. & Weinberg, R. A. The basics of epithelial-mesenchymal transition. *J Clin Invest*, 2009, 119(6):1420-8
- Kane, C. J., Mallin, K., Ritchey, J., Cooperberg, M. R., et al. Renal cell cancer stage migration: analysis of the National Cancer Data Base. *Cancer*, 2008, 113(1):78-83
- Kang, H. M., Ahn, S. H., Choi, P., Ko, Y. A., et al. Defective fatty acid oxidation in renal tubular epithelial cells has a key role in kidney fibrosis development. *Nat Med*, 2015, 21(1):37-46
- Kariolis, M. S., Miao, Y. R., Diep, A., Nash, S. E., et al. Inhibition of the GAS6/AXL pathway augments the efficacy of chemotherapies. *J Clin Invest*, 2017, 127(1):183-198
- KDIGO. KDIGO 2012 Clinical Practice Guideline for the Evaluation and Management of Chronic Kidney Disease. *Kidney International*, 2013, 3(1):1-163
- Keller, G., Zimmer, G., Mall, G., Ritz, E., et al. Nephron number in patients with primary hypertension. *N Engl J Med*, 2003, 348(2):101-8
- King, T. E., Jr., Pardo, A. & Selman, M. Idiopathic pulmonary fibrosis. *Lancet*, 2011, 378(9807):1949-61
- Knoop, T., Vikse, B. E., Mwakimonga, A., Leh, S., et al. Long-term outcome in 145 patients with assumed benign immunoglobulin A nephropathy. *Nephrol Dial Transplant*, 2017, 32(11):1841-1850
- Kocjan, B. J., Hosnjak, L. & Poljak, M. Commercially available kits for manual and automatic extraction of nucleic acids from formalin-fixed, paraffin-embedded (FFPE) tissues. *Acta Dermatovenerol Alp Pannonica Adriat*, 2015, 24(3):47-53
- Kopp, J. B. TGF-beta signaling and the renal tubular epithelial cell: too much, too little, and just right. *J Am Soc Nephrol*, 2010, 21(8):1241-3
- Korshunov, V. A. Axl-dependent signalling: a clinical update. *Clin Sci (Lond)*, 2012, 122(8):361-8
- Kuncio, G. S., Neilson, E. G. & Havery, T. Mechanisms of tubulointerstitial fibrosis. *Kidney Int*, 1991, 39(3):550-6
- Lamouille, S., Xu, J. & Derynck, R. Molecular mechanisms of epithelial-mesenchymal transition. *Nat Rev Mol Cell Biol*, 2014, 15(3):178-96

- Larsen, I. K., Moller, B, Johannesen, T. B., Laronningen, S, et al. Cancer Registry of Norway. Cancer in Norway 2016 - Cancer incidence, mortality, survival and prevalence in Norway. *Cancer registry of Norway*, 2017, 1-103
- Lathia, J. D. & Liu, H. Overview of Cancer Stem Cells and Stemness for Community Oncologists. *Target Oncol*, 2017, 12(4):387-399
- LeBleu, V. S., Taduri, G., O'Connell, J., Teng, Y., et al. Origin and function of myofibroblasts in kidney fibrosis. *Nat Med*, 2013, 19(8):1047-53
- Lee, J. E., Hankinson, S. E. & Cho, E. Reproductive factors and risk of renal cell cancer: the Nurses' Health Study. *Am J Epidemiol*, 2009, 169(10):1243-50
- Lee, J. E., Hunter, D. J., Spiegelman, D., Adami, H. O., et al. Alcohol intake and renal cell cancer in a pooled analysis of 12 prospective studies. *J Natl Cancer Inst*, 2007, 99(10):801-10
- Lee, S., Huen, S., Nishio, H., Nishio, S., et al. Distinct macrophage phenotypes contribute to kidney injury and repair. *J Am Soc Nephrol*, 2011, 22(2):317-26
- Leibovich, B. C., Blute, M. L., Cheville, J. C., Lohse, C. M., et al. Prediction of progression after radical nephrectomy for patients with clear cell renal cell carcinoma: a stratification tool for prospective clinical trials. *Cancer*, 2003, 97(7):1663-71
- Lemley, K. V. & Kriz, W. Anatomy of the renal interstitium. *Kidney Int*, 1991, 39(3):370-81
- Levey, A. S., Stevens, L. A., Schmid, C. H., Zhang, Y. L., et al. A new equation to estimate glomerular filtration rate. *Ann Intern Med*, 2009, 150(9):604-12
- Levi, F., Ferlay, J., Galeone, C., Lucchini, F., et al. The changing pattern of kidney cancer incidence and mortality in Europe. *BJU Int*, 2008, 101(8):949-58
- Levin, A., Tonelli, M., Bonventre, J., Coresh, J., et al. Global kidney health 2017 and beyond: a roadmap for closing gaps in care, research, and policy. *Lancet*, 2017, 390(10105):1888-1917
- Liang, L., Sun, H., Zhang, W., Zhang, M., et al. Meta-Analysis of EMT Datasets Reveals Different Types of EMT. *PLoS One*, 2016, 11(6):e0156839
- Liu, B. C., Tang, T. T., Lv, L. L. & Lan, H. Y. Renal tubule injury: a driving force toward chronic kidney disease. *Kidney Int*, 2018, 93(3):568-579
- Liu, E., Hjelle, B. & Bishop, J. M. Transforming genes in chronic myelogenous leukemia. *Proc Natl Acad Sci U S A*, 1988, 85(6):1952-6
- Liu, F. X., Rutherford, P., Smoyer-Tomic, K., Prichard, S., et al. A global overview of renal registries: a systematic review. *BMC Nephrol*, 2015, 1631
- Ljungberg, B., Bensalah, K., Canfield, S., Dabestani, S., et al. EAU guidelines on renal cell carcinoma: 2014 update. *Eur Urol*, 2015, 67(5):913-24
- Lopez-Novoa, J. M. & Nieto, M. A. Inflammation and EMT: an alliance towards organ fibrosis and cancer progression. *EMBO Mol Med*, 2009, 1(6-7):303-14
- Lovisa, S., LeBleu, V. S., Tampe, B., Sugimoto, H., et al. Epithelial-to-mesenchymal transition induces cell cycle arrest and parenchymal damage in renal fibrosis. *Nat Med*, 2015, 21(9):998-1009
- Lovisa, S., Zeisberg, M. & Kalluri, R. Partial Epithelial-to-Mesenchymal Transition and Other New Mechanisms of Kidney Fibrosis. *Trends Endocrinol Metab*, 2016, 27(10):681-695
- Lowrance, W. T., Thompson, R. H., Yee, D. S., Kaag, M., et al. Obesity is associated with a higher risk of clear-cell renal cell carcinoma than with other histologies. *BJU Int*, 2010, 105(1):16-20
- Lu, Y., Stamm, C., Nobre, D., Pruijm, M., et al. Changing trends in end-stage renal disease patients with diabetes. *Swiss Med Wkly*, 2017, 147:w14458
- Ludwig, K. F., Du, W., Sorrelle, N. B., Wnuk-Lipinska, K., et al. Small-Molecule Inhibition of Axl Targets Tumor Immune Suppression and Enhances Chemotherapy in Pancreatic Cancer. *Cancer Res*, 2018, 78(1):246-255
- Lundberg, E., Fagerberg, L., Klevebring, D., Matic, I., et al. Defining the transcriptome and proteome in three functionally different human cell lines. *Mol Syst Biol*, 2010, 6, article number 450
- Ma, L. J. & Fogo, A. B. PAI-1 and kidney fibrosis. *Front Biosci (Landmark Ed)*, 2009, 142028-41
- Mack, M. & Yanagita, M. Origin of myofibroblasts and cellular events triggering fibrosis. *Kidney Int*, 2015, 87(2):297-307
- Mahimkar, R., Alfonso-Jaume, M. A., Cape, L. M., Dahiya, R., et al. Graded activation of the MEK1/MT1-MMP axis determines renal epithelial cell tumor phenotype. *Carcinogenesis*, 2011, 32(12):1806-14

- Maisonneuve, P., Agodoa, L., Gellert, R., Stewart, J. H., et al. Cancer in patients on dialysis for end-stage renal disease: an international collaborative study. *Lancet*, 1999, 354(9173):93-9
- Mak, M. P., Tong, P., Diao, L., Cardnell, R. J., et al. A Patient-Derived, Pan-Cancer EMT Signature Identifies Global Molecular Alterations and Immune Target Enrichment Following Epithelial-to-Mesenchymal Transition. *Clin Cancer Res*, 2016, 22(3):609-20
- Massague, J. TGFbeta in Cancer. *Cell*, 2008, 134(2):215-30
- Matsushita, K., van der Velde, M., Astor, B. C., Woodward, M., et al. Chronic Kidney Disease Prognosis Consortium: Association of estimated glomerular filtration rate and albuminuria with all-cause and cardiovascular mortality in general population cohorts: a collaborative meta-analysis. *Lancet*, 2010, 375(9731):2073-81
- Meertens, L., Labeau, A., Dejarnac, O., Cipriani, S., et al. Axl Mediates ZIKA Virus Entry in Human Glial Cells and Modulates Innate Immune Responses. *Cell Rep*, 2017, 18(2):324-333
- Mejean, A., Ravaud, A., Thezenas, S., Colas, S., et al. Sunitinib Alone or after Nephrectomy in Metastatic Renal-Cell Carcinoma. *N Engl J Med*, 2018, 379(5):417-427
- Meng, X. M., Chung, A. C. & Lan, H. Y. Role of the TGF-beta/BMP-7/Smad pathways in renal diseases. *Clin Sci (Lond)*, 2013, 124(4):243-54
- Meng, X. M., Nikolic-Paterson, D. J. & Lan, H. Y. TGF-beta: the master regulator of fibrosis. *Nat Rev Nephrol*, 2016, 12(6):325-38
- Meng, X. M., Zhang, Y., Huang, X. R., Ren, G. L., et al. Treatment of renal fibrosis by rebalancing TGF-beta/Smad signaling with the combination of asiatic acid and naringenin. *Oncotarget*, 2015, 6(35):36984-97
- Meyer, A. S., Zweemer, A. J. & Lauffenburger, D. A. The AXL Receptor is a Sensor of Ligand Spatial Heterogeneity. *Cell Syst*, 2015, 1(1):25-36
- Mezni, I., Galichon, P., Mongi Bacha, M., Xu-Dubois, Y. C., et al. Urinary mRNA analysis of biomarkers to epithelial mesenchymal transition of renal allograft. *Nephrol Ther*, 2018, 14(3):153-161
- Moch, H., Cubilla, A. L., Humphrey, P. A., Reuter, V. E., et al. The 2016 WHO Classification of Tumours of the Urinary System and Male Genital Organs-Part A: Renal, Penile, and Testicular Tumours. *Eur Urol*, 2016, 70(1):93-105
- Moore, B. B., Murray, L., Das, A., Wilke, C. A., et al. The role of CCL12 in the recruitment of fibrocytes and lung fibrosis. *Am J Respir Cell Mol Biol*, 2006, 35(2):175-81
- Moreno, J. A., Yuste, C., Gutierrez, E., Sevillano, A. M., et al. Haematuria as a risk factor for chronic kidney disease progression in glomerular diseases: A review. *Pediatr Nephrol*, 2016, 31(4):523-33
- Mosser, D. M. & Edwards, J. P. Exploring the full spectrum of macrophage activation. *Nat Rev Immunol*, 2008, 8(12):958-69
- Motzer, R. J., Haas, N. B., Donskov, F., Gross-Goupil, M., et al. Randomized Phase III Trial of Adjuvant Pazopanib Versus Placebo After Nephrectomy in Patients With Localized or Locally Advanced Renal Cell Carcinoma. *J Clin Oncol*, 2017, 35(35):3916-3923
- Motzer, R. J., Ravaud, A., Patard, J. J., Pandha, H. S., et al. Adjuvant Sunitinib for High-risk Renal Cell Carcinoma After Nephrectomy: Subgroup Analyses and Updated Overall Survival Results. *Eur Urol*, 2018a, 73(1):62-68
- Motzer, R. J., Tannir, N. M., McDermott, D. F., Aren Frontera, O., et al. Nivolumab plus Ipilimumab versus Sunitinib in Advanced Renal-Cell Carcinoma. *N Engl J Med*, 2018b, 378(14):1277-1290
- Mount, D. B. Thick ascending limb of the loop of Henle. *Clin J Am Soc Nephrol*, 2014, 9(11):1974-86
- Myers, S. H., Brunton, V. G. & Unciti-Broceta, A. AXL Inhibitors in Cancer: A Medicinal Chemistry Perspective. *J Med Chem*, 2016, 59(8):3593-608
- Nagai, K., Arai, H., Yanagita, M., Matsubara, T., et al. Growth arrest-specific gene 6 is involved in glomerular hypertrophy in the early stage of diabetic nephropathy. *J Biol Chem*, 2003, 278(20):18229-34
- Neelisetty, S., Alford, C., Reynolds, K., Woodbury, L., et al. Renal fibrosis is not reduced by blocking transforming growth factor-beta signaling in matrix-producing interstitial cells. *Kidney Int*, 2015, 88(3):503-14
- Nieto, M. A., Huang, R. Y., Jackson, R. A. & Thiery, J. P. EMT: 2016. *Cell*, 2016, 166(1):21-45
- Nigam, S. K., Wu, W., Bush, K. T., Hoenig, M. P., et al. Handling of Drugs, Metabolites, and Uremic Toxins by Kidney Proximal Tubule Drug Transporters. *Clin J Am Soc Nephrol*, 2015, 10(11):2039-49

- O'Bryan, J. P., Frye, R. A., Cogswell, P. C., Neubauer, A., et al. *axl*, a transforming gene isolated from primary human myeloid leukemia cells, encodes a novel receptor tyrosine kinase. *Mol Cell Biol*, 1991, 11(10):5016-31
- Ochodnický, P., Lattenist, L., Ahdi, M., Kers, J., et al. Increased Circulating and Urinary Levels of Soluble TAM Receptors in Diabetic Nephropathy. *Am J Pathol*, 2017, 187(9):1971-1983
- Ogurtsova, K., da Rocha Fernandes, J. D., Huang, Y., Linnenkamp, U., et al. IDF Diabetes Atlas: Global estimates for the prevalence of diabetes for 2015 and 2040. *Diabetes Res Clin Pract*, 2017, 12840-50
- Olson, J, L. Renal Disease Caused by Hypertension. In Jennette, C. E., et al. (Eds.) *Heptinstall's Pathology of the Kidney, 7th Edition*. Philadelphia, PA, USA. Wolters Kluwer. 2015, Vol. 2, 849-883. 978-1-4511-4411-6
- Olson, J, L. & Laszik, Z, G. Diabetic nephropathy. In Jennette, C. E., et al. (Eds.) *Heptinstall's Pathology of the Kidney, 7th Edition*. Philadelphia, PA, USA. Wolters Kluwer. 2015, Vol. 2, 897-933. 978-1-4511-4411-6
- Ovadya, Y. & Krizhanovsky, V. A new Twist in kidney fibrosis. *Nat Med*, 2015, 21(9):975-7
- Palmer, L. G. & Schnermann, J. Integrated control of Na transport along the nephron. *Clin J Am Soc Nephrol*, 2015, 10(4):676-87
- Palsdottir, H. B., Hardarson, S., Petursdottir, V., Jonsson, A., et al. Incidental detection of renal cell carcinoma is an independent prognostic marker: results of a long-term, whole population study. *J Urol*, 2012, 187(1):48-53
- Pantuck, A. J., An, J., Liu, H. & Rettig, M. B. NF-kappaB-dependent plasticity of the epithelial to mesenchymal transition induced by Von Hippel-Lindau inactivation in renal cell carcinomas. *Cancer Res*, 2010, 70(2):752-61
- Parker, W. P., Cheville, J. C., Frank, I., Zaid, H. B., et al. Application of the Stage, Size, Grade, and Necrosis (SSIGN) Score for Clear Cell Renal Cell Carcinoma in Contemporary Patients. *Eur Urol*, 2017, 71(4):665-673
- Patard, J. J., Leray, E., Rioux-Leclercq, N., Cindolo, L., et al. Prognostic value of histologic subtypes in renal cell carcinoma: a multicenter experience. *J Clin Oncol*, 2005, 23(12):2763-71
- Paunas, T. I. F., Finne, K., Leh, S., Marti, H. P., et al. Glomerular abundance of complement proteins characterized by proteomic analysis of laser-captured microdissected glomeruli associates with progressive disease in IgA nephropathy. *Clin Proteomics*, 2017, 1430
- Pearce, D., Soundararajan, R., Trimpert, C., Kashlan, O. B., et al. Collecting duct principal cell transport processes and their regulation. *Clin J Am Soc Nephrol*, 2015, 10(1):135-46
- Pennacchietti, S., Michieli, P., Galluzzo, M., Mazzone, M., et al. Hypoxia promotes invasive growth by transcriptional activation of the met protooncogene. *Cancer Cell*, 2003, 3(4):347-61
- Perazella, M. A., Dreicer, R. & Rosner, M. H. Renal cell carcinoma for the nephrologist. *Kidney Int*, 2018, 94(3):471-483
- Pichler, M., Hutterer, G. C., Chromecki, T. F., Jesche, J., et al. Renal cell carcinoma stage migration in a single European centre over 25 years: effects on 5- and 10-year metastasis-free survival. *Int Urol Nephrol*, 2012, 44(4):997-1004
- Pollak, M. R., Quaggin, S. E., Hoenig, M. P. & Dworkin, L. D. The glomerulus: the sphere of influence. *Clin J Am Soc Nephrol*, 2014, 9(8):1461-9
- Ponomarenko, E. A., Poverennaya, E. V., Ilgisonis, E. V., Pyatnitskiy, M. A., et al. The Size of the Human Proteome: The Width and Depth. *Int J Anal Chem*, 2016, article ID 7436849
- Poplawski, P., Rybicka, B., Boguslawska, J., Rodzik, K., et al. Induction of type 1 iodothyronine deiodinase expression inhibits proliferation and migration of renal cancer cells. *Mol Cell Endocrinol*, 2017, 44258-67
- Powles, T., Albiges, L., Staehler, M., Bensalah, K., et al. Updated European Association of Urology Guidelines Recommendations for the Treatment of First-line Metastatic Clear Cell Renal Cancer. *Eur Urol*, 2017, 73311-315
- Puri, T. S., Shakaib, M. I., Chang, A., Mathew, L., et al. Chronic kidney disease induced in mice by reversible unilateral ureteral obstruction is dependent on genetic background. *Am J Physiol Renal Physiol*, 2010, 298(4):F1024-32
- Ranjit, S., Dobrinskikh, E., Montford, J., Dvornikov, A., et al. Label-free fluorescence lifetime and second harmonic generation imaging microscopy improves quantification of experimental renal fibrosis. *Kidney Int*, 2016, 90(5):1123-1128
- Rastaldi, M. P., Ferrario, F., Giardino, L., Dell'Antonio, G., et al. Epithelial-mesenchymal transition of tubular epithelial cells in human renal biopsies. *Kidney Int*, 2002, 62(1):137-46

- Rasti, A., Madjd, Z., Abolhasani, M., Mehrazma, M., et al. Cytoplasmic expression of Twist1, an EMT-related transcription factor, is associated with higher grades renal cell carcinomas and worse progression-free survival in clear cell renal cell carcinoma. *Clin Exp Med*, 2017, 18(2):177-190
- Ravaud, A., Motzer, R. J., Pandha, H. S., George, D. J., et al. Adjuvant Sunitinib in High-Risk Renal-Cell Carcinoma after Nephrectomy. *N Engl J Med*, 2016, 375(23):2246-2254
- Read, S. A., Tay, E. S., Shahidi, M., O'Connor, K. S., et al. Hepatitis C Virus Driven AXL Expression Suppresses the Hepatic Type I Interferon Response. *PLoS One*, 2015, 10(8):e0136227
- Reilly, R. F. & Ellison, D. H. Mammalian distal tubule: physiology, pathophysiology, and molecular anatomy. *Physiol Rev*, 2000, 80(1):277-313
- Reisaeter, A. V. Annual Report 2016. The Norwegian Renal Registry (Norsk Nyreregister). Renal Unit, OUS-Rikshospitalet, Oslo, Norway, 2016, 1-14.
<http://www.nephro.no/registry.html>
- Richeldi, L., Collard, H. R. & Jones, M. G. Idiopathic pulmonary fibrosis. *Lancet*, 2017, 389(10082):1941-1952
- Rini, B. I. & Atkins, M. B. Resistance to targeted therapy in renal-cell carcinoma. *Lancet Oncol*, 2009, 10(10):992-1000
- Rockey, D. C., Bell, P. D. & Hill, J. A. Fibrosis--A Common Pathway to Organ Injury and Failure. *N Engl J Med*, 2015, 373(1):96
- Rodder, S., Scherer, A., Korner, M. & Marti, H. P. A subset of metzincins and related genes constitutes a marker of human solid organ fibrosis. *Virchows Arch*, 2011, 458(4):487-96
- Rodder, S., Scherer, A., Raulf, F., Berthier, C. C., et al. Renal allografts with IF/TA display distinct expression profiles of metzincins and related genes. *Am J Transplant*, 2009, 9(3):517-26
- Rohrmann, S., Linseisen, J., Overvad, K., Lund Wurtz, A. M., et al. Meat and fish consumption and the risk of renal cell carcinoma in the European prospective investigation into cancer and nutrition. *Int J Cancer*, 2015, 136(5):E423-31
- Ruan, H., Li, X., Yang, H., Song, Z., et al. Enhanced expression of caveolin-1 possesses diagnostic and prognostic value and promotes cell migration, invasion and sunitinib resistance in the clear cell renal cell carcinoma. *Exp Cell Res*, 2017, 358(2):269-278
- Salmasi, A., Faiena, I., Drakaki, A. & Pantuck, A. J. Re: Adjuvant Sunitinib in High-risk Renal-cell Carcinoma After Nephrectomy. *Eur Urol*, 2018, 74(1):119-121
- Schmidt, L. S. & Linehan, W. M. Molecular genetics and clinical features of Birt-Hogg-Dube syndrome. *Nat Rev Urol*, 2015, 12(10):558-69
- Schneider, V. A., Graves-Lindsay, T., Howe, K., Bouk, N., et al. Evaluation of GRCh38 and de novo haploid genome assemblies demonstrates the enduring quality of the reference assembly. *Genome Res*, 2017, 27(5):849-864
- Schoumacher, M. & Burbridge, M. Key Roles of AXL and MER Receptor Tyrosine Kinases in Resistance to Multiple Anticancer Therapies. *Curr Oncol Rep*, 2017, 19(3):19
- Schulman, G., Berl, T., Beck, G. J., Remuzzi, G., et al. Risk factors for progression of chronic kidney disease in the EPPIC trials and the effect of AST-120. *Clin Exp Nephrol*, 2018, 22(2):299-308
- Shaw, T. J. & Martin, P. Wound repair: a showcase for cell plasticity and migration. *Curr Opin Cell Biol*, 2016, 4229-37
- Shen, S. S., Krishna, B., Chirala, R., Amato, R. J., et al. Kidney-specific cadherin, a specific marker for the distal portion of the nephron and related renal neoplasms. *Mod Pathol*, 2005, 18(7):933-40
- Sheridan, C. First Axl inhibitor enters clinical trials. *Nat Biotechnol*, 2013, 31(9):775-6
- Shuch, B., Amin, A., Armstrong, A. J., Eble, J. N., et al. Understanding pathologic variants of renal cell carcinoma: distilling therapeutic opportunities from biologic complexity. *Eur Urol*, 2015, 67(1):85-97
- Siegel, R. L., Miller, K. D. & Jemal, A. Cancer statistics, 2018. *CA Cancer J Clin*, 2018, 68(1):7-30
- Silva, G. B. D. Junior, Pinto, J. R., Barros, E. J. G., Farias, G. M. N., et al. Kidney involvement in malaria: an update. *Rev Inst Med Trop Sao Paulo*, 2017, 59e53
- Skogstrand, T., Leh, S., Paliege, A., Reed, R. K., et al. Arterial damage precedes the development of interstitial damage in the nonclipped kidney of two-kidney, one-clip hypertensive rats. *J Hypertens*, 2013, 31(1):152-9
- Skrunes, R., Svarstad, E., Reisaeter, A. V., Marti, H. P., et al. End Stage Renal Disease Predicts Increased Risk of Death in First Degree Relatives in the Norwegian Population. *PLoS One*, 2016, 11(11):e0165026

- Souma, T., Suzuki, N. & Yamamoto, M. Renal erythropoietin-producing cells in health and disease. *Front Physiol*, 2015, 6:167
- Sprangers, B., Nair, V., Launay-Vacher, Vincent, Riella, Leonardo V., et al. Risk factors associated with post-kidney transplant malignancies: an article from the Cancer-Kidney International Network. *Clinical Kidney Journal*, 2017, 1-15
- Spruessel, A., Steimann, G., Jung, M., Lee, S. A., et al. Tissue ischemia time affects gene and protein expression patterns within minutes following surgical tumor excision. *Biotechniques*, 2004, 36(6):1030-7
- Stanifer, J. W., Jing, B., Tolan, S., Helmke, N., et al. The epidemiology of chronic kidney disease in sub-Saharan Africa: a systematic review and meta-analysis. *Lancet Glob Health*, 2014, 2(3):e174-81
- Stanifer, J. W., Muir, A., Jafar, T. H. & Patel, U. D. Chronic kidney disease in low- and middle-income countries. *Nephrol Dial Transplant*, 2016, 31(6):868-74
- Staufer, K., Dengler, M., Huber, H., Marculescu, R., et al. The non-invasive serum biomarker soluble Axl accurately detects advanced liver fibrosis and cirrhosis. *Cell Death Dis*, 2017, 8(10):e3135
- Stitt, T. N., Conn, G., Gore, M., Lai, C., et al. The anticoagulation factor protein S and its relative, Gas6, are ligands for the Tyro 3/Axl family of receptor tyrosine kinases. *Cell*, 1995, 80(4):661-70
- Strupler, M., Pena, A. M., Hernest, M., Tharoux, P. L., et al. Second harmonic imaging and scoring of collagen in fibrotic tissues. *Opt Express*, 2007, 15(7):4054-65
- Subramanya, A. R. & Ellison, D. H. Distal convoluted tubule. *Clin J Am Soc Nephrol*, 2014, 9(12):2147-63
- Tan, T. Z., Miow, Q. H., Miki, Y., Noda, T., et al. Epithelial-mesenchymal transition spectrum quantification and its efficacy in deciphering survival and drug responses of cancer patients. *EMBO Mol Med*, 2014, 6(10):1279-93
- Tapmeier, T. T., Fearn, A., Brown, K., Chowdhury, P., et al. Pivotal role of CD4+ T cells in renal fibrosis following ureteric obstruction. *Kidney Int*, 2010, 78(4):351-62
- Theis, R. P., Dolwick Grieb, S. M., Burr, D., Siddiqui, T., et al. Smoking, environmental tobacco smoke, and risk of renal cell cancer: a population-based case-control study. *BMC Cancer*, 2008, 8:387
- Tondel, C., Vikse, B. E., Bostad, L. & Svarstad, E. Safety and complications of percutaneous kidney biopsies in 715 children and 8573 adults in Norway 1988-2010. *Clin J Am Soc Nephrol*, 2012, 7(10):1591-7
- Tsai, C. W., Lin, S. Y., Kuo, C. C. & Huang, C. C. Serum Uric Acid and Progression of Kidney Disease: A Longitudinal Analysis and Mini-Review. *PLoS One*, 2017, 12(1):e0170393
- Tsai, W. C., Wu, H. Y., Peng, Y. S., Ko, M. J., et al. Risk Factors for Development and Progression of Chronic Kidney Disease: A Systematic Review and Exploratory Meta-Analysis. *Medicine (Baltimore)*, 2016, 95(11):e3013
- Tveitars, M. K., Skogstrand, T., Leh, S., Helle, F., et al. Matrix Metalloproteinase-2 Knockout and Heterozygote Mice Are Protected from Hydronephrosis and Kidney Fibrosis after Unilateral Ureteral Obstruction. *PLoS One*, 2015, 10(12):e0143390
- Uhlen, M., Fagerberg, L., Hallstrom, B. M., Lindskog, C., et al. Proteomics. Tissue-based map of the human proteome. *Science*, 2015, 347(6220):1260419
- UICC (2017) *TNM Classification of Malignant Tumours, 8th Edition*, Wiley Blackwell. 978-1-119-26357-9
- USRDS. United States Renal Data System. USRDS annual data report 2017: Epidemiology of kidney disease in the United States. National Institute of Diabetes and Digestive and Kidney Diseases, Bethesda, MD. 2017, <https://www.usrds.org/adr.aspx>
- van der Mijn, J. C., Broxterman, H. J., Knol, J. C., Piersma, S. R., et al. Sunitinib activates Axl signaling in renal cell cancer. *Int J Cancer*, 2016, 138(12):3002-10
- van Dijk, E. L., Auger, H., Jaszczyszyn, Y. & Thernes, C. Ten years of next-generation sequencing technology. *Trends Genet*, 2014, 30(9):418-26
- Vatten, L. J., Trichopoulos, D., Holmen, J. & Nilsen, T. I. Blood pressure and renal cancer risk: the HUNT Study in Norway. *Br J Cancer*, 2007, 97(1):112-4
- Vikse, B. E., Irgens, L. M., Leivestad, T., Hallan, S., et al. Low birth weight increases risk for end-stage renal disease. *J Am Soc Nephrol*, 2008a, 19(1):151-7
- Vikse, B. E., Irgens, L. M., Leivestad, T., Skjaerven, R., et al. Preeclampsia and the risk of end-stage renal disease. *N Engl J Med*, 2008b, 359(8):800-9

- von Ahlfen, S., Missel, A., Bendrat, K. & Schlumpberger, M. Determinants of RNA quality from FFPE samples. *PLoS One*, 2007, 2(12):e1261
- Wang, F. & Xu, Y. Body mass index and risk of renal cell cancer: a dose-response meta-analysis of published cohort studies. *Int J Cancer*, 2014, 135(7):1673-86
- Wang, Z., Divanyan, A., Jour'd'heuil, F. L., Goldman, R. D., et al. Vimentin expression is required for the development of EMT-related renal fibrosis following unilateral ureteral obstruction in mice. *Am J Physiol Renal Physiol*, 2018, 315(4):F769-F780
- Weaver, V. M., Fadrowski, J. J. & Jaar, B. G. Global dimensions of chronic kidney disease of unknown etiology (CKDu): a modern era environmental and/or occupational nephropathy? *BMC Nephrol*, 2015, 16145
- Webster, A. C., Nagler, E. V., Morton, R. L. & Masson, P. Chronic Kidney Disease. *Lancet*, 2017, 389(10075):1238-1252
- Weikert, S., Boeing, H., Pischon, T., Olsen, A., et al. Fruits and vegetables and renal cell carcinoma: findings from the European prospective investigation into cancer and nutrition (EPIC). *Int J Cancer*, 2006, 118(12):3133-9
- Weikert, S., Boeing, H., Pischon, T., Weikert, C., et al. Blood pressure and risk of renal cell carcinoma in the European prospective investigation into cancer and nutrition. *Am J Epidemiol*, 2008, 167(4):438-46
- WHO. European Health Information Gateway: Autopsy rate for all deaths. Accessed on 19.06.2018. World Health Organization, Regional Office for Europe 2018. https://gateway.euro.who.int/en/indicators/hfa_545-6410-autopsy-rate-for-all-deaths/
- Wilhelm, M., Schlegl, J., Hahne, H., Gholami, A. M., et al. Mass-spectrometry-based draft of the human proteome. *Nature*, 2014, 509(7502):582-7
- Wisniewski, J. R. Proteomic sample preparation from formalin fixed and paraffin embedded tissue. *J Vis Exp*, 2013, 79:e50589
- Wnuk-Lipinska, K., Davidsen, K., Blø, M., Engelsen, A., et al. BGB324, a selective small molecule inhibitor of receptor tyrosine kinase AXL, abrogates tumor intrinsic and microenvironmental immune suppression and enhances immune checkpoint inhibitor efficacy in lung and mammary adenocarcinoma models [abstract nr 626]. In: Proceedings of the American Association for Cancer Research Annual Meeting 2017; 2017 Apr 1-5; Washington, DC. *AACR; Cancer Res*, 2017, 77(13 Suppl):
- Wolk, A., Lindblad, P. & Adami, H. O. Nutrition and renal cell cancer. *Cancer Causes Control*, 1996, 7(1):5-18
- Wozniak, M. B., Brennan, P., Brenner, D. R., Overvad, K., et al. Alcohol consumption and the risk of renal cancers in the European prospective investigation into cancer and nutrition (EPIC). *Int J Cancer*, 2015, 137(8):1953-66
- Xu-Dubois, Y. C., Galichon, P., Brocheriou, I., Baugey, E., et al. Expression of the transcriptional regulator snail1 in kidney transplants displaying epithelial-to-mesenchymal transition features. *Nephrol Dial Transplant*, 2014, 29(11):2136-44
- Yakes, F. M., Chen, J., Tan, J., Yamaguchi, K., et al. Cabozantinib (XL184), a novel MET and VEGFR2 inhibitor, simultaneously suppresses metastasis, angiogenesis, and tumor growth. *Mol Cancer Ther*, 2011, 10(12):2298-308
- Yanagita, M., Arai, H., Ishii, K., Nakano, T., et al. Gas6 regulates mesangial cell proliferation through Axl in experimental glomerulonephritis. *Am J Pathol*, 2001, 158(4):1423-32
- Yang, H. C., Zuo, Y. & Fogo, A. B. Models of chronic kidney disease. *Drug Discov Today Dis Models*, 2010, 7(1-2):13-19
- Yao, D., Dai, C. & Peng, S. Mechanism of the mesenchymal-epithelial transition and its relationship with metastatic tumor formation. *Mol Cancer Res*, 2011, 9(12):1608-20
- Yu, H., Liu, R., Ma, B., Li, X., et al. Axl receptor tyrosine kinase is a potential therapeutic target in renal cell carcinoma. *Br J Cancer*, 2015, 113(4):616-25
- Yule, M., Chisamore, M., Wnuk-Lipinska, M., Davidsen, K., et al. Combination of bemcentinib (BGB324) - a first-in-class selective, oral Axl inhibitor - with pembrolizumab in patients with triple negative breast cancer and adenocarcinoma of the lung. Poster. Presented at the ASCO-SITC Clinical Immuno-Oncology Symposium, San Francisco, CA, January 25-27 2018. 2018,
- Zeisberg, M., Hanai, J., Sugimoto, H., Mammoto, T., et al. BMP-7 counteracts TGF-beta1-induced epithelial-to-mesenchymal transition and reverses chronic renal injury. *Nat Med*, 2003, 9(7):964-8

- Zeisberg, M. & Kalluri, R. Physiology of the Renal Interstitium. *Clin J Am Soc Nephrol*, 2015, 10(10):1831-40
- Zeisberg, M. & Neilson, E. G. Mechanisms of tubulointerstitial fibrosis. *J Am Soc Nephrol*, 2010, 21(11):1819-34
- Zeng, W., Glicksberg, B. S., Li, Y. & Chen, B. Selecting precise reference normal tissue samples for cancer research using a deep learning approach. *bioRxiv*, 2018, 10.1101/336909
- Zhang, G., Wang, M., Zhao, H. & Cui, W. Function of Axl receptor tyrosine kinase in non-small cell lung cancer. *Oncol Lett*, 2018, 15(3):2726-2734
- Zhang, S., Jia, Z., Yan, Z. & Yang, J. Consumption of fruits and vegetables and risk of renal cell carcinoma: a meta-analysis of observational studies. *Oncotarget*, 2017, 8(17):27892-27903
- Zhao, A. J., Qian, Y. Y., Sun, H., Hou, X., et al. Screening for gastric cancer with magnetically controlled capsule gastroscopy in asymptomatic individuals. *Gastrointest Endosc*, 2018, 88(3):466-474 e1
- Zhao, H., Dong, Y., Tian, X., Tan, T. K., et al. Matrix metalloproteinases contribute to kidney fibrosis in chronic kidney diseases. *World J Nephrol*, 2013, 2(3):84-9
- Zhao, M., Kong, L., Liu, Y. & Qu, H. dbEMT: an epithelial-mesenchymal transition associated gene resource. *Sci Rep*, 2015, 5:11459
- Zhao, Y. L., Zhu, R. T. & Sun, Y. L. Epithelial-mesenchymal transition in liver fibrosis. *Biomed Rep*, 2016, 4(3):269-274
- Zhen, Y., Lee, I. J., Finkelman, F. D. & Shao, W. H. Targeted inhibition of Axl receptor tyrosine kinase ameliorates anti-GBM-induced lupus-like nephritis. *J Autoimmun*, 2018, 93:37-44
- Zhen, Y., Priest, S. O. & Shao, W. H. Opposing Roles of Tyrosine Kinase Receptors Mer and Axl Determine Clinical Outcomes in Experimental Immune-Mediated Nephritis. *J Immunol*, 2016, 197(6):2187-94
- Zheng, M., Lv, L. L., Cao, Y. H., Zhang, J. D., et al. Urinary mRNA markers of epithelial-mesenchymal transition correlate with progression of diabetic nephropathy. *Clin Endocrinol (Oxf)*, 2012, 76(5):657-64
- Zheng, X., Carstens, J. L., Kim, J., Scheible, M., et al. Epithelial-to-mesenchymal transition is dispensable for metastasis but induces chemoresistance in pancreatic cancer. *Nature*, 2015, 527(7579):525-530
- Zhou, L., Liu, X. D., Sun, M., Zhang, X., et al. Targeting MET and AXL overcomes resistance to sunitinib therapy in renal cell carcinoma. *Oncogene*, 2016, 35(21):2687-97
- Zhu, Y., Xu, L., Zhang, J., Xu, W., et al. Klotho suppresses tumor progression via inhibiting PI3K/Akt/GSK3beta/Snail signaling in renal cell carcinoma. *Cancer Sci*, 2013, 104(6):663-71
- Zisman, A., Pantuck, A. J., Dorey, F., Said, J. W., et al. Improved prognostication of renal cell carcinoma using an integrated staging system. *J Clin Oncol*, 2001, 19(6):1649-57

ORIGINAL RESEARCH

Clear Cell Renal Cell Carcinoma is linked to Epithelial-to-Mesenchymal Transition and to Fibrosis

Lea Landolt¹, Øystein Eikrem^{1,2}, Philipp Strauss¹, Andreas Scherer^{3,4}, David H. Lovett⁵, Christian Beisland^{1,6}, Kenneth Finne¹, Tarig Osman¹, Mohammad M. Ibrahim¹, Gro Gausdal⁷, Lavina Ahmed⁷, James B. Lorens^{7,8}, Jean Paul Thiery^{8,9}, Tuan Zea Tan¹⁰, Miroslav Sekulic¹ & Hans-Peter Marti^{1,2}

1 Department of Clinical Medicine, University of Bergen, Bergen, Norway

2 Department of Medicine, Haukeland University Hospital, Bergen, Norway

3 Spheromics, Kontiolahti, Finland

4 Institute for Molecular Medicine Finland (FIMM), University of Helsinki, Helsinki, Finland

5 Department of Medicine, San Francisco VAMC, University of California San Francisco, San Francisco, California

6 Department of Urology, Haukeland University Hospital, Bergen, Norway

7 BerGenBio AS, Bergen, Norway

8 Department of Biomedicine, Center for Cancer Biomarkers, University of Bergen, Bergen, Norway

9 INSERM UMR 1186, Integrative Tumor Immunology and Genetic Oncology, Gustave Roussy, EPHE, Fac. de médecine-Univ. Paris-Sud, Université Paris-Saclay, Villejuif, France

10 Science Institute of Singapore, National University of Singapore, Singapore, Singapore

Keywords

Clear cell renal cell carcinoma, epithelial-to-mesenchymal transition, fibrosis.

Correspondence

Hans-Peter Marti, University of Bergen, Department of Clinical Medicine, Haukeland University Hospital, Laboratory Building, 5th floor, Jonas Liesvei 65 5021 Bergen, Norway.
Tel: +47 940 30 929
Fax: +47 55 58 96 43
E-mail: hans-peter.marti@uib.no

Funding Information

Lea Landolt and Øystein Eikrem have received a PhD scholarship from the University of Bergen, Bergen, Norway. Studies were funded in part by an open project grant (number 912167) from the Western Health Region of Norway (Helse Vest).

Received: 24 March 2017; Revised: 27 April 2017; Accepted: 1 May 2017

doi: 10.14814/phy2.13305

Physiol Rep, 5 (11), 2017, e13305,
<https://doi.org/10.14814/phy2.13305>

Abstract

Clear cell renal cell carcinoma (ccRCC) represents the most common type of kidney cancer with high mortality in its advanced stages. Our study aim was to explore the correlation between tumor epithelial-to-mesenchymal transition (EMT) and patient survival. Renal biopsies of tumorous and adjacent nontumorous tissue were taken with a 16 g needle from our patients ($n = 26$) undergoing partial or radical nephrectomy due to ccRCC. RNA sequencing libraries were generated using Illumina TruSeq[®] Access library preparation protocol and TruSeq Small RNA library preparation kit. Next generation sequencing (NGS) was performed on Illumina HiSeq2500. Comparative analysis of matched sample pairs was done using the Bioconductor Limma/voom R-package. Liquid chromatography-tandem mass spectrometry and immunohistochemistry were applied to measure and visualize protein abundance. We detected an increased generic EMT transcript score in ccRCC. Gene expression analysis showed augmented abundance of *AXL* and *MMP14*, as well as down-regulated expression of *KL* (klotho). Moreover, microRNA analyses demonstrated a positive expression correlation of miR-34a and its targets *MMP14* and *AXL*. Survival analysis based on a subset of genes from our list EMT-related genes in a publicly available dataset showed that the EMT genes correlated with ccRCC patient survival. Several of these genes also play a known role in fibrosis. Accordingly, recently published classifiers of solid organ fibrosis correctly identified EMT-affected tumor samples and were correlated with patient survival. EMT in ccRCC linked to fibrosis is associated with worse survival and may represent a target for novel therapeutic interventions.

Introduction

Renal cell carcinoma, also named renal cell adenocarcinoma, comprises over 80% of primary renal neoplasms and is among the ten most frequent forms of cancer in both men and women (Escudier et al. 2016). Clear cell renal cell carcinoma (ccRCC) represents the most common (75–85%) form of renal cell carcinomas and is one of the most lethal genitourinary cancers. Up to a quarter of patients display distal metastases or advanced regional disease at the time of presentation and diagnosis.

Morbidity and mortality of advanced ccRCC is high. Patients with metastatic ccRCC have a 5-year survival of between 0 and 32% depending upon their risk stage at time of diagnosis (Escudier et al. 2016). Therefore, the identification of new mechanisms, biomarkers and related treatment targets is of great clinical importance for the management of ccRCC patients.

Our study focuses on the role of epithelial-to-mesenchymal transition (EMT) as one of the initial steps toward the development of fibrosis, and its potential role in ccRCC. EMT was first described in the 1980s and is physiologically involved in embryogenesis and in pathological states, such as development of solid organ fibrosis. EMT is also associated with tumor invasiveness and distal metastasis (Gjerdum et al. 2010; Thiery and Lim 2013; Lovisa et al. 2015; Piva et al. 2016). EMT defines a process, where epithelial cells lose their polarity and barrier integrity and develop a mesenchymal phenotype, which includes acquired motility. The acquisition of a mesenchymal phenotype in part results from the loss of intercellular junctions and from the reorganization of the actin cytoskeleton to promote migratory behavior (Thiery and Sleeman 2006; Kidd et al. 2014). Moreover, EMT renders cancer cells immune-evasive, drug-resistant, and contributes to the metastatic cascade (Gjerdum et al. 2010; Fleuren et al. 2014; Reichl et al. 2015; Zhou et al. 2016b). Thus, activation of EMT is a key process that promotes local invasion, distal metastasis and drug resistance (Gjerdum et al. 2010). The identification of the signaling pathways leading to activation of EMT programs in cancer should provide new insights into cell plasticity and therapeutic interventions to optimize health care delivery. Accordingly, EMT has been shown to play a key role in the progression of both experimental and human ccRCC (Yu et al. 2015; Piva et al. 2016; Zhou et al. 2016a).

Different molecules and pathways are associated with the control of EMT, including transforming growth factor β (TGF β), fibroblast growth factor (FGF), and klotho (KL) (Thiery and Sleeman 2006; Doi et al. 2011; Grande et al. 2015). Known EMT triggers are cytokines such as TGF β and FGF. TGF β and EGF lead to the activation of

transcriptional factors including SNAIL1 and SNAIL2, TWIST, ZEB1 and ZEB2 which induce gene expression patterns favoring EMT development (Lamouille et al. 2014; Grande et al. 2015; Lovisa et al. 2015). As a consequence, down-regulation of E-cadherin (CDH1), an epithelial marker involved in intercellular connections, and up-regulation of vimentin (VIM), a mesenchymal marker, are typically observed in EMT. However, carcinoma cells can adopt multiple intermediate, possibly metastable stages (Nieto et al. 2016).

The transcription factors SNAIL1, ZEB1, and ZEB2 induce the expression of matrix metalloproteinases (MMPs). MMPs are crucial mediators of cancer EMT as they influence tumor behavior, especially invasiveness, by proteolysis of extracellular matrix (ECM) (Kalluri and Neilson 2003; Jorda et al. 2005; Thiery et al. 2009; Mahimkar et al. 2011; Lamouille et al. 2014). The principal MMPs involved in cancer are MMP2, MMP9 and most notably MMP14 (Seiki et al. 2003; Mahimkar et al. 2011; Lamouille et al. 2014). Increased expression of MMP2 and MMP9 is associated with poor prognosis in ccRCC (Kallakury et al. 2001; Chen et al. 2014; Mikami et al. 2016). Expression of MMP14, also known as MT1MMP, correlates with the extent of renal epithelial tumor EMT and invasive capacity (Mahimkar et al. 2011). Mutation or hypermethylation-induced inactivation of the tumor suppressor gene Von-Hippel-Lindau (VHL) increases activity of the mitogen-activated protein kinase (MEK) protein. Sustained activation of the MEK1 module leads to the higher expression of MMP14 and is related to the degree of EMT. In accordance, the activity of the MEK1/MMP14 signaling module is highly correlated with tumor nuclear grade and invasiveness of ccRCC (Mahimkar et al. 2011).

The AXL receptor tyrosine kinase, with its main ligand growth arrest-specific 6 (GAS6), is emerging as another important promoter and regulator of EMT (Gjerdum et al. 2010). High expression of AXL and its pathway can be detected in various cancers including acute myeloid leukemia, prostate, breast, lung, and skin cancers (Axelrod and Pienta 2014). AXL, along with MERTK and TYRO3, is a member of the TAM receptor family (Korshunov 2012). Binding of GAS6 leads to the oligomerization of AXL with tyrosine phosphorylation and activation of a down-stream signaling cascade (Jorda et al. 2005). AXL-mediated EMT is known to be important for ccRCC progression (Yu et al. 2015; Zhou et al. 2016b).

Both AXL and MMP14 mRNA's are targeted by miR-34a, which represents an important microRNA in cancer development (Jia et al. 2014; Li et al. 2015). MiR-34a represents a mediator of p53-dependent tumor inhibition, and its low expression correlates with worse prognosis in several cancers (Fritz et al. 2015).

The aim of this study, which includes mRNA and to a more limited extent miRNA sequencing and proteomics, is to describe in detail the dysregulation of EMT and its related genes in a cohort of ccRCC patients and to determine if the results have prognostic value in other patient cohorts.

Methods

Patients and renal tissues

This study includes renal tissue from 26 patients with ccRCC who attended Haukeland University Hospital in Bergen Norway and underwent partial or radical (full) nephrectomy from November 2013 until September 2015, as published previously (Eikrem et al. 2016a,b). Two additional patients were excluded because of a mixture of carcinoma and normal tissue in the respective biopsies. Renal core biopsies of tumorous and adjacent noncancerous normal tissue, as judged by histopathology, were

taken with a 16 g needle perioperatively. Core biopsies of tumorous and adjacent non-tumorous tissues were formalin-fixed and paraffin-embedded (FFPE), as described (Eikrem et al. 2016a).

Patients (10 females and 16 males) had a mean age of 57.4 ± 12 years (58.2 ± 11 years for females and 56.9 ± 12.9 years for males). All patients had tumor-negative lymph nodes and no metastases. Detailed patient characteristics are summarized in Table 1.

The regional Ethics Committee of Western Norway approved our studies (REC West no. 78/05). All participants provided written consent as requested by our Ethics Committee.

RNA extraction and quality assessment for next generation sequencing

Total RNA was extracted from FFPE stored kidney core biopsies using the miRNeasy FFPE kit (Qiagen) as reported (Eikrem et al. 2016a; Landolt et al. 2016).

Table 1. Patient characteristics.

Patient ID	Age (year)	Gender	BMI (kg/m ²)	Nephrectomy type	eGFR (mL/min/1.73 m ²)	TNM-stage	Fuhrmann grade (1–3)	Cancer stage (1–4)	Leibovich score (0–11)	Sample usage
9	70	Male	24	Partial	>60	pT1AcN0cM0	2	1	0	R
10	69	Male	34	Partial	>60	pT3AcN0cM0	2	2	4	R
11	37	Male	27	Partial	>60	pT1AcN0cM0	2	1	0	R
13	63	Male	24	Full	40	pT3AcN0cM0	4	2	8	R
15	68	Male	28	Partial	>60	pT1AcN0cM0	2	1	0	R
18	78	Male	27	Full	47	pT3AcN0cM0	2	2	4	R, P
19	71	Female	22	Full	>60	pT2aN0cM0	1	2	4	R
21	53	Female	25	Full	55	pT1 BcN0cM0	2	1	2	R, P
22	49	Male	25	Partial	>60	pT1 BcN0cM0	2	1	3	R, P
27	46	Male	31	Full	>60	pT2BcN0cM0	3	2	5	R, P
29	54	Female	29	Partial	>60	pT1AcN0cM0	2	1	0	R, P
31	67	Male	25	Partial	>60	pT1AcN0cM0	1	1	0	R, P
32	36	Male	23	Partial	>60	pT1AcN0cM0	3	1	1	R
33	48	Male	28	Partial	>60	pT1AcN0cM0	1	1	0	R, P
39	71	Male	25	Full	59	pT3AcN0cM0	4	3	8	R, M, P
44	74	Female	23	Full	>60	pT3AcN0cM0	2	3	4	R, M, P
46	53	Female	24	Partial	>60	pT1AcN0cM0	1	1	0	R, M, P
50	72	Female	19	Full	>60	pT1 BcN0cM0	2	1	3	R, M
53	46	Female	44	Full	>60	pT2AcN0cM0	2	2	3	R, M, P
55	44	Female	23	Full	>60	pT3AcN0cM0	3	3	5	R, M
57	63	Female	28	Full	>60	pT1AcN0cM0	2	1	0	R, M
59	52	Female	29	Partial	>60	pT1AcN0cM0	2	1	0	R, M
63a	55	Male	28	Partial	>60	pT1AcN0cM0	3	1	1	R, M
63b	44	Male	20	Partial	>60	pT1AcN0cM0	2	1	0	R, M
64	52	Male	26	Full	>60	pT1 BcN0cM0	3	1	4	R, M
65	57	Male	24	Full	>60	pT2AcN0cM0	3	2		R, M

Characteristic patient ($n = 26$) features at the time of surgery. eGFR was calculated with the MDRD formula. Full nephrectomy is equivalent to radical nephrectomy. The "Cancer Stage" was determined based on the European Association of Urology (EAU) Guidelines on renal cell carcinoma: 2014 update (Gjerdrum et al. 2010). Leibovich score: 1 = low risk, 2 = intermediate risk, 3 = high risk (Leibovich et al. 2003). Sample usage: "R", mRNA sequencing; "M", microRNA (miR) sequencing; "P", proteomics.

Quality and quantity of extracted RNA were assessed using the Agilent RNA 6000 Nano Kit on a 2100 Bioanalyzer instrument (Agilent Technologies, Santa Clara, CA).

We calculated the DV₂₀₀ value (the percentage of RNA fragments longer than 200 nucleotides) as a measure to estimate the quality of RNA necessary for sequencing (Huang et al. 2015; Eikrem et al. 2016a; Landolt et al. 2016). The mean DV₂₀₀ values (95% CI) of the samples of 26 patients (with each tumorous and non-tumorous FFPE samples) were 65.7% (58.9–72.4%); a minimum level of 30% is required for sequencing (Huang et al. 2015; Eikrem et al. 2016a).

RNA library preparation and sequencing

RNA sequencing libraries were prepared using the TruSeq RNA Access library kit (Illumina, Inc., San Diego, CA, USA) for mRNA sequencing ($n =$ all 26 patients) or the TruSeq Small RNA Library Preparation Kits (Illumina Inc, San Diego, CA) for miRNA sequencing (subgroup of $n = 12$ patients, as shown in Table 1) according to the manufacturer's protocol. RNA sequencing was performed on a HiSeq2500 instrument (Illumina, San Diego, CA) according to the manufacturer's protocol and as described previously (Eikrem et al. 2016a,b).

Sequencing data are available via Gene Expression Omnibus, <https://www.ncbi.nlm.nih.gov/geo/>; GSE76207 and GSE82122.

Bioinformatics of RNA sequencing

Assembly of reads and alignment of the contigs to the Human Genome Assembly GRCh38 were guided by Tophat and Bowtie. For the mRNA expression data of 52 samples from 26 patients, an empirical expression filter was applied, which left genes with at least 3 counts per million (cpm) in at least 19 samples.

A list of 483 EMT genes was compiled from three publicly available sources (<http://dbemt.bioinfo-minzhao.org/>; (Chen et al. 2014; Groger et al. 2012)), and supplemented by the addition of genes involved in EMT based on our own study interest, as described below.

For the microRNA expression data of 22 samples from 11 patients, an empirical expression filter was applied, which left microRNA species with at least 3 cpm in at least nine samples.

Comparative analysis was done using the voom/Limma R-package. Differential gene expression with a moderated paired t -test was defined as Benjamini-Hochberg adjusted $P \leq 0.05$, and an absolute fold change of ≥ 2 .

Survival analyses using mRNA or microRNA were performed using two tools, (<http://bioinformatica.mty.itesm.mx:8080/Biomatec/SurvivaX.jsp>), and SurvMicro ([\[bioinformatica.mty.itesm.mx:8080/Biomatec/Survmicro.jsp\]\(http://bioinformatica.mty.itesm.mx:8080/Biomatec/Survmicro.jsp\)\), respectively. For the mRNA analysis we used 468 samples from the TCGA ccRCC dataset; for the microRNA analysis we employed 217 HiSeq samples from TCGA. Further data analysis and visualization was performed with JMP Pro 11 \(\[www.sas.com\]\(http://www.sas.com\)\), and Graphpad version 6 and 7 \(\[www.graphpad.com\]\(http://www.graphpad.com\)\).](http://</p></div><div data-bbox=)

Classifier analysis was performed as recently published (Rodder et al. 2009, 2011). The classifier consisted of a panel of metzincins and related genes (MARGS), and the algorithm linear discriminant analysis. The analysis was performed in JMP Pro 11 (www.sas.com). The ccRCC dataset was treated as the test set, as the classifiers had been trained already in other datasets (Rodder et al. 2009, 2011).

Transcriptomic EMT score

A generic EMT score was computed for each of the RNA-seq samples using a method described previously (Tan et al. 2014). Briefly, using an EMT signature derived from bladder, breast, colorectal, lung, gastric, and ovarian cancers, a two-sample Kolmogorov-Smirnov test was performed to assess the extent of EMT enrichment. A high enrichment score of the EMT signature indicate a sample to be more mesenchymal-like, whereas a low enrichment score indicates a sample to be more epithelial-like.

Proteomics

This investigation was performed in a subgroup of patients ($n = 11$) from our total subject cohort ($n = 26$), as indicated in Table 1. Protein and peptide extraction: After deparaffinization with xylene, tissue sections (10 μm) were lysed by suspension in 20 μL lysis solution [0.1 mol/L Tris-HCl pH 8, 0.1 mol/L dithiothreitol (DTT), 4% sodium dodecyl sulphate (SDS)] and heated at 99°C for 60 min. Filter aided sample preparation (FASP) was performed as described (Wisniewski 2013). Eluted peptides were desalted and cleaned using Oasis HLB μ Elution plates (Waters, Milford, Mass.), and protein concentrations were measured by A280 using Nano-Drop (Thermo Scientific). The samples were analyzed with a 180 min LC gradient on a Q-Exactive HF (Thermo Scientific) connected to a Dionex Ultimate NCR-3500RS LC system.

We used label-free protein quantification: Raw data from the MS was processed using Progenesis LC-MS software (version 4.0, Nonlinear Dynamics, UK) with default settings. Features were searched with searchGUI (version 2.2.2) and PeptideShaker (version 1.2.2) applying the UniprotKB/SwissProt human database (downloaded from Uniprot August 2015, 20,197 entries). Precursor mass

tolerance was set at 10 parts per million, and product mass tolerance at 0.5 Dalton. Carbamidomethylation of cysteines and oxidation of methionines were set as fixed and variable modifications, respectively. Two missed cleavages were allowed, and false discovery rate was set at 1%.

Immunohistochemistry

Immunohistochemistry (IHC) of *AXL*, *CDH1*, *MMP14*, and *VIM* was performed on 3 and 4 μm thick FFPE sections following standard methodology. The following primary antibodies were used: *AXL* (1H12, BerGenBio AS, Bergen, Norway, (Nalwoga et al. 2016)), *CDH1* (monoclonal mouse anti-E-cadherin, clone NHC-38, Dako, Agilent Technologies, Santa Clara, CA, USA, catalogue number: MA5-12547), *MMP14* (monoclonal rabbit anti-MMP14, Abcam, Cambridge, UK, catalogue number: EP1264Y) and *VIM* (monoclonal mouse anti-vimentin, clone V9, Dako, Agilent Technologies, Santa Clara, CA, USA, catalogue number: M072529-2). Slides were incubated with the specified antibodies, such as *AXL* 1 $\mu\text{g}/\text{mL}$, *CDH1* 1:200 and *VIM* 1:1000, for 1 h at room temperature. *MMP14* antibodies 1:1200 were applied overnight at 4°C. Sections were counterstained with hematoxylin (Dako, catalogue number: CS70030-2), then dehydrated and cover-slipped.

Results

The hypothesis underlying this study was that a transition from normal renal structure to ccRCC is characterized by EMT. To test this hypothesis and to characterize the extent of EMT in ccRCC, we determined gene expression levels of EMT genes from ccRCC patient biopsies and compared them to levels in matched, adjacent, normal tissue. Patient characteristics are summarized in Table 1. Importantly, no patient had signs of metastases.

Increased generic EMT score in renal cell carcinoma

We first assessed whether gene expression changes could be used to reflect the degree of EMT in the samples. To that end, we employed an EMT score calculation, which is based on the enrichment score of 315 genes, as previously described (Tan et al. 2014). A higher EMT score indicates greater mesenchymal characteristics. Accordingly, a lower EMT score reflects a more epithelial-like phenotype.

Figure 1 shows that the EMT score of normal non-cancerous kidney tissue samples indicates a relatively mesenchymal-like value. However, in 25 of 26 sample pairs,

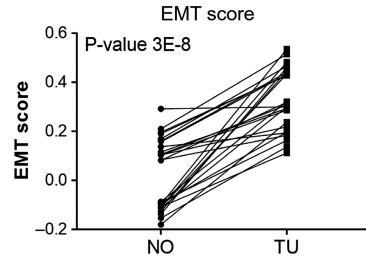


Figure 1. Epithelial-Mesenchymal Transition (EMT) score of 26 adjacent normal-tumor pairs from renal clear cell carcinoma patients. *P*-value shown is computed by matched-pairs two-sided Wilcoxon signed rank test. NO, normal, non-carcinoma tissues; TU, respective ccRCC samples.

the EMT score values were significantly higher in ccRCC (TU) samples as compared to the matched normal (NO) sample. Importantly, there was neither a difference comparing normal, non-cancer tissues obtained from partial versus radical nephrectomy nor effects of age, sex or cancer stage on the degree of EMT score (data not shown).

The data also show that in our dataset EMT score alone cannot be used as indicator of ccRCC, since the individual scores of NO and TU samples are not clearly separated. The value of this analysis lies in the increase of the EMT score from NO to the respective matched TU sample.

Alterations in EMT gene expression distinct renal cell carcinoma from normal tissue and correlate with cancer stage

We have investigated alterations in the gene expression pattern on the mRNA and on the miRNA level as well as to a lesser degree on the protein level.

Analysis of mRNA abundances

We compiled a list of EMT-related genes from three public sources and our own data. The study by Chen et al. (2014) used microarray data to identify 46 EMT genes in normal and primary ccRCC. Gröger and colleagues performed a meta-analysis of cancer gene expression studies in primary cell cultures and concluded on a core set of 131 EMT genes with relevance in tumor progression (Groger et al. 2012). Further we extracted 357 genes from the dbEMT database (<http://dbemt.bioinfo-minzhao.org/>), (Zhao et al. 2015). Surprisingly, only six genes were common to all three datasets (*CDH1*, *CDH2*, *FN*, *MMP2*, *VIM*, and *ZEB1*). The inclusion of other relevant genes, such as *GAS6* and *AKT3*, resulted in a gene list

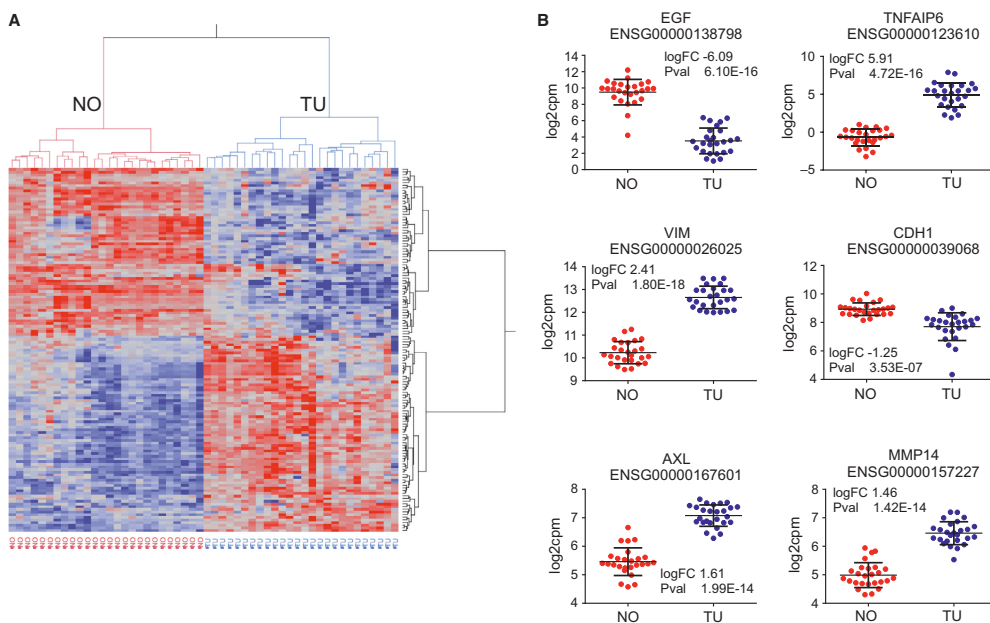


Figure 2. RNA sequencing data analysis. (A) Unsupervised hierarchical cluster analysis with 137 differentially expressed EMT-related mRNA. The samples segregate into two large clusters, the normal ("NO") samples, and the ccRCC samples ("TU"). (B) Scatterplot illustration of expression levels of selected genes.

comprising 483 EMT-related genes implicated in ccRCC. In the gene expression analysis of matched ccRCC and adjacent normal biopsy samples from 26 patients ($n = 52$ samples), 399 of these 483 EMT-related genes (83%) passed the expression filter (see Material and Methods) and were retained in the analysis. Of those 399 genes, 137 were differentially expressed (absolute $\log_{2}FC > 1$, adjusted $P < 0.05$). Of the 315 genes used in the EMT score analysis, 71 were included in the list of 399 detected EMT-related genes, and 39 were differentially expressed.

Unsupervised hierarchical cluster analysis illustrates how the normalized expression values of the 137 mRNAs led to the formation of two distinct clusters of samples, consisting of normal and tumor samples, respectively (Fig. 2A). Genes with the largest fold changes in tumor tissue compared to normal tissue included *EGF* and *TNFAIP6*. Scatterplots for selected genes are shown in Figure 2B.

Twenty genes with the largest absolute fold change of mRNA abundance and smallest P -values are shown in Table 2. From this list, three genes were detected and confirmed by proteomics, as described below. Other upregulated, important EMT-related genes, which

were not present in the list of the top 20 genes, were *SNAIL1*, *TGF β 1*, and *CTNNB1* (β -catenin); data not shown.

To analyze the contribution of the 137 variables (differentially expressed genes) toward explaining the data structure (i.e., variance), we applied principal component analysis (PCA), as depicted in Figure 3. The normalized expression data for the differentially expressed mRNA explained 58.7% of the variance in principal component 1 (PC1) and leads to a visual separation of the normal and the tumor samples (Fig. 3A). The biplot in Figure 3B represents both the samples (illustrated as black points) and vectors of the variable contribution (or loadings, in red) to represent the data structure. As in the PCA, the axes of the biplot are the principal components. Vectors that point in the same direction correspond to variables that have similar response profiles. The loadings represent correlations between the input variables and the principal component scores; they can be negative or positive. Extraction of the loadings of the variables for PC1, and ranking them by the largest to smallest absolute value identifies the mRNA variables with the largest contribution to PC1, which explains the difference between

Table 2. Differentially expressed genes.

ENSEMBL_ID	Symbol	RNAseq				Proteomics			
		log FC (TU/NO)	abs ClogFC (TU/NO)	t	P value	adj P value	log FC (TU/NO)	P value	adj P value
ENSG00000138798	EGF	-6.09	6.09	-16.69	6.10E-16	9.96E-14			
ENSG00000123610	TNFAIP6	5.91	5.91	16.86	4.72E-16	8.02E-14			
ENSG00000171004	HS6ST2	-5.61	5.61	-12.87	3.53E-13	1.06E-11			
ENSG00000135374	ELF5	-5.54	5.54	-11.52	4.77E-12	8.54E-11			
ENSG00000159263	SIM2	-5.29	5.29	-10.55	3.45E-11	4.44E-10			
ENSG00000198910	L1CAM	-4.34	4.34	-13.61	9.37E-14	3.85E-12	10.43	8.18E103	2.77E102
ENSG00000136943	CTSL2	-3.94	3.94	-11.14	1.02E-11	1.59E-10			
ENSG00000137648	TMPRSS4	-3.60	3.60	-6.34	7.96E-07	2.90E-06			
ENSG00000107485	GATA3	-3.59	3.59	-18.14	7.30E-17	1.87E-14			
ENSG00000198780	FAM169A	-3.45	3.45	-12.67	5.17E-13	1.43E-11			
ENSG00000146674	IGFBP3	3.38	3.38	19.75	8.31E-18	4.18E-15	3.26	1.23E-03	6.70E-03
ENSG00000113083	LOX	3.35	3.35	11.59	4.09E-12	7.52E-11			
ENSG00000104413	ESRP1	-2.99	2.99	-6.16	1.28E-06	4.48E-06			
ENSG00000106541	AGR2	-2.97	2.97	-3.76	8.03E-04	1.60E-03			
ENSG00000184937	WT1	-2.97	2.97	-8.16	7.88E-09	4.72E-08			
ENSG00000113578	FGF1	-2.95	2.95	-9.64	2.51E-10	2.33E-09			
ENSG00000118526	TCF21	-2.85	2.85	-9.10	8.57E-10	6.83E-09			
ENSG00000101144	BMP7	-2.75	2.75	-3.87	6.05E-04	1.24E-03			
ENSG00000112715	VEGFA	2.72	2.72	14.91	1.01E-14	7.68E-13			
ENSG00000038427	VCAN	2.72	2.72	7.92	1.41E-08	7.97E-08	3.01	3.90E-05	6.15E-04

Top 20 differentially expressed EMT genes (sorted by decreasing absolute \log_2 fold change in mRNA abundance) and available proteomics results.

normal and tumor samples. As shown in the list of ten mRNA with largest absolute loadings for PC1 (Fig. 3C), *ITGA5* has the largest contribution, *AXL* and *MMP14* rank 6th and 9th, respectively, indicating their importance in explaining the data structure, similarity and difference between samples.

Next, we analyzed whether any mRNA expression profiles were correlated with cancer stage, as described by us and others (von Roemeling et al. 2014; Eikrem et al. 2016a). We correlated the \log_2 cpm expression values of the EMT genes, which were obtained from the LIMMA/VOOM analysis in R Bioconductor, to the cancer stage applying a bivariate polynomial fitting algorithm. *CAVI* had the largest absolute correlation, followed by *VIM*, *IGFBP3*, and *ITGA1*. Interestingly, the expression levels did not increase from the stage 2 to stage 3, and in some cases even decreased. These results are depicted in Figure 4.

Figure 5 summarizes the expression data obtained for *MMP14*. Besides RNA-sequencing, we applied proteomics, and immunohistochemistry. Using these three technologies, we could confirm RNA abundance as well as protein abundance of *MMP14*, revealing an approximate twofold higher average expression level in ccRCC tumor specimens compared to normal samples. Note, only one

patient showed an inexplicable decrease on *MMP14* in ccRCC as analyzed by proteomics.

Applying proteomics and IHC, we also detected increased abundance of protein of *AXL*, and *VIM*, in ccRCC, and decreased abundance of *CDH1*, thereby supporting RNA sequencing data, as depicted in Figure 6A and B. In addition, Figure 6A indicates that there could be some stromal cells detectable next to *CDH1*-positive tubules, which may explain in part the relatively high EMT values of some carcinoma-adjacent normal kidney samples (Fig. 1).

Analysis of microRNA expression

Expanding our analysis of gene expression data to the analysis of those microRNAs with involvement in EMT, we sequenced microRNAs from 12 ccRCC samples and the 12 respective normal specimens from our patient cohort, followed by pairwise comparison of their abundance as done for mRNA. Most of the patient material is shared between the microRNA and the mRNA studies. MicroRNAs associated with EMT were identified from the literature (Zhang and Ma 2012; Zaravinos 2015). The respective results are shown in Table 3. *Mir-34a*, which targets *AXL* and *MMP14* (Jia et al. 2014; Li et al. 2015) is

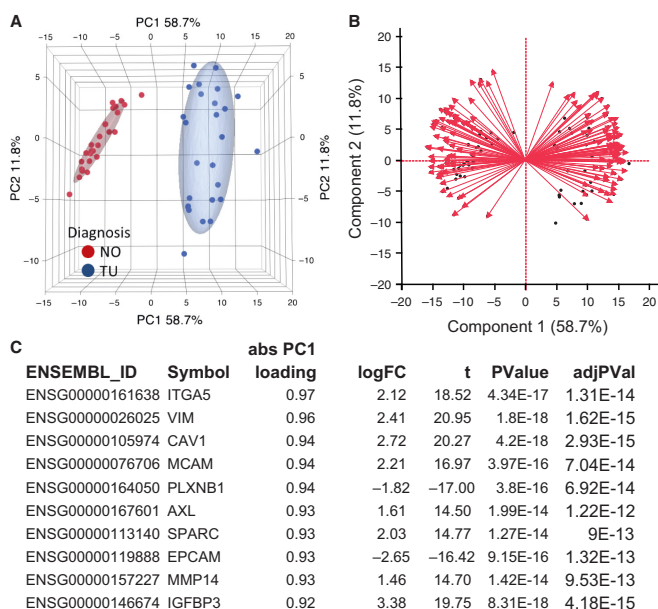


Figure 3. Principal component analysis with differentially expressed EMT genes. (A) Principal component analysis (PCA) with 137 differentially expressed EMT-mRNA. The sample groups “healthy” (normal, NO) and “ccRCC” (tumor, TU) are separated along the principal component 1 (PC1). Ellipsoids indicate the 95th percentile of data points per group. (B) The biplot demonstrates the samples as dots, and the contribution of each variable toward the explanation of the variance of the data as red arrows. Each arrow can be attributed a value, the loading score. (C) Ten mRNA with the largest absolute loading scores. ITGA5, AXL and MMP14 are among the mRNAs with the largest loading scores.

one of the most significantly affected microRNAs. The expression levels of these three microRNA and mRNA species are found to be strongly positively correlated in our datasets (Fig. 7).

Expression of tumor EMT-genes and also of fibrosis-related genes correlates with patient survival

However, while mir-34a is highly expressed in high-risk ccRCC groups, it did not correlate with patient survival in 217 ccRCC samples (see Material and Methods; data not shown). *MMP14* and *AXL* on the other hand are significantly associated with patient survival, being higher expressed in high-risk groups within 468 human ccRCC samples (Fig. 8A–D).

KL (klotho) has recently been shown to inhibit *TGFβ1* and to decrease renal fibrosis and cancer metastasis (Doi et al. 2011). As *KL* was differentially expressed in our dataset (fold change TU/NO -3.43, *P*-value 2.15E-07), we tested the effect on patient survival on 468 samples of the TCGA clear cell carcinoma dataset implemented (Material

and Methods). In accordance with the literature, lower expression levels of *KL* indicated lower patient survival (Risk Group Hazard Ratio 3.61, *P*-value 4.41E-14), as shown in Figure 8E–F.

Finally, we evaluated combinations of differentially expressed genes. A set of four collagen genes with an expression very tightly correlated across the samples (*COL1A1*, *COL1A2*, *COL3A1*, and *COL5A1*; correlation 0.8 ± 0.025) outperformed *MMP14* and *AXL* (Risk Group Hazard Ratio 3.19, *P*-value 1.11E-11). All collagen genes are higher expressed in high-risk group and correlated with patient survival (Figure 9A and B).

Furthermore, we tested various combinations of genes from the set of 20 genes highest fold changes between NO and TU (Table 2). A set of 11 genes allowed us to predict patient survival to a much better degree than any individual gene we tested (Risk Group Hazard Ratio 4.28, *P*-value 1.32E-15), as shown in Figure 9C and D.

The member genes of two gene sets, the collagen-based set (Fig. 9A and B) and the panel of 11 genes (Fig. 9C and D), underscore the tight link between EMT and fibrosis development. Notably, EMT and its intermediate

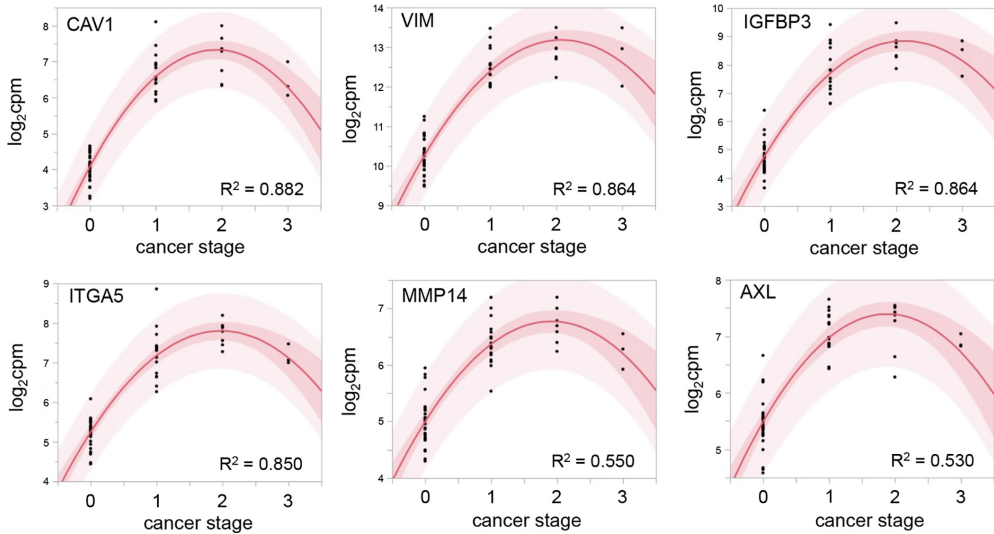


Figure 4. Bivariate polynomial regression of the mRNA abundance and cancer stage. *CAV1*, *VIM*, *IGFBP3*, and *ITGA5* were the mRNAs with strongest regression. The expression level for all mRNAs declined in samples with the highest tumor stage. The dark red area is the confidence limit for the expected fitted mean, the light red area displays the confidence limits for the individual predicted value. The confidence limits reflect variation in the error and variation in the parameter estimates. Cancer stage (see also Table 1) is indicated as numerical values from 1 to 3, with 0 indicating tumor-unaffected status corresponding to the respective noncancerous normal tissues.

states have recently been identified as key promoters of organ fibrosis (Nieto et al. 2016). Amongst the genes of the two sets, especially collagens 1 and 3, but also 5 can be augmented in solid organ fibrosis, including the kidney (Mak et al. 2016). Moreover, the EMT drivers $TGF\beta$ and epithelial growth factor (EGF) are also linked to the promotion of fibrosis development (Kok et al. 2014; Grande et al. 2015).

Therefore, in a subsequent step, we applied our previously described fibrosis classifier in humans, which is based on metzincins and related genes (MARGS). The classifier was successfully applied in renal allografts (classifier with 19 MARGS genes) and in solid human organ fibrosis (classifier with 10 of the 19 MARGS genes), (Rodder et al. 2009, 2011). This fibrosis classifier was also validated across species in rat fibrosis models (Marti et al. 2014, 2016). Both models classified all samples correctly into normal and ccRCC samples (Fig. 10) despite the fact that the majority of our tumor samples ($n = 24$) had areas of intra-tumor stroma and/or evidence of fibrosis, as judged by light microscopy (data not shown).

We also tested the performance of the MARGS classifiers with respect to the patient survival. The 19-gene panel classifier had a Risk Group Hazard Ratio of 3.6

(P -value $4E-12$), and the 10-gene MARGS classifier of solid organ fibrosis a Risk Group Hazard Ratio of 2.97 (P -value $7.3E-9$).

Discussion

This study provides additional evidence for the pathophysiological and prognostic role of EMT gene expression in the development of ccRCC. To the best of our knowledge, this is the first report combining mRNA/miRNA next generation sequencing with proteomics in FFPE ccRCC tissues, and linking results to fibrosis. Firstly, we observed an increased EMT score in ccRCC. Thereafter, we have analyzed several individual genes and finally, we have obtained two prognostic EMT-related gene sets consisting of four and eleven genes, respectively. Many of these genes are also linked to fibrosis development.

Numerous genes are involved in EMT and their selection for analysis ultimately remains incomplete. We decided to first use an established, generic EMT score for an initial EMT screening, as published by members of our group (Tan et al. 2014). The respective results indicated that our dataset can be used to address whether EMT-related genes play a role in ccRCC. It also

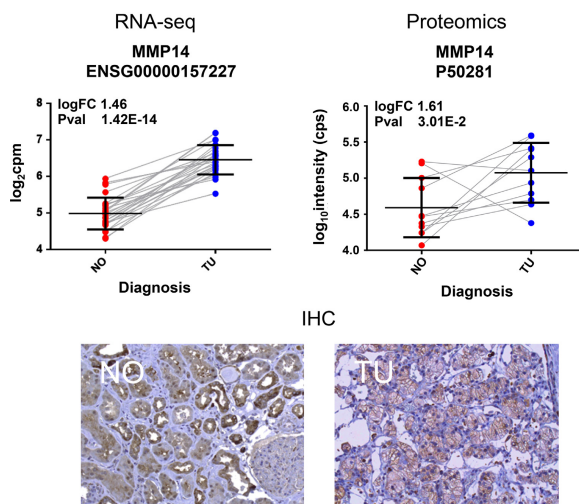


Figure 5. Detection of expression changes of MMP14 in ccRCC. Top left ("RNA-seq"): MMP14 mRNA is about 1.46-logfold increased in ccRCC. Matched normal samples from the same patients are connected by a line to illustrate the expression change. Top right ("Proteomics"): Increased abundance of MMP14 protein in ccRCC. Two samples, patients 27 and 29, showed decrease in MMP14 expression in ccRCC. In RNA sequencing data, *MMP14* mRNA levels were increased in ccRCC also for these two patients. Matched normal and ccRCC samples from the same patient are connected to illustrate the expression change. Bottom ("IHC"): Representative immunohistochemistry (IHC) results showing the increased detection of MMP14 epitope in a ccRCC sample ("TU") in comparison to the matched healthy ("NO") sample from the same patient.

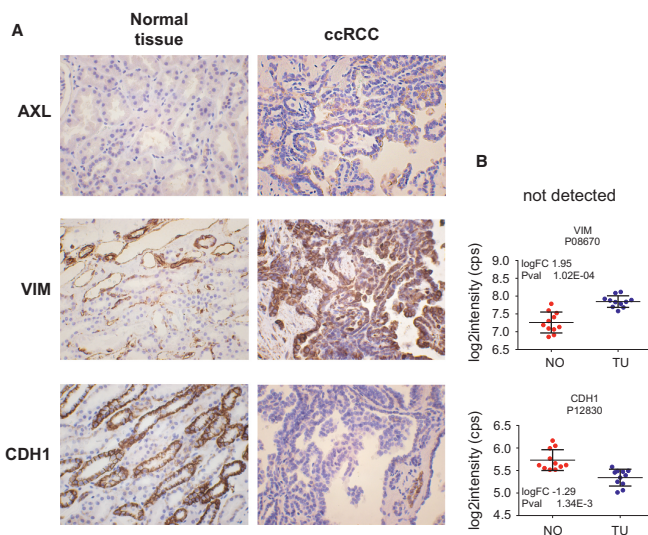


Figure 6. Representative immunohistochemistry (IHC) analyses of protein abundance by proteomics of three genes involved in EMT. Protein level of AXL and VIM were increased in ccRCC, while CDH1 protein was decreased (A). IHC results are supported by proteomics data for VIM and CDH1 (B). AXL protein was not detected in the proteomics dataset.

Table 3. Differentially expressed microRNA (mir).

microRNA	micro RNA			Target mRNA					
	Precursor	FC (TU vs. NO)	P value	adj. P value	ENSEMBL ID	Symbol	FC (TU/NO)	P value	adj. P value
hsa-miR-200b-3p	hsa-mir-200b	-2.53	2.99E-04	8.95E-04	ENSG0000039068	CDH1	-2.38	3.53E-07	1.40E-06
hsa-miR-200b-5p	hsa-mir-200b	-2.34	1.48E-04	5.10E-04	ENSG00000169554	ZEB2	1.54	4.38E-07	1.71E-06
hsa-miR-200c-3p	hsa-mir-200c	-39.12	6.84E-09	3.59E-07	ENSG00000148516	ZEB1			
hsa-miR-141-5p	hsa-mir-141	-30.31	1.25E-07	2.29E-06	ENSG00000168036	CTNNB1	1.16	3.20E-03	5.71E-03
hsa-miR-141-3p	hsa-mir-141	-17.64	1.08E-07	2.18E-06					
hsa-miR-429	hsa-mir-429	-2.34	4.36E-05	1.83E-04					
hsa-miR-30a-3p	hsa-mir-30a	-3.09	4.54E-07	5.87E-06	ENSG00000167601	AXL	3.05	1.99E-14	1.22E-12
hsa-miR-30a-5p	hsa-mir-30a	-2.32	1.50E-05	7.48E-05	ENSG00000157227	MMP14	2.74	1.42E-14	9.53E-13
hsa-miR-34a-3p	hsa-mir-34a	4.97	7.79E-08	2.04E-06					
hsa-miR-34a-5p	hsa-mir-34a	2.73	4.66E-06	2.80E-05	ENSG00000124216	SNAIL1	1.78	1.21E-03	2.33E-03
hsa-miR-34c-5p	hsa-mir-34c	2.55	1.42E-02	2.58E-02	ENSG00000128710	HOXD10	-2.82	1.06E-08	6.13E-08
hsa-miR-203a-3p	hsa-mir-203a	-2.26	1.44E-02	2.60E-02	ENSG00000156299	TIAM1	1.92	5.66E-09	3.55E-08
hsa-miR-10b-5p	hsa-mir-10b	-2.72	1.44E-09	1.26E-07	ENSG00000150593	PDCD4	1.35	5.59E-07	2.11E-06
hsa-miR-21-3p	hsa-mir-21	6.23	1.05E-07	2.18E-06	ENSG00000140416	TPM1	1.79	6.67E-07	2.47E-06
hsa-miR-31-3p	hsa-mir-31	-3.07	8.92E-03	1.71E-02	ENSG00000156299	TIAM1	1.92	5.66E-09	3.55E-08
hsa-miR-155-5p	hsa-mir-155	9.62	5.31E-08	1.86E-06	ENSG0000067560	RHOA	1.16	3.05E-04	6.59E-04
hsa-miR-194-3p	hsa-mir-194-2	-3.21	3.47E-04	1.00E-03	ENSG00000170558	CDH2	1.79	2.69E-05	7.13E-05
hsa-miR-204-5p	hsa-mir-204	-4.25	1.50E-04	5.14E-04	ENSG00000134873	CLDN10	-4.95	8.69E-11	9.58E-10
hsa-miR-204-3p	hsa-mir-204	-3.96	4.97E-05	2.02E-04	ENSG00000113946	CLDN16	-25.37	5.29E-10	4.48E-09
hsa-miR-138-5p	hsa-mir-138-2	-12.09	2.01E-05	9.40E-05	ENSG00000164007	CLDN19	-26.79	8.10E-13	2.00E-11
hsa-miR-138-3p	hsa-mir-138-1	-12.01	1.78E-05	8.72E-05	ENSG00000105329	TGFB1	2.80	6.14E-14	2.77E-12
hsa-miR-9-5p	hsa-mir-9-1	-6.32	2.73E-04	8.36E-04	ENSG00000124216	SNAIL1	1.78	1.21E-03	2.33E-03
hsa-miR-10a-5p	hsa-mir-10a	-3.77	1.12E-06	1.05E-05	ENSG0000039068	CDH1	-2.38	3.53E-07	1.40E-06
hsa-miR-10a-3p	hsa-mir-10a	-2.71	1.86E-05	8.94E-05					
hsa-miR-335-5p	hsa-mir-335	-2.85	2.03E-05	9.40E-05					

Relevant microRNA in EMT. Expression changes of microRNAs and their target mRNAs in ccRCC compared with normal tissue.

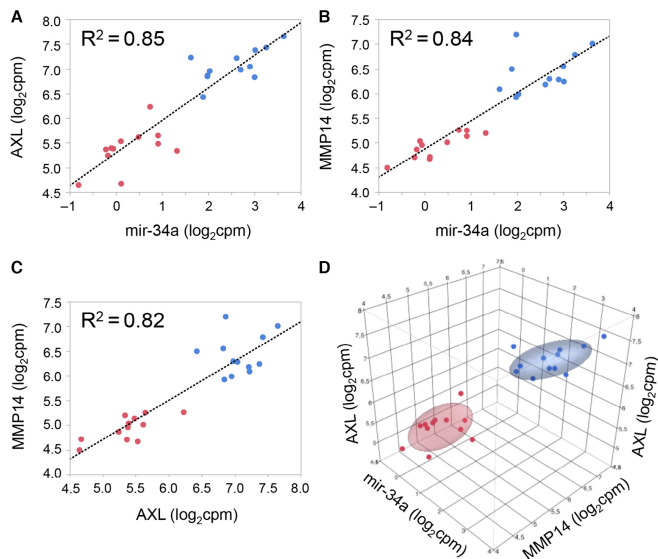


Figure 7. Correlation of expression levels of miR-34a and target genes *AXL* and *MMP14*. Pearson correlation of expression levels of miR-34a and the target genes *AXL* (A) and *MMP14* (B), of *AXL* and *MMP14* (C), and all miR-34a and *AXL* and *MMP14* (D). Red dots indicate normal samples, blue dots ccRCC tumor samples. Ellipsoids indicate the 95th percentile of data points per group.

demonstrates that samples adjacent to tumor and histologically cancer-negative can display a gene expression pattern consistent certain degree of EMT development.

Thereafter, detailed gene expression analyses were primarily based on the dbEMT database containing 357 genes, as this is a curated gene list based on experimental evidence extracted manually from respective publications.

EMT indeed plays an important role in renal cell carcinoma, which supports the ultimate goal and rationale for EMT-directed therapeutic strategies for these patients (Piva et al. 2016). Our comprehensive approach is best exemplified by the description of the up-regulated *MMP14* by investigations on all levels, such as mRNA sequencing, proteomics, and immunohistochemistry, as well as by the analysis of its regulator miR-34a. Notably, *MMP14* is - together with *AXL*, caveolin 1 (*CAV1*) and *ITGA5* - among the top genes contributing to the differentiation of cancer from normal tissue. Expression levels of miR-34a and target genes *AXL* and *MMP14* are closely correlated among each other and clearly separate tumor from adjacent normal tissue.

The integrin *ITGA5* is expressed by renal carcinoma cells but its exact function remains to be determined (Poplawski et al. 2017). Based on our findings, this molecule warrants further exploration. *CAV1* expression

displayed the largest absolute correlation with tumor stage, followed by *VIM*, *IGFBP3*, and *ITGA1*. *CAV1* has not been described in the context of EMT in ccRCC, but it is over-expressed in hepatocellular carcinoma and promotes cancer cell invasion via inducing EMT (Gai et al. 2014). Accordingly, increased expression of *CAV1* can predict a poor prognosis of patients with ccRCC (Steffens et al. 2011).

Our results have implications for prognosis of ccRCC. Higher *MMP14* and *AXL* mRNA levels are associated with lower patient survival. Nevertheless, their common regulator miR-34a, although highly produced in high-risk ccRCC, does not have prognostic value in terms of patient survival. In accordance with our results, *AXL* inhibition represents an emerging treatment option in oncology (Feneyrolles et al. 2014). A selective small molecule *Axl* kinase inhibitor (BGB324) is currently in Phase II clinical trials for acute myeloid leukemia, melanoma and non-small cell lung cancer. *AXL* inhibition in experimental ccRCC models is beneficial indicating a new therapeutic option (Yu et al. 2015).

AXL and miR-34a are engaged in a complex auto-regulation circuit, which involves targeting of *AXL* by miR-34a, while at the same time *AXL* overexpression leads to increased expression of miR-34a via *ELK1* (Cho et al.

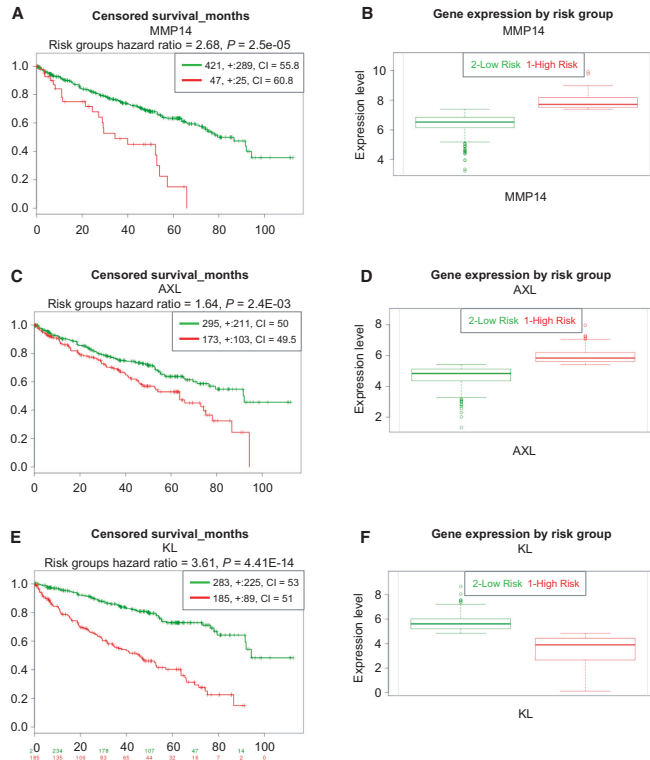


Figure 8. Survival analysis for patients with ccRCC based on individual genes. Higher mRNA expression levels of *MMP14* (A and B), and *AXL* (C and D) are significantly associated with worse survival. Higher *KL* mRNA expression levels are significantly associated with improved patient outcome (E and F).

2016). These data may help explain the concordant up-regulation of *AXL* and *miR-34a* in our datasets.

Contrary to our data, *miR-34* expression levels did not correlate to *AXL* mRNA abundance in a previous ccRCC investigation (Fritz et al. 2015). We do not have a clear explanation for this discrepancy beyond the known ccRCC heterogeneity. However, in that study, levels of *miR-34a* were also increased in ccRCC but not associated with patient outcome, as it is the case for the present investigation (Fritz et al. 2015).

MMP14 represents an increasingly recognized but complex mediator of EMT and ccRCC. *MMP14* is a known target of *miR-34a* (Jia et al. 2014). In our analysis, we observe positive correlation between the expression levels of *MMP14* and *miR-34a*. This could be explained by the fact that *MMP14* is not exclusively regulated by *miR-34a*.

In this respect, we must consider the complex network of *miR-34a*, which targets several MMPs, including *MMP14*, and represses their expression. Higher expression of another microRNA, *miR-21*, decreases the expression of genes coding for TIMPs, such as *TIMP3*, which then in turn leads to an increase in invasion-promoting MMPs (Chernov and Strongin 2011). Importantly, *TIMP3* is a strong inhibitor of *MMP14* (Will et al. 1996). Thus, the MMP regulation pattern is not always linear and unidirectional, but rather includes several checkpoints and multi-directional paths. Furthermore, control of MMP expression and activity is remarkably complex, including at the level of transcription, cellular compartmentalization, zymogen activation, and enzyme inhibition (Baker et al. 2002). *MMP14* is also connected to EGFR, since *MMP14* exerts a positive effect on the MEK1/MAPK axis

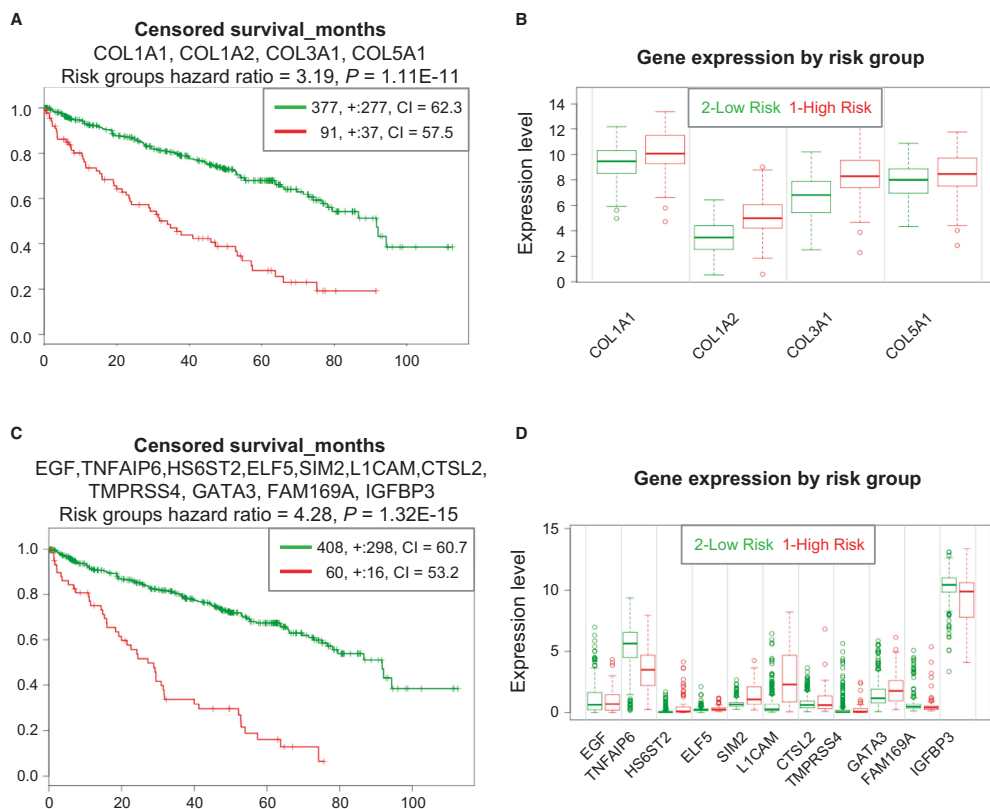


Figure 9. Survival analysis for patients with ccRCC based on two gene panels. Performance of a panel of four collagen genes with co-expression in the matched pairs data (A and B). Performance of a panel of eleven genes with superior rank hazard ratio, and their expression level in risk groups (C and D). The genes have been selected based on their performance in the survival analysis from a set of 20 genes with highest TU/NO-fold change listed in Table 2.

through transactivation of the EGFR (Mahimkar et al. 2011). Indeed, *EGFR* is more than twofold up-regulated in our ccRCC patient cohort (data not shown). The expression level of *EGFR* was previously found to be associated with high ccRCC tumor grade and worse prognosis (Dordevic et al. 2012; Minner et al. 2012).

Klotho (KL) can affect EMT via an interaction with SNAIL. *KL* inhibits the PI3K/Akt/GSK3beta/Snail pathway and decreased *KL* expression negatively correlates with ccRCC patient survival in the literature (Zhu et al. 2013; Gigante et al. 2015). In this respect, Klotho reduces epithelial-mesenchymal transition and cellular invasion in renal cell carcinoma (Zhu et al. 2013). Thus, our data regarding higher *KL* expression favoring better patient

survival are in accordance with the literature. *KL* is a gene encoding a transmembrane protein with anti-aging and tumor suppression functions (Kuro-o et al. 1997; Xie et al. 2013; O'Sullivan et al. 2016). In kidneys, *KL* is naturally present in the proximal tubules, where it increases phosphaturic processes by modulating the activity of renal phosphate transporters. Decreased expression levels of *KL* are also associated with oxidative stress (O'Sullivan et al. 2016).

Despite observations that many individual genes can be used at the mRNA level to indicate better or worse prognosis, a combined set comprising several genes may eventually give the best predictive value. Accordingly, we have designed the two novel candidate prognostic marker sets

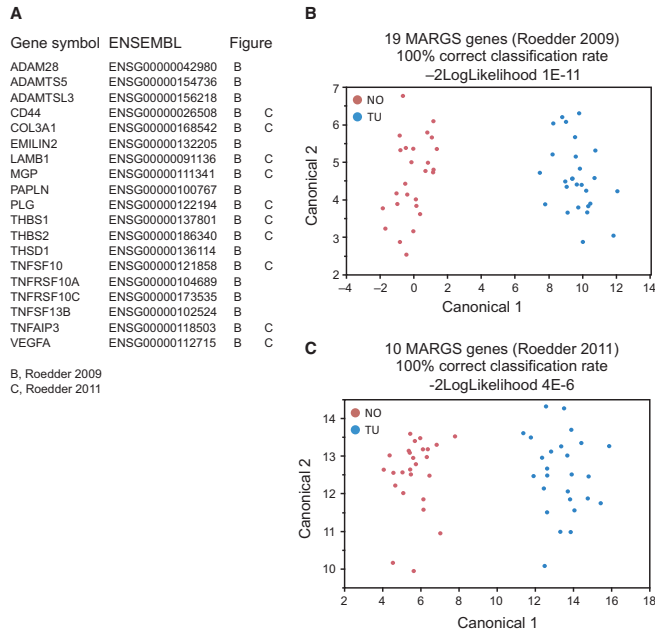


Figure 10. Fibrosis classifier. Two MARGS-based classifiers of fibrosis are diagnostic of ccRCC. Most of the genes of the classifier panels which had been developed to diagnose interstitial fibrosis in renal allografts (19 genes, (Rodder et al. 2009)), and solid organ fibrosis (10 genes, (Rodder et al. 2011)) are differentially expressed in the ccRCC dataset (A). Applying linear discriminant analysis with the 19-gene panel (B) or with the 10-gene panel (C) has a 100% correct classification rate, and indicates a role of fibrosis in ccRCC.

representing mRNA abundances of a limited number of genes to best predict patient survival.

Our results further support a close relationship between EMT and fibrosis development. Several genes of our prognostic gene sets, such as collagens and EGF, are known to bridge EMT and fibrosis. Accordingly, our previously described MARGS-based fibrosis classifier identified all our cancer samples correctly and was also correlated with patient survival. Our results may lead to better early identification of tissues undergoing EMT and potentially fibrosis in the onset of ccRCC, and they support development of new treatment avenues. Nevertheless, our study has some limitations. The sample size of kidney biopsies ($n = 52$) from our ccRCC patient cohort is limited. Furthermore, there is cellular heterogeneity in the tumors and adjacent normal tissues. Hence, our results are a summation of this variability, but reflecting the real life clinical situation. The issue of cell-specificity regarding gene expression must be addressed in the future by tissue microdissection or even by single cell sequencing.

Conclusion

EMT linked to fibrosis represents a prominent feature in ccRCC, which is closely associated with worse patient survival. Therefore, EMT-related genes represent a promising target for future therapeutic interventions.

Acknowledgments

We are thankful to the other local urologists for participation in biopsy harvesting. The Genomics Core Facility (GCF), Norwegian University of Science and Technology (NTNU) performed the library preparation, sequencing and partly the bioinformatics analysis. GCF is funded by the Faculty of Medicine at NTNU and by the Central Norway Regional Health Authority.

Conflict of Interest

No disclosures and no conflict of interest to be reported.

References

- Axelrod, H., and K. J. Pienta. 2014. Axl as a mediator of cellular growth and survival. *Oncotarget* 5:8818–8852.
- Baker, A. H., D. R. Edwards, and G. Murphy. 2002. Metalloproteinase inhibitors: biological actions and therapeutic opportunities. *J. Cell Sci.* 115:3719–3727.
- Chen, D., M. Gassenmaier, M. Maruschke, R. Riesenberg, H. Pohla, C. G. Stief, et al. 2014. Expression and prognostic significance of a comprehensive epithelial-mesenchymal transition gene set in renal cell carcinoma. *J. Urol.* 191:479–486.
- Chernov, A. V., and A. Y. Strongin. 2011. Epigenetic regulation of matrix metalloproteinases and their collagen substrates in cancer. *Biomol. Concepts* 2:135–147.
- Cho, C. Y., J. S. Huang, S. G. Shiah, S. Y. Chung, J. D. Lay, Y. Y. Yang, et al. 2016. Negative feedback regulation of AXL by miR-34a modulates apoptosis in lung cancer cells. *RNA* 22:303–315.
- Doi, S., Y. Zou, O. Togao, J. V. Pastor, G. B. John, L. Wang, et al. 2011. Klotho inhibits transforming growth factor-beta1 (TGF-beta1) signaling and suppresses renal fibrosis and cancer metastasis in mice. *J. Biol. Chem.* 286: 8655–8665.
- Dordevic, G., Dordevic, G., Matusan Ilijas, K., Hadzisejdic, I., Maricic, A., Grahovac, B., et al. 2012. EGFR protein overexpression correlates with chromosome 7 polysomy and poor prognostic parameters in clear cell renal cell carcinoma. *J. Biomed. Sci.* 19:40.
- Eikrem, O., C. Beisland, K. Hjelle, A. Flatberg, A. Scherer, L. Landolt, et al. 2016a. transcriptome sequencing (rnaseq) enables utilization of formalin-fixed, paraffin-embedded biopsies with clear cell renal cell carcinoma for exploration of disease biology and biomarker development. *PLoS ONE* 11:e0149743.
- Eikrem, O. S., P. Strauss, C. Beisland, A. Scherer, L. Landolt, A. Flatberg, et al. 2016b. Development and confirmation of potential gene classifiers of human clear cell renal cell carcinoma using next-generation RNA sequencing. *Scand. J. Urol.* 50:452–462.
- Escudier, B., C. Porta, M. Schmidinger, N. Rioux-Leclercq, A. Bex, V. Khoo, et al. 2016. Renal cell carcinoma: ESMO clinical practice guidelines for diagnosis, treatment and follow-up. *Ann. Oncol.* 27:v58–v68.
- Feneyrolles, C., A. Spenlinhauer, L. Guiet, B. Fauvel, B. Dayde-Cazals, P. Warnault, et al. 2014. Axl kinase as a key target for oncology: focus on small molecule inhibitors. *Mol. Cancer Ther.* 13:2141–2148.
- Fleuren, E. D., M. H. Hillebrandt-Roeffen, U. E. Flucke, D. M. Te Loo, O. C. Boerman, W. T. van der Graaf, et al. 2014. The role of AXL and the in vitro activity of the receptor tyrosine kinase inhibitor BGB324 in Ewing sarcoma. *Oncotarget* 5:12753–12768.
- Fritz, H. K., A. Gustafsson, B. Ljunberg, Y. Ceder, H. Axelsson, and B. Dahlback. 2015. The Axl-Regulating tumor suppressor miR-34a is increased in ccrcc but does not correlate with Axl mRNA or Axl protein levels. *PLoS ONE* 10:e0135991.
- Gai, X., Z. Lu, K. Tu, Z. Liang, and X. Zheng. 2014. Caveolin-1 is up-regulated by GLI1 and contributes to GLI1-driven EMT in hepatocellular carcinoma. *PLoS ONE* 9:e84551.
- Gigante, M., G. Lucarelli, C. Divella, G. S. Netti, P. Pontrelli, C. Cafiero, et al. 2015. Soluble serum alphaklotho is a potential predictive marker of disease progression in clear cell renal cell carcinoma. *Medicine* 94:e1917.
- Gjerdrum, C., C. Tiron, T. Hoiby, I. Stefansson, H. Haugen, T. Sandal, et al. 2010. Axl is an essential epithelial-to-mesenchymal transition-induced regulator of breast cancer metastasis and patient survival. *Proc. Natl Acad. Sci. USA* 107:1124–1129.
- Grande, M. T., B. Sanchez-Laorden, C. Lopez-Blau, C. A. De Frutos, A. Boutet, M. Arevalo, et al. 2015. Snail1-induced partial epithelial-to-mesenchymal transition drives renal fibrosis in mice and can be targeted to reverse established disease. *Nat. Med.* 21:989–997.
- Groger, C. J., M. Grubinger, T. Waldhor, K. Vierlinger, and W. Mikulits. 2012. Meta-analysis of gene expression signatures defining the epithelial to mesenchymal transition during cancer progression. *PLoS ONE* 7:e51136.
- Huang, W., M. Goldfischer, S. Babyeva, Y. Mao, K. Volyanskyy, N. Dimitrova, et al. 2015. Identification of a novel PARP14-TFE3 gene fusion from 10-year-old FPFE tissue by RNA-seq. *Genes Chromosom. Cancer.* <https://doi.org/10.1002/gcc.22261>.
- Jia, L. F., S. B. Wei, K. Mitchelson, Y. Gao, Y. F. Zheng, Z. Meng, et al. 2014. miR-34a inhibits migration and invasion of tongue squamous cell carcinoma via targeting MMP9 and MMP14. *PLoS ONE* 9:e108435.
- Jorda, M., D. Olmeda, A. Vinyals, E. Valero, E. Cubillo, A. Llorens, et al. 2005. Upregulation of MMP-9 in MDCK epithelial cell line in response to expression of the Snail transcription factor. *J. Cell Sci.* 118:3371–3385.
- Kallakury, B. V., S. Karikhalli, A. Haholu, C. E. Sheehan, N. Azumi, and J. S. Ross. 2001. Increased expression of matrix metalloproteinases 2 and 9 and tissue inhibitors of metalloproteinases 1 and 2 correlate with poor prognostic variables in renal cell carcinoma. *Clin. Cancer Res.* 7:3113–3119.
- Kalluri, R., and E. G. Neilson. 2003. Epithelial-mesenchymal transition and its implications for fibrosis. *J. Clin. Invest.* 112:1776–1784.
- Kidd, M. E., D. K. Shumaker, and K. M. Ridge. 2014. The role of vimentin intermediate filaments in the progression of lung cancer. *Am. J. Respir. Cell Mol. Biol.* 50:1–6.
- Kok, H. M., L. L. Falke, R. Goldschmeding, and T. Q. Nguyen. 2014. Targeting CTGF, EGF and PDGF pathways to prevent progression of kidney disease. *Nat. Rev. Nephrol.* 10:700–711.
- Korshunov, V. A. 2012. Axl-dependent signalling: a clinical update. *Clin. Sci. (Lond.)* 122:361–368.

- Kuro-o, M., Y. Matsumura, H. Aizawa, H. Kawaguchi, T. Suga, T. Utsugi, et al. 1997. Mutation of the mouse *klotho* gene leads to a syndrome resembling ageing. *Nature* 390:45–51.
- Lamouille, S., J. Xu, and R. Derynck. 2014. Molecular mechanisms of epithelial-mesenchymal transition. *Nat. Rev. Mol. Cell Biol.* 15:178–196.
- Landolt, L., H. P. Marti, C. Beisland, A. Flatberg, and O. Eikrem. 2016. RNA extraction for RNA sequencing of archival renal tissues. *Scand. J. Clin. Lab. Invest.* 76: 426–434.
- Leibovich, B. C., M. L. Blute, J. C. Cheville, C. M. Lohse, I. Frank, E. D. Kwon, et al. 2003. Prediction of progression after radical nephrectomy for patients with clear cell renal cell carcinoma: a stratification tool for prospective clinical trials. *Cancer* 97:1663–1671.
- Li, R., X. Shi, F. Ling, C. Wang, J. Liu, W. Wang, et al. 2015. MiR-34a suppresses ovarian cancer proliferation and motility by targeting AXL. *Tumour Biol.* 36:7277–7283.
- Lovisa, S., V. S. LeBleu, B. Tampe, H. Sugimoto, K. Vадnagara, J. L. Carstens, et al. 2015. Epithelial-to-mesenchymal transition induces cell cycle arrest and parenchymal damage in renal fibrosis. *Nat. Med.* 21:998–1009.
- Mahimkar, R., M. A. Alfonso-Jaume, L. M. Cape, R. Dahiya, and D. H. Lovett. 2011. Graded activation of the MEK1/MT1-MMP axis determines renal epithelial cell tumor phenotype. *Carcinogenesis* 32:1806–1814.
- Mak, K. M., C. Y. Png, and D. J. Lee. 2016. Type V collagen in health, disease, and fibrosis. *Anat. Rec. (Hoboken)* 299:613–629.
- Marti, H. P., J. C. Fusco, J. C. Kwekel, A. Anagnostopoulou, and A. Scherer. 2014. Metzincins and related genes in experimental renal ageing: towards a unifying fibrosis classifier across species. *Nephrol. Dial. Transplant.* 29:1177–1185.
- Marti, H. P., A. Jeffs, A. Scherer, J. Leader, C. Leader, J. Bedford, et al. 2016. Renal fibrosis mRNA classifier: validation in experimental lithium-induced interstitial fibrosis in the rat kidney. *PLoS ONE* 11:e0168240.
- Mikami, S., M. Oya, R. Mizuno, T. Kosaka, M. Ishida, N. Kuroda, et al. 2016. Recent advances in renal cell carcinoma from a pathological point of view. *Pathol. Int.* 66:481–490.
- Minner, S., D. Rump, P. Tennstedt, R. Simon, E. Burandt, L. Terracciano, et al. 2012. Epidermal growth factor receptor protein expression and genomic alterations in renal cell carcinoma. *Cancer* 118:1268–1275.
- Nalwoga, H., L. Ahmed, J. B. Arnes, H. Wabinga, and L. A. Akslen. 2016. Strong expression of hypoxia-inducible factor-1alpha (HIF-1alpha) is associated with *axl* expression and features of aggressive tumors in african breast cancer. *PLoS ONE* 11:e0146823.
- Nieto, M. A., R. Y. Huang, R. A. Jackson, and J. P. Thiery. 2016. EMT. *Cell* 166:21–45.
- O'Sullivan, E. D., J. Hughes, and D. A. Ferenbach. 2016. Renal aging: causes and consequences. *J. Am. Soc. Nephrol.* 28:14.
- Piva, F., M. Giuliotti, M. Santoni, G. Occhipinti, M. Scarpelli, A. Lopez-Beltran, et al. 2016. Epithelial to mesenchymal transition in renal cell carcinoma: implications for cancer therapy. *Mol. Diagn. Ther.* 20:111–117.
- Poplawski, P., B. Rybicka, J. Boguslawska, K. Rodzik, T. J. Visser, A. Nauman, et al. 2017. Induction of type 1 iodothyronine deiodinase expression inhibits proliferation and migration of renal cancer cells. *Mol. Cell. Endocrinol.* 442:58–67.
- Reichl, P., M. Dengler, F. van Zijl, H. Huber, G. Fuhrlinger, C. Reichel, et al. 2015. Axl activates autocrine transforming growth factor-beta signaling in hepatocellular carcinoma. *Hepatology* 61:930–941.
- Rodder, S., A. Scherer, F. Raulf, C. C. Berthier, A. Hertig, L. Couzi, et al. 2009. Renal allografts with IF/TA display distinct expression profiles of metzincins and related genes. *Am. J. Transplant.* 9:517–526.
- Rodder, S., A. Scherer, M. Korner, and H. P. Marti. 2011. A subset of metzincins and related genes constitutes a marker of human solid organ fibrosis. *Virchows Arch.* 458:487–496.
- von Roemeling, C. A., D. C. Radisky, L. A. Marlow, S. J. Cooper, S. K. Grebe, P. Z. Anastasiadis, et al. 2014. Neuronal pentraxin 2 supports clear cell renal cell carcinoma by activating the AMPA-selective glutamate receptor-4. *Can. Res.* 74:4796–4810.
- Seiki, M., N. Koshikawa, and I. Yana. 2003. Role of pericellular proteolysis by membrane-type 1 matrix metalloproteinase in cancer invasion and angiogenesis. *Cancer Metastasis Rev.* 22:129–143.
- Steffens, S., A. J. Schrader, H. Blasig, G. Vetter, H. Eggers, W. Trankenschuh, et al. 2011. Caveolin 1 protein expression in renal cell carcinoma predicts survival. *BMC Urol.* 11:25.
- Tan, T. Z., Q. H. Miow, Y. Miki, T. Noda, S. Mori, R. Y. Huang, et al. 2014. Epithelial-mesenchymal transition spectrum quantification and its efficacy in deciphering survival and drug responses of cancer patients. *EMBO Mol. Med.* 6:1279–1293.
- Thiery, J. P., and C. T. Lim. 2013. Tumor dissemination: an EMT affair. *Cancer Cell* 23:272–273.
- Thiery, J. P., and J. P. Sleeman. 2006. Complex networks orchestrate epithelial-mesenchymal transitions. *Nat. Rev. Mol. Cell Biol.* 7:131–142.
- Thiery, J. P., H. Acloque, R. Y. Huang, and M. A. Nieto. 2009. Epithelial-mesenchymal transitions in development and disease. *Cell* 139:871–890.
- Will, H., S. J. Atkinson, G. S. Butler, B. Smith, and G. Murphy. 1996. The soluble catalytic domain of membrane type 1 matrix metalloproteinase cleaves the propeptide of progelatinase A and initiates autoproteolytic activation. Regulation by TIMP-2 and TIMP-3. *J. Biol. Chem.* 271:17119–17123.
- Wisniewski, J. R. 2013. Proteomic sample preparation from formalin fixed and paraffin embedded tissue. *J. Vis. Exp.* 50589.

- Xie, B., J. Chen, B. Liu, and J. Zhan. 2013. Klotho acts as a tumor suppressor in cancers. *Pathol. Oncol. Res.* 19:611–617.
- Yu, H., R. Liu, B. Ma, X. Li, H. Y. Yen, Y. Zhou, et al. 2015. Axl receptor tyrosine kinase is a potential therapeutic target in renal cell carcinoma. *Br. J. Cancer* 113:616–625.
- Zaravinos, A. 2015. The regulatory role of MicroRNAs in EMT and cancer. *J. Oncol.* 2015:865816.
- Zhang, J., and L. Ma. 2012. MicroRNA control of epithelial-mesenchymal transition and metastasis. *Cancer Metastasis Rev.* 31:653–662.
- Zhao, M., L. Kong, Y. Liu, and H. Qu. 2015. dbEMT: an epithelial-mesenchymal transition associated gene resource. *Sci. Rep.* 5:11459.
- Zhou, D., V. Kannappan, X. Chen, J. Li, X. Leng, J. Zhang, et al. 2016a. RBP2 induces stem-like cancer cells by promoting EMT and is a prognostic marker for renal cell carcinoma. *Exp. Mol. Med.* 48:e238.
- Zhou, L., X. D. Liu, M. Sun, X. Zhang, P. German, S. Bai, et al. 2016b. Targeting MET and AXL overcomes resistance to sunitinib therapy in renal cell carcinoma. *Oncogene* 35:2687–2697.
- Zhu, Y., L. Xu, J. Zhang, W. Xu, Y. Liu, H. Yin, et al. 2013. Klotho suppresses tumor progression via inhibiting PI3K/Akt/GSK3beta/Snail signaling in renal cell carcinoma. *Cancer Sci.* 104:663–671.

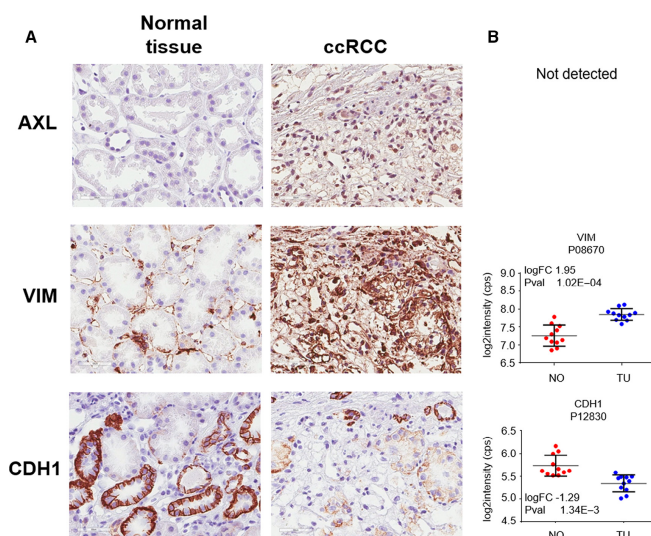
doi: 10.14814/phy2.13671

Clear Cell Renal Cell Carcinoma is linked to Epithelial-to-Mesenchymal Transition and to Fibrosis

Lea Landolt, Øystein Eikrem, Philipp Strauss, Andreas Scherer, David H. Lovett, Christian Beisland, Kenneth Finne, Tarig Osman, Mohammad M. Ibrahim, Gro Gausdal, Lavina Ahmed, James B. Lorens, Jean Paul Thiery, Tuan Zea Tan, Miroslav Sekulic & Hans-Peter Marti

Physiol Rep, 5 (11), 2017, e13305, <https://doi.org/10.14814/phy2.13305>

Figure 6 supplied in the article was incorrect. The correct version is given below.



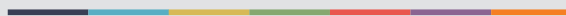
The authors apologise for the error.

Reference

Landolt, L., Ø. Eikrem, P. Strauss, A. Scherer, D. H. Lovett, C. Beisland, K. Finne, T. Osman, M. M. Ibrahim, G. Gausdal, L. Ahmed, J. B. Lorens, J. P. Thiery, T. Z. Tan, M. Sekulic, and H.-P. Marti. Clear cell renal cell carcinoma is linked to epithelial-to-mesenchymal transition and to fibrosis. *Physiol. Rep.* 5:e13305. <https://doi.org/10.14814/phy2.13305>



Graphic design: Communication Division, UIB / Print: Skjipes Kommunikasjon AS



uib.no

ISBN: 978-82-308-3582-1